

Geomorphic process chains in high-mountain regions - A review and classification approach for natural hazards assessment

Peter Adolf Mani¹, Simon Keith Allen¹, Stephen G Evans², Jeffrey Kargel³, Martin Mergili⁴, Dmitry A Petrakov⁵, and Markus Stoffel¹

¹University of Geneva

²University of Waterloo

³U of AZ

⁴Institute of Applied Geology, BOKU University, Vienna

⁵Moscow State University

November 26, 2022

Abstract

Human populations and infrastructure in high mountain regions are exposed to a wide range of natural hazards, the frequency, magnitude, and location of which are extremely sensitive to climate change. In cases where several hazards can occur simultaneously or where the occurrence of one event will change the disposition of another, assessments need to account for complex process chains. While process chains are widely recognized as a major threat, no systematic analysis has been undertaken. We therefore assemble a broad set of process chain events from across the globe to establish new understanding on the factors that directly trigger or alter the disposition for subsequent events in the chain. Based on this new understanding, we derive a novel classification scheme and parameters to aid natural hazard assessment. Most process chains in high mountains are commonly associated with glacier retreat or permafrost degradation. Regional differences exist in the nature and rate of sequencing—some process chains are almost instantaneous, while other linkages are delayed. Process chains involving rapid sequences are difficult to predict or mitigate, and impacts are often devastating. We demonstrate that process chains are initialized most frequently as threshold failures, being the result of gradual landscape weakening and not due to the occurrence of a distinct trigger. The co-occurrence of fluvial processes or activation of sediment deposition areas increases the reach of process chains. Climate change is therefore expected to increase the reach of events in the future, as glacial environments transform into sediment-rich paraglacial and fluvial landscapes.

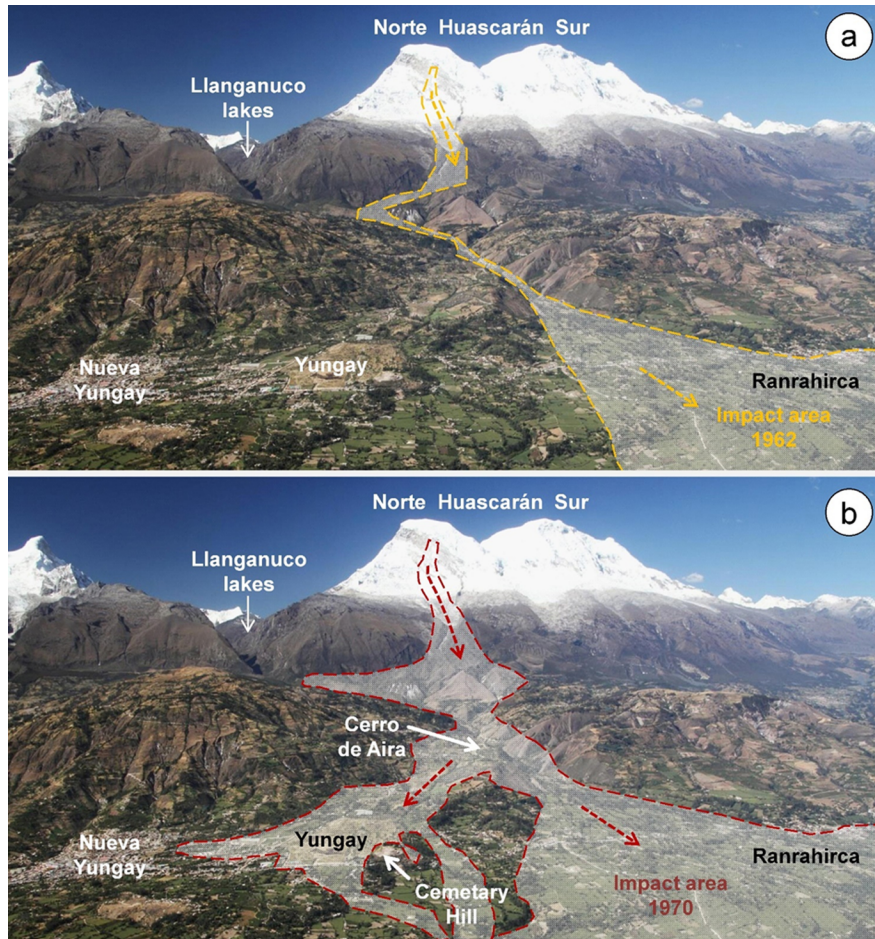
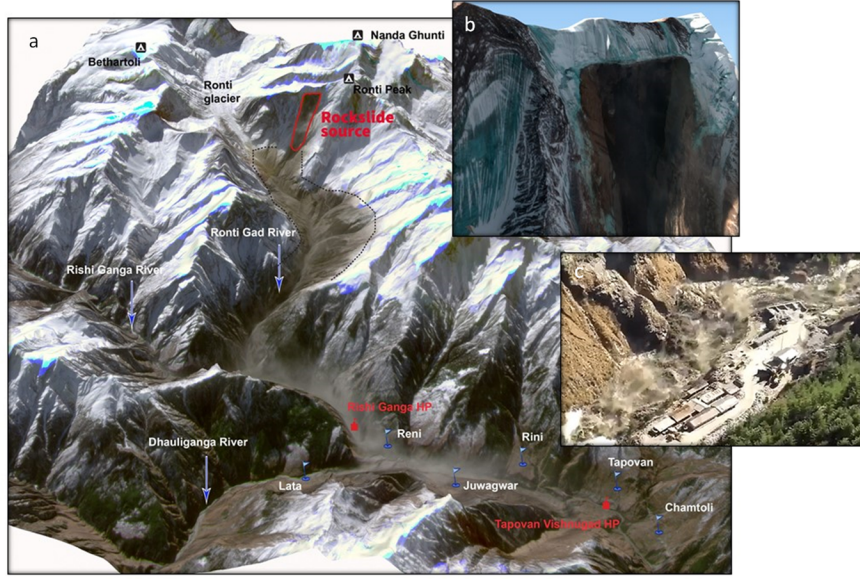
		Subsequent process (triggered or increased probability)							
		RFA	SIA	DF	LA	SL	FL	GLOF	
Triggering process	EQ								
	VO								
	PRE								
	MEL								
Initial process	TF								
	RFA								
	SIA								
	DF								
	LA								
	SL								
	FL								
	GLOF								

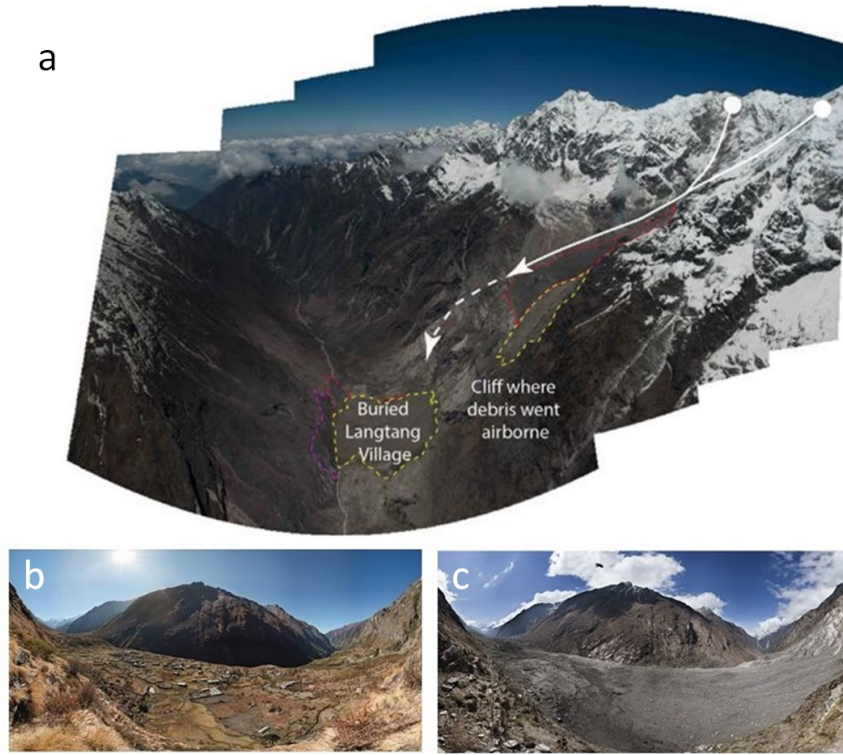
EQ: Earthquake
 VO: Volcanic eruption
 PRE: Heavy precipitation
 MEL: Snow or ice melt
 TF: Threshold failure
 RFA: Rockfall and rock avalanche
 SIA: Snow and ice avalanche
 DF: Debris flow
 LA: Lahar
 SL: Slide
 FL: Flood
 GLOF: Glacier lake outburst flood

Symbol	Explanation
	Process triggers subsequent hazard
	Process increases the probability of subsequent hazard
	Process both triggers and increases the probability of subsequent hazard

Type of Movement		Type of Material			
		Rock	Soil ^{*)}	Ice	Snow
Falls (including topples)		Rockfall		Icefall	
Slides		Rockslide (rotational, planar)	Soilslide (rotational, planar)	Glacial surge	
Flows	Dry	Rock avalanche		Ice avalanche	Dry snow avalanche
	Wet	Debris flow			Wet snow avalanche
		Lahar			

^{*)} Soil: including boulder, debris, gravel, sand, silt, mud, clay





Geomorphic process chains in high-mountain regions – A review and classification approach for natural hazards assessment

Peter Mani¹, Simon Allen¹, Stephen G. Evans², Jeffrey S. Kargel³, Martin Mergili⁴, Dmitry Petrakov⁵, Markus Stoffel^{1,6,7}

¹ Institute for Environmental Sciences, University of Geneva, Switzerland

² Department of Earth & Environmental Sciences, Centre for Environmental and Information Technology, University of Waterloo, Ontario, Canada

³ Planetary Science Institute, University of Arizona, Tucson, AZ, USA

⁴ Institute of Geography and Regional Science, University of Graz, Graz, Austria

⁵ Faculty of Geography, M.V. Lomonosov Moscow State University, Moscow, Russia

⁶ Dendrolab.ch, Department of Earth Sciences, University of Geneva, Geneva, Switzerland

⁷ Department of F.A. Forel for Environmental and Aquatic Sciences, University of Geneva, Geneva, Switzerland

Key Points

- High mountain hazard process chains commonly are associated with glacier retreat or permafrost degradation.
- Process chains are initialized most frequently by threshold failure, which is a result of long-lasting landscape weakening.
- An important implication of climate change is that we can expect an increase in the reach of process chain events in the future.

Abstract

Human populations and infrastructure in high mountain regions are exposed to a wide range of natural hazards, the frequency, magnitude, and location of which are extremely sensitive to climate change. In cases where several hazards can occur simultaneously or where the occurrence of one event will change the disposition of another, assessments need to account for complex process chains. While process chains are widely recognized as a major threat, no systematic analysis has been undertaken. We therefore assemble a broad set of process chain events from across the globe to establish new understanding on the factors that directly trigger or alter the disposition for subsequent events in the chain. Based on this new understanding, we derive a novel classification scheme and parameters to aid natural hazard assessment.

Most process chains in high mountains are commonly associated with glacier retreat or permafrost degradation. Regional differences exist in the nature and rate of sequencing—some process chains are almost instantaneous, while other linkages are delayed. Process chains involving rapid sequences are difficult to predict or mitigate, and impacts are often devastating. We demonstrate that process chains are initialized most frequently as threshold failures, being the result of gradual landscape weakening and not due to the occurrence of a distinct trigger. The co-occurrence of fluvial processes or activation of sediment deposition areas increases the reach of process chains. Climate change is therefore expected to increase the reach of events in the future, as glacial environments transform into sediment-rich paraglacial and fluvial landscapes.

Keywords: Debris flow, Landslides, Multihazards, Disasters, Cryosphere, Climate impact, Trigger

1. Introduction

1.1 Mountain Regions and Mountain Hazards

Mountain regions make up 24% of global land area (35.8 million km²; Kapos et al., 2000) and are home to 12% of the world's population (Hock et al., 2019) as well as of 15–20% of worldwide tourism with an annual turnover estimated to US\$ 70–90 billion (UNEP, 2007). Mountains are also home to vital infrastructure

including that related to water supply and the generation of hydroelectric power (Farinotti et al., 2019). They are characterized by sharp topographic gradients, resulting in a high local elevation range, distinctive meteorological conditions and – under most circumstances – glacial, paraglacial and periglacial environments which define the mountain cryosphere. Often in combination with enhanced tectonic activity, mountain regions are therefore home to a wide range of catastrophic natural hazard processes (Stäubli et al., 2018), including various types of gravitational processes, (rock/debris avalanches, rockfalls, landslides and debris flows), massive glacial instability, snow avalanches and a range of types of floods generated by heavy rains or lake outburst. As a result, almost 1 billion people who inhabit mountain regions are potentially exposed to or affected by the occurrence of catastrophic processes and the severe impacts that accompany them including fatalities, damage to settlements, and destruction of infrastructure (Hock et al., 2019).

Over the past decade (2012-2022), a number of major disasters (defined here as having killed more than 10 people) have occurred in the world’s mountain regions. Examples include 1) India (2013) - the floods and landslides in the June 2013 Uttarakhand disaster that were triggered by unusually heavy, very early monsoon rainfall in the northern part of India, claiming more than 5,700 lives (Nair and Singh, 2014) 2) Nepal (2015) - the M7.8 Gorkha earthquake in Nepal triggered about 25,000 landslides, rockfalls and ice avalanches (Fujita et al., 2017; Kargel et al., 2016; Lacroix, 2016). In this event, about 8,200 people died and several villages as well as important infrastructure were destroyed by mass movements (Roback et al., 2018; Zhao, 2016). 3) Salkantay, Peru (2020) – an outburst flood triggered by a rock/ice avalanche caused fatalities in the valley downstream (Wilca et al., 2021), 4) European Alps (2020) - abnormally heavy rainfall in early October 2020 caused widespread devastation of settlements and infrastructure in the southern French and Italian Alps, with more than 20 killed or reported missing (Carrega and Michelot, 2021; Payrastre and Nicolle, 2021). 5) Chamoli, India (2021) – a huge rock/ice avalanche rapidly transformed into an extraordinarily large and mobile debris flow. More than 200 people were killed or are missing (Shugar et al., 2021). In addition, a number of large-scale catastrophic events have occurred in the world’s mountain regions with less fatalities and/or damage to infrastructure, e.g. the twin glacier collapse in Aru Mountains, Tibet in 2016 (Gilbert et al., 2018), the 2020 landslide at Elliot Creek, British Columbia (Geertsema et al., 2022) or a glacier lake outburst flood in 2020 at Jinwuco (Tibet) (Zheng et al., 2021b).

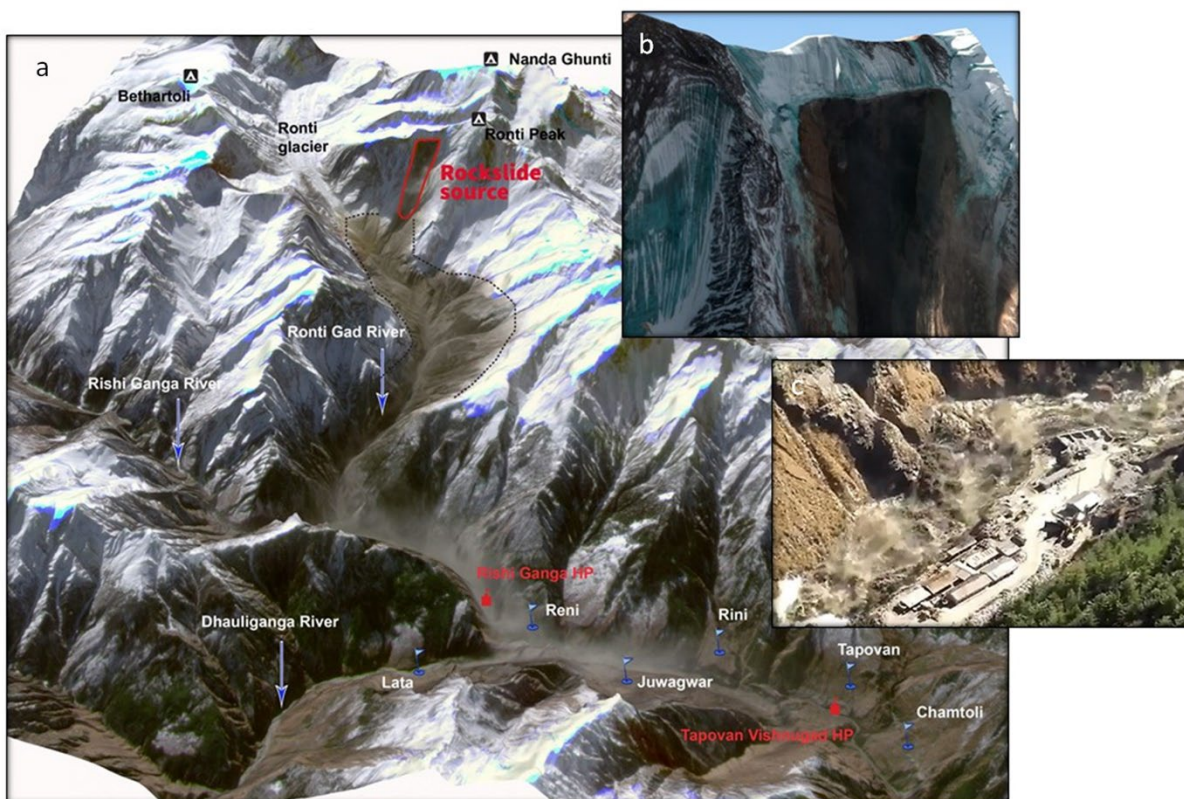


Figure 1. A real-time perspective of the Chamoli process chain (a), showing origin of the rockslide and the path of the debris flow captured on a satellite image at 10:30 Indian Standard Time, just before the front of the flow reached the Tapovan Hydropower Project site (CubeSat image reused with permission from (Shrestha, AB et al., 2021)). The dust cloud accompanying the flow is clearly visible. The dotted black line shows the sediment and dust deposited in the river valley. The release zone of the rock/ice avalanche is shown in red and in the enlarged image (b) (CNES and Airbus DS, Pléiades image processed by E. Berthier and S. Gascoïn and reused with permission). Inset image is a screenshot taken from a video, showing the debris flood around 2km below the Topovan hydropower site (c) (reused with permission from Anand Bahuguna).

Detailed knowledge and assessment of natural hazard processes is therefore key when it comes to sustaining livelihoods in mountain regions, limiting vulnerability, reducing disaster risk and, enhancing adaptive capacity of humans and their infrastructure in mountain ranges worldwide where ongoing and future climate change will likely increase negative impacts (Hock et al., 2019).

Our understanding and the assessment of natural hazard processes in mountain regions has improved substantially over recent decades and especially since the 1992 Earth Summit in Rio de Janeiro during which mountain regions received political recognition for the unique role they play in global sustainability through the adoption of Chapter 13 on Sustainable Mountain Development (Agenda 21, 1992). An important next step was the Sendai Framework for Disaster Risk Reduction 2015–2030 (United Nations Office for Disaster Risk Reduction). In the Sendai document, the “understanding of disaster risk” is given highest priority. To achieve this aim, it is necessary “to promote comprehensive surveys on multi-hazard disaster risks and the development of regional disaster risk assessments and maps, including climate change scenarios”. These efforts resulted in the development of a suite of assessment methods for catastrophic hazard processes.

As a result of their complexity and widespread occurrence, a range of approaches exist for landslide hazard assessment: Hungr (2016) summarizes methodological advances that have been achieved in monitoring and remote sensing as well as in the analytical methods for landslide susceptibility, runout and hazard assessment. For torrential catchments debris flows are the most important process. Iverson (2014) presents the actual perspective of debris-flow behavior, debris flow models and the hazard assessment. In the case of rockfall hazards, for instance, both quantitative (model based) and qualitative (rating systems) assessment methods have been developed (Mavrouli et al., 2014, Ferrari et al., 2016). For snow avalanches, Bründl et al. (2010) present an overview of advances in defining scenarios as a basis for the hazard assessment and numerical modelling of runout distance and other flow parameters for hazard zoning. Specifically for the mountain cryosphere, guidelines for the assessment of glacial and permafrost hazards have been produced by a Scientific Standing Group of the International Association of Cryospheric Sciences IACS and the International Permafrost Association IPA (GAPHAZ, 2017).

Despite these advances, major challenges still persist, especially in cases where interactions between different hazard processes occur, thereby changing the nature, magnitude, and reach (runout distance) of a catastrophic event. Such interactions can be manifold but can be summarized under the term “multi-hazard” (e.g. Kappes et al. 2012, van Westen et al. 2014). In general, a multi-hazard event is characterized by a close spatial and/or temporal proximity of different processes that contribute to a single event and involves the occurrence of multiple processes in a single hazard event. This occurrence of multiple processes in a single hazard event may lead to a greater impact on communities and infrastructure than individual hazards and may reduce resilience and recovery (Liu et al., 2016).

1.2 Definitions of Multi-Hazard

In general, a multi-hazard event is characterized by a close spatial and temporal proximity and a cause-effect relation of multiple processes within a single hazard event. The term “multi-hazard” has been defined in various ways. Kappes et al. (2012) presents 16 different terms for the relations within multi-hazard processes. Following Schauwecker et al. (2019), this term can be assigned to two main types of interactions between single processes:

- A single overall driver triggers a similar process in a cluster of events that are independent of each other, yet are nearly coincident in space and/or time. For instance, a heavy rain event may cause

flooding and landslides (including debris flows) in a mountain region. An example is the case in August 2005 in the Bernese Oberland (Switzerland), where a large area underwent intense slope and channel processes (Rickenmann et al., 2016). This type of multi-hazard can be termed a compound event (Schauwecker et al., 2019; Zscheischler et al., 2018).

- A hazard process triggers a sequence of processes that are spatially linked in rapid sequence or delayed time. A first example (rapid sequence) involves a rock avalanche entering a lake, which in turn generates a tsunami displacing water downstream to generate a debris flood/debris flow. A second example (delayed time) can be when a landslide blocks a river, which leads to the formation of a lake. A delayed collapse of the dam following overtopping results in a flood wave, which can trigger further landslides due to bank destabilization. For this type of interaction, the terms “cascade effect” or “process chain” are used (e.g. Gilbert et al., 2018; Kirschbaum et al., 2019; Mergili et al., 2020a; Schauwecker et al., 2019).

Gill and Malamud (2016) likewise emphasize that a multi-hazard event can be more than a spatial or temporal overlap of different hazard processes (multi-layer single hazard) because it can also involve the interaction between the different hazard processes.

Liu et al. (2016) present a systematic classification of hazard interactions, differentiating independent, mutual, parallel and serial relationships. Their description of serial relationship coincides with the description of process chains or process cascade in other publications. Pescaroli and Alexander (2015) for instance, give a definition of cascading disasters and cascading effects in which cascades of disasters related to technical systems are described, some of them triggered by natural processes (e.g. tsunamis, floods, storm surges). They distinguish between linear sequences of events and non-linear paths of cascades. While linear interactions can still be analyzed relatively easily, non-linear interactions can trigger network effects that result in complex system behavior, such as feedbacks or bifurcations.

Kappes et al. (2010) distinguish two types of relations between hazard interactions that are crucial in natural hazards management, namely (i) those in which one process triggers near-instantaneously the next (cascades, domino effects); and (ii) those in which the disposition of one hazard is altered by another (delayed). In the case of altered disposition, a longer period normally elapses between the two processes, leaving some time for intervention planning. In situations where one process triggers another process (in a cascading manner or a domino effect), processes follow one another almost instantaneously without leaving time for intervention or emergency measures (Baer et al., 2017; Walter et al., 2020). From an applications viewpoint, the time sequencing either giving or denying options to reduce harm is key. Is there adequate time for an intervention, such as a self-evacuation or a rescue of threatened people, or an engineered disaster mitigation? In the case of a rapidly progressing event, such as a glacial lake outburst flood (GLOF), if a real-time early warning system exists (quite rare) and the resident population has been trained to respond, then evacuations from a small village may be possible in minutes. Lacking hazard early warning or the required response training, a GLOF or landslide dam-induced flood may effectively be nearly instantaneous. In the case of a landslide blockage of a river, a rescue may take days, and an engineered solution may take place in days to months. Hence, whether a process chain is viewed as near instantaneous or delayed depends on the specific circumstances and what is at risk. However, we avoid a rigid definition of the timeframes of events and responses, as terms like “near instantaneous” and “delayed” may be readily understandable.

1.3 Process Chains

We focus on catastrophic natural hazards in mountain regions and examine process chains resulting from geomorphic cascades (cf. Schauwecker et al., 2019), where a hazard process triggers a sequence of other processes in a single overall event. We also include linear and non-linear interactions following the concept provided by Pescaroli and Alexander (2015) as well as direct triggering and disposition change according to Kappes et al. (2010). Interactions with technical and/or social systems are not part of our analysis. Therefore, in brief, we define “process chains in mountain regions” as a sequence of natural hazard processes in a single event, where one process transforms in one or more subsequent processes that are spatially linked, and where the transformation occurs either nearly instantaneously or is delayed by changing the disposition of

the subsequent processes. Process chains can amplify the impact of the initial event and increase the area affected (e.g., Evans et al., 2021).

Numerous examples of process chains in geomorphic events are found in the European Alps. They include 1) rock avalanches triggering rock-snow avalanches (e.g., in the Mont Blanc area (Deline et al., 2011)) 2) the rock avalanches from Pizzo Cengalo in Grisons (Switzerland) leading to massive debris flows (Baer et al., 2017; Frank et al., 2019; Mergili et al., 2020a; Walter et al., 2020), and 3) the process chain that resulted from the destabilization of a rock mass and subsequent rockfalls from the east face of the Eiger (Bernese Oberland, Switzerland) (Werder et al., 2010).

Examples of process chains have also been described from other mountain regions. In the Andes, for example, Evans et al. (2009) described two events of rock-ice avalanches at Nevado Huascarán (Peru) that transformed into debris flows. The second event in 1970 was triggered by an earthquake. In the Himalayas, Cook et al. (2018) and Sattar et al. (2022) assessed an outburst flood at the Gongbatongshacuo Lake, which produced many slope processes along the Zhangzangbo River and subsequent damages to buildings and infrastructure 40 km downstream. Ruiz-Villanueva et al. (2017) provided an overview of landslide-dammed lake outburst floods across the Hindu Kush-Karakoram-Himalayas. For the Tien Shan mountains in Central Asia, Zaginaev et al. (2016) described a series of debris flows triggered by englacial water pocket outbursts (and/or glacier lake outburst floods) and described the implications that these process chains have for hazard assessment.

The complexity of process chains presents important challenges in modelling for mountain hazard assessment. Several studies have employed models to analyze the process chains, e.g. Barla and Barla (2001) for the Brenva Glacier rock avalanche in the Mont Blanc area and Schneider et al. (2014) for the glacier lake outburst flood at Nevado Hualcán in Peru. Likewise, Worni et al. (2014) evaluated the usability of numerical models for the simulation of process cascades, with a focus on GLOFs. Mergili et al. (2020b) used a GIS-based model to evaluate different hypothesis for the GLOF event that occurred 1941 at the Lake Palcacocha. A broader overview of models for dam breach processes and flood or debris flow propagation is presented by Westoby et al. (2014). In modelling such complex processes, uncertainty is an important issue. Using the example of a GLOF event on Mount Hualcán, Schaub et al. (2016) discuss the effect of scenario elaboration and uncertainty propagation on the outcome of the simulation of process chains. Uncertainty in the simulation of process chains is also an issue in the analyses of the Huascarán events (Mergili et al., 2018b), the multi-lake outburst flood in the Santa Cruz valley (Mergili et al., 2018a), both in Peru and the Pizzo Cengalo event (Mergili et al., 2020a).

1.4 Process Chains and Climate Change in Mountain Regions

The ongoing and accelerating anthropogenic warming (Arias et al., 2021) has led to substantial changes in high-mountain environments (Beniston et al., 2018; Gobiet et al., 2014; IPCC, 2019). Climate change impacts on natural hazards can occur through changes in the amount or peak intensity of precipitation, changing balances of the physical state of precipitation (snow:rain ratio), by increased melting rates of ice and snow, initiation of basal melting of glaciers or introduction of surface melt or rainwater to glacier beds, development of glacial lakes, thawing of permafrost with melting of ground ice, or by changes in vegetation. Since these individual climate change effects normally do not occur in isolation, multiple climate change effects can be active. The hazard responses can involve a change in hazard intensity or frequency (increasing or decreasing), a shift in their location to higher elevation or a different aspect on a mountain range, a shift from one kind of hazard to another, or a change in the linkages within hazard process chains. The impacts of these climate change related influences on hazard activity are further modulated by changing exposure to hazards, including increases in human populations and infrastructure in mountain regions.

Atmospheric warming has well-documented impacts on snow, ice and permafrost, and this is altering the frequency, magnitude and location of related natural hazards in the mountain cryosphere (Hock et al., 2019) and thus, is expected to have increased the probability for process chains to occur (Shugar et al., 2021) and to increase their complexity. The number and area of glacier lakes has increased in most mountain regions of the globe (Shugar et al., 2020), and changes in the decadal occurrences of GLOFs has oscillated (Harrison

et al., 2018), but it remains uncertain whether the frequency of GLOFs has increased over the longer term as is widely supposed (Harrison et al., 2018; Veh et al., 2022; Veh et al., 2019). Snow avalanches involving wet snow have increased in several regions and mostly at higher elevations (Ballesteros-Cánovas et al., 2018; Stoffel and Corona, 2018), whereas snow avalanches have become much less frequent at lower altitudes (Castebrunet et al., 2014; Giacona et al., 2021). As a consequence of increases in temperature and snowfall limits, rain-on-snow floods have increased in winter, but have started to decrease in spring (Freudiger et al., 2014). With ongoing climate change rain-induced snowmelt floods will likely become more frequent at high elevations in winter over decades to come (Beniston and Stoffel, 2016; Morán-Tejeda et al., 2016). Such floods may cease to be a hazard in some lower elevation regions, though thunderstorm cloudburst type run-off floods may increase in those areas.

Evans and Clague (1994) provided examples from the Canadian Cordillera and the Andes where climate change has likely altered the disposition (readiness or susceptibility (Allen et al., 2022)) of natural hazard processes in the periglacial and glacial domain. In their Special Report on EXtreme events and disasters (SREX; Field et al., 2012), the Intergovernmental Panel on Climate Change (IPCC) did not take process chains explicitly into account, whereas the IPCC Special Report on the Ocean and Cryosphere in a Changing Climate (IPCC, 2019) discussed process chains explicitly, including the effect of climate change on GLOF processes (Harrison et al., 2018; Huggel et al., 2020; Shugar et al., 2020; Zheng et al., 2021b) and increasing landslide hazards (Gruber and Haeblerli, 2007; Stoffel et al., 2014b).

1.5 Objective of the study

Despite the recent inclusion of process chains in IPCC's climate change assessments, progress made in the field as well as the substantial body of literature existing on individual case studies of process chains, no attempt has been made so far to analyze process chains systematically with the aim to provide an overview of the characteristics of process chains in the mountain environment. The objective of this study, therefore, is to fill this gap by (i) assembling a broad list of process chains resulting from geomorphic cascades from mountain regions across the world. This is based on a broad literature search. We then (ii) typify events by applying a classification scheme containing both characteristics and parameters of process chains. For this the information from literature and additional sources is stored in a database. Based on the classification, we (iii) derive a series of parameters that are relevant for natural hazard assessment, and (iv) highlight the relevance of climate change for the different process chains discussed.

2. Classification approach

2.1 Classification scheme

The classification scheme for the characterization of process chain events consists of a set of parameters that are grouped into classes (Table 1). The parameters are selected in terms of their relevance for natural hazard assessment, their availability in the literature, or the possibility of deriving them from globally available spatial datasets. The classes are described in more detail in the following chapters.

Table 1. Classification scheme for the characterization of process chain events. For the different aspects (classes) of process chains, distinct characteristics (parameters) are defined.

Class	Parameters
Spatial context	Region (glacier region from GTN-G) Location (mountain, valley, region) Coordinates (lat/lon)
Processes involved	Triggering process that initiates the process chain Initial process of the process chain Sequence of subsequent processes (cf. box with relevant processes)
Process interaction	Direct triggering of secondary processes (yes/no) Increasing disposition for secondary processes (yes/no)
Starting zone parameters	Elevation of starting zone (m asl) Local elevation range (meters radius) Seismicity (peak Ground Acceleration (PGA)) Lithology (lithological classification) Permafrost (classes of permafrost zonation index (PZI)) Stream order of basin
Amplifying effects	Snow entrainment (yes/no) Ice entrainment (yes/no) Fine grained loose material (yes/no) Fluvial processes involved (yes/no) Lakes involved (yes/no)
Volume	Initial volume (m ³ (order of magnitude)) Total volume mobilized (m ³ (order of magnitude))
Trajectory parameters	Average slope (degree) Reach (kilometers) Large retention areas (yes/no)
Potential impact of climate change	Existing effect on the event (amplifying/indifferent/diminishing) Future influence (by 2100) (amplifying/indifferent/diminishing)

2.2 Spatial context

The location where a process chain occurs is basic information. Beside the precise location given by the geographic **coordinates**, and the local name of the **location**, the events are assigned to one of the GTN-G Glacier **Regions** (Global Terrestrial Network For Glaciers, 2017). The aim of the GTN-G is to make glacier data easily accessible to a broader audience (Gärtner-Roer et al., 2019). Here it is used for the geographic classification of the events. The elevation can be used within a regional classification.

2.3 Processes involved in process chains

Related to process chains three types of processes are distinguished here: (i) **triggering** processes initiating a process chain but are not part of the process chain, (ii) **initial** processes representing the first process in a process chain and (iii) **subsequent** processes in a process chain. Whereas geomorphic phenomena constitute the most common initial and subsequent processes, triggering processes can also include tectonic and hydro-meteorological phenomena. The nature of the processes involved determines under which conditions a process can occur and – accordingly – a process chain can develop. The boundary of the system under consideration is the earth's surface and atmosphere without the oceans. As such, we do not consider tsunamis caused by landslides into fiords.

For the definition and visualization of the process chains considered in this study we utilize the matrix proposed by Gill and Malamud (2014). As the focus of this review is on mountain regions, the selection of

processes is limited to seven gravitational and hydrological processes, that can be part of a process chain (Figure 2). In addition, four tectonic and hydro-meteorological processes are defined as external triggering processes that are not part of a process chain. However not all process chains are triggered by distinct processes, but are the result of long-term landscape weakening processes that lead to threshold failure.

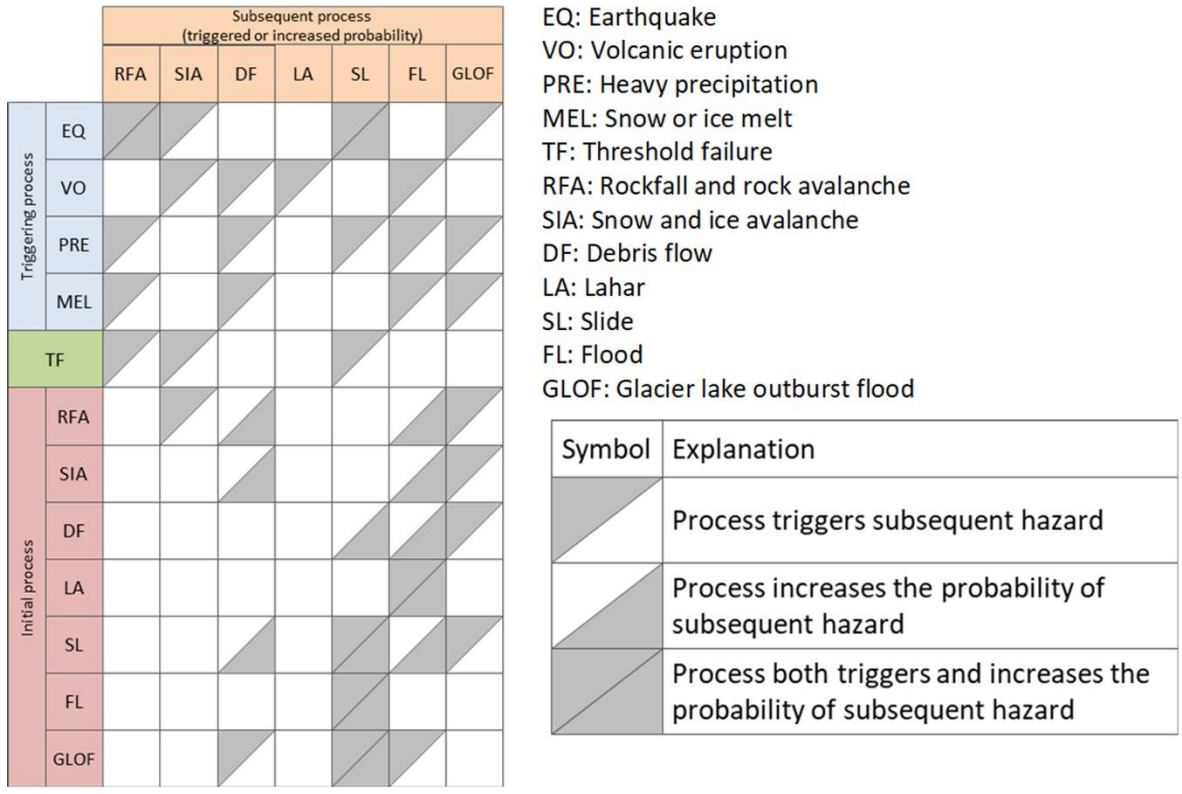


Figure 2. Identification of the hazard processes considered in the classification and type of interaction between triggering, initial and subsequent hazard (according to Gill and Malamud (2014)). The matrix shows which of the primary processes can trigger a secondary process and/or increase the probability of a secondary process.

External processes triggering process chains

Tectonic processes

Earthquakes (EQ in Figure 2) are caused by a sudden slip of a fault that results in ground shaking and radiated seismic energy. Earthquakes can also be triggered by the movement of magma in volcanoes. Seismic disruption is an important factor in mountain landscape development (Fan et al., 2019). Often earthquake shaking triggers further hazard processes such as landslides (e.g., rockfalls and rock avalanches; (Tanyaş et al., 2017)) which may generate process chains. Furthermore, earthquakes can weaken the mountain landscape without immediately triggering a failure (Gischig et al., 2016) reducing the threshold for the initiation of slope-related geomorphic cascades

Volcanic eruptions (VO in Figure 2) are limited to ice-clad volcanoes in this paper. Volcano-ice interactions are manifold and can trigger different processes. Eruptions can generate substantial volumes of water by melting snow and ice (Pierson et al., 1990). In combination with the easy-to-mobilize pyroclastic deposits, lahars can occur. Pyroclastic flows can erode and incorporate snow and transform into debris flows (Granados et al., 2021).

Hydro-meteorological processes

Heavy rains (PRE in Figure 2) are a frequent trigger of slope and fluvial processes. Long-lasting intense but not necessarily extreme rainfall over several days to months can trigger shallow and deep-seated slides (e.g. Stanley et al., 2020). Moreover, the same process can trigger rock avalanches and rockslides by increasing hydrostatic pressure in joints of rock walls (McCull and Draebing, 2019). Large rainfall volume can also trigger GLOF's when water level rises and erodes the damming moraine (e.g. Allen et al., 2015). Torrential rainfall of very high intensity is often the trigger for debris flows on mountain slopes or in steep channels (e.g. Singh et al., 2018). Further, heavy rainfall following earthquakes frequently triggers debris flows and other types of landslides in seismically weakened landscapes (Kargel et al., 2016).

Intense snow and ice melting are other processes that can supply large volumes of water and thereby trigger landslide processes (including debris flows) comparable to long-lasting rainfall (Moreiras et al., 2012; Mostbauer et al., 2018; Vergara Dal Pont et al., 2020). Very large volumes of water can result from rain-on-snow (ROS) events (e.g. Beniston and Stoffel, 2016; Morán-Tejeda et al., 2016; Musselman et al., 2018; Pomeroy et al., 2016).

Landscape-weakening processes

Threshold failures (TF in Figure 2) do not involve a distinct trigger to generate a process chain. Instead, they result from landscape-weakening processes. Various processes cause a gradual change in landscape resistance until a critical threshold is reached. The weakening of surficial rock masses by freeze-thaw-cycles (manifested by crack widening), permafrost degradation, or seismic shock are examples of processes that cause landscape weakening, increasing the susceptibility to slope failure.

Processes forming process chains (initial and subsequent processes)

The hazardous geomorphic processes that are considered in this analysis of process chains can be split into two groups, (i) hillslope and (ii) channel processes.

Hillslope processes

Hillslope processes are classified based on Hungr et al. (2014). Considering the focus of this analysis some modifications are made. Movement types (e.g., slope spread, sagging or liquefaction) with little relevance in process chains in mountain regions are omitted. Further, snow and ice are added as material types. The following processes are abstracted (with modification) from the Hungr et al. (2014) classification (Figure 3):

Rockfall: Abrupt, downward movement of rock fragments, that detach from steep rock slopes or cliffs. The falling material usually strikes the lower slope at angles less than the angle of fall, causing bouncing and rolling. The falling fragments may break on impact. Bouncing and rolling may continue until the terrain flattens. The velocity of detached masses in free fall is very rapid to extremely rapid.

Icefall: Ice falls from glacier fronts consisting of ice blocks are a natural ablation process of alpine glaciers. The dynamics of ice falls are identical to those of rockfall, except for the relative weakness of ice blocks which disintegrate on impact (Hungr et al., 2014).

Rockslide: Parts of detached bedrock that initially slide along a concave (rotational) or planar (translational) surface. In rock, translational slides are more frequent than rotational slides because of presence of planar discontinuities in the failing rock mass (Evans et al., 2006). Rockslides in mountain regions may be very large and catastrophic in nature. Steep high relief generates high velocities, comparable to rockfalls and rock avalanches (Selby, 1993). In the mountain cryosphere rockslides may contain considerable volumes of ice either from the starting zone or entrained from glaciers during the movement downslope (Evans et al., 2021).

Soilslide: As with the rockslides concave and planar sliding surfaces are distinguished. In homogeneous, clay or silt-rich soils sliding processes can occur along a concave surface (rotational slide). In inhomogeneous granular material (gravel, sand, debris) more or less planar sliding surfaces develop (translational slide). With increased velocity, the slide mass of translational failures may disintegrate and develop into a debris flow (Selby, 1993) thus forming a process chain.

Glacial surge: Surging is a quasiperiodic oscillation of glaciers between long periods (tens to hundreds of years) of slow flow and shorter periods of typically 10–1000 times faster flow (Murray et al., 2003). During a

surge, the flow velocity increases abruptly (up to 100 times faster than normal), and fast flow is maintained over some time (1–15 years) and over a wide area. (Jiskoot, 2011). Surging glaciers can block rivers in tributary or main valleys (e.g. Häusler et al., 2016).

Rock avalanche: A process mostly developing from large rockslides or rock falls. During downslope motion, the material disintegrates rapidly and travels as an extremely rapid flow of fragmented rock. The mobility (or runout distance) of rock avalanches increases systematically with volume of the event (Hungar et al., 2014; Schneider et al., 2011). Rock avalanches that occur in high mountain cryosphere often contain a substantial ice component (Evans et al., 2021).

Debris flow: A flow-like mass movement, consisting of an unsorted mixture of water, coarse debris and more or less fine sediments. The grain size distribution is a major factor in determining debris flow rheology. (Hungar, 2013). Hutchinson (1990) distinguishes between channelized and hillslope varieties (here the hillslope type). Debris flows can develop high erosive force and move large volume of sediments over distances in excess of 10 km.

Ice avalanche: Ice that detaches from glacier tongues on steep slopes or from hanging glaciers shatter to small pieces and develops to an avalanche comparable to a snow avalanche. (Margret and Funk, 1999). Detachments occur typically (i) from the steep frontal section of a glacier (so called cliff situations), or (ii) from a sloping glacier bed (so-called ramp or slab situation) (Alean, 1985). In rare cases, very large-volume detachments of entire low-angled glacier tongues have been observed (Leinss et al., 2021), with the detachments appearing to be linked to the presence of soft deformable glacier beds, polythermal ice, and possibly surging glaciers (Kääb et al., 2021)

Snow avalanches: A process that can be classified by three criteria: (i) the manner of starting (loose snow or slab avalanche), (ii) the form of movement (flow or powder avalanche) and (iii) the water content in the snow (dry or wet-snow avalanche) (McClung and Schaerer, 2006). Slab avalanches from dry snow can develop to powder avalanches and reach high front velocities of about 50 m/s and consequently, will tend to overrun terrain features in their path. Wet snow flow avalanches will move more slowly (5 – 10 m/s) and are more easily diverted or channeled by terrain features such as gullies. (Stethem, 2013)

Lahar: Eruptions on ice clad volcanoes produce complex interactions between hot lava and pyroclastic material, snow and/or ice, resulting in intensive melt producing high volumes of free water. Together with the pyroclastic deposits develop lahars (volcanic debris flows) (Major and Newhall, 1989). Lahars may also develop on volcanoes when pyroclastic material is mobilized by heavy rains. This process is comparable to debris flows or hyperconcentrated flows but is limited to volcanoes. (Sigurdsson et al., 2015). Lahars can develop fast travel velocities and have a very erosive effect.

Type of Movement		Type of Material			
		Rock	Soil *)	Ice	Snow
Falls (including topples)		Rockfall		Icefall	
Slides		Rockslide (rotational, planar)	Soilslide (rotational, planar)	Glacial surge	
Flows	Dry	Rock avalanche		Ice avalanche	Dry snow avalanche
	Wet	Debris flow			Wet snow avalanche
			Lahar		
*) Soil: including boulder, debris, gravel, sand, silt, mud, clay					

Figure 3. Classification of landslide processes based on Hungr et al. (2014) modified by a) adding the material types ice and snow and b) reducing the hillslope processes relevant for process chains in mountain areas.

Channel processes

Debris flow can occur on open hillslopes and in constrained channels. For a definition, please consult the “hillslope process” paragraph.

Debris flood can occur in steep channels if during extreme floods the stream bed is destabilized. The transport rate can reach values far exceeding normal bed load transport. In contrast to debris flows the movement of sediment still relies on the tractive forces of water (Hungr et al., 2014).

Floods result from an overflow of a river channel. In mountain environments, floods occur when the flow capacity of river and stream channels is exceeded due to heavy, intense, or continuous rainfall or when the absorptive capacity of the soils is exceeded (Hong et al., 2013). In many cases floods include sediment transport. Quantities of sediment transported can cover a wide range, from low concentrated bedload or suspended sediment transport to hyperconcentrated flow (Pierson et al., 1987).

Glacier lake outburst floods (GLOFs) are broadly defined herein as the sudden release of a lake that has formed either at the side, in front, within, beneath or on the surface of a glacier (see Emmer, 2016). Natural dams that impound a water reservoir may be composed primarily of glacial ice, morainic debris, or bedrock (Iturrizaga, 2011; Ruiz-Villanueva et al., 2017). Outburst floods may also occur from landslide dams and are known as landslide lake outburst floods (LLOFs; cf. Ruiz-Villanueva et al. (2017))

2.4 Process interactions

The timespan between the initial or antecedent and the subsequent process covers a large range. In some cases, as for example in the Pizzo Cengalo-Val Bondasca (Swiss Alps) event 2017, one process (the debris flow) in the process chain is **directly** triggered by the antecedent process (the rockslide). In other cases, the initial process creates conditions for secondary processes in the chain. The delay until the subsequent process occurs can be days, months, or years. In the Hattian Bala case (Kashmir), for example, a landslide dam that was emplaced by an earthquake in 2005 partly breached in 2010 (Dunning et al., 2007; Konagai and Sattar, 2012).

To distinguish direct and delayed interaction a threshold must be defined whereupon a sharp limit is not productive. In fact, a range of time is more appropriate. Therefore, in this study we define for direct triggering a timeframe from seconds to one day. A disposition change or delayed response is presumed if the subsequent process in a chain starts within days to a few years. In this study we do not consider processes in a chain occurring over more than ten years.

Direct and delayed interactions may not be mutually exclusive as evidenced by the two rock avalanche events leading to debris flows in the Bondasca valley in 2011 and 2017, where only the latter rock avalanche triggered debris flows directly (Evans et al., 2021; Mergili et al., 2020a; Walter et al., 2020). Another example is the Wenchuan earthquake where beside direct, co-seismic process chains, a large number of delayed interactions occurred involving landslides and landslide dams (Huang and Li, 2014; Zhang et al., 2016). Figure 2 therefore shows the different possible interactions between processes, but also the types of interactions that can occur over time.

The relation between single processes constituting a process chain is fundamental for natural hazards management as it will change the nature, magnitude, probability of occurrence and threat of a natural hazard process in areas at risk. In case of direct triggering of the subsequent process in a chain, very little time remains for administration and/or first responders to put (organizational) protective measures into place. On the other hand, where the initial process do not directly trigger a subsequent process, but its disposition is changed, this can be addressed with the implementation of protective measures or other response strategies.

2.5 Starting zone characteristics

The disposition of the processes involved in process chains depends on a multitude of environmental properties. The key properties listed in Table 2 are used for the characterisation of the starting zones, provided that this information is deducible from the literature.

While the **elevation** of the starting zone itself is not a determining factor for the formation of process chains, it does allow to derive the relevant altitude range for the origin of process chains occurring in a given region. The **relative relief** or local elevation range (LER) calculated between the highest and the lowest point within a predefined radius around the starting point is an indication of the gravitational forces and thus for the gain of energy in the starting zone. Where LER is large, high potential energy transforms to heat that, in the case of rock/ice avalanches, can melt the ice and cause high mobility of the mobilized material (Shugar et al., 2021). Furthermore, high gravitational forces cause a massive shattering of rock which generates loose debris that can be easily mobilized. LER values are calculated from the SRTM 30 m DTM with a vertical accuracy of 4.31 m (± 14.09 m) in mountain regions (Uuemaa et al., 2020). For each starting point of a process chain, the range between the highest and the lowest point within a radius of 0.5 km, 1.0 km and 5.0 km is derived.

The **lithology** of rock and sediments is, in combination with the types and orientations of discontinuities, a determining factor for slope stability. Dip slope failures, for instance, preferentially occur in sedimentary lithology due to the stratification of bedrock. In this study, the basis for lithological characterization is the global lithological map database GLiM (Hartmann and Moosdorf, 2012), provided in the Living Atlas of ESRI. Meanwhile, the effect of **seismicity** is twofold. On the one hand, it can trigger processes or even process chains as was the case in Langtang valley (Nepal) in April 2015 (Kargel et al., 2016; Lacroix, 2016; Roback et al., 2018) or in the Andes, where the 1970 Huascarán event was triggered by an earthquake (Evans et al., 2009). On the other hand seismicity can gradually destabilize rock bodies and thus increase the disposition for failure over time (Gischig et al., 2016; Kargel et al., 2016). Seismic characterization was based on the GSHAP global seismic hazard map available in the Global Seismic Hazard Assessment Program (Shedlock et al., 2000). The map shows peak ground acceleration with a probability of 10% to be exceeded in 50 years. Values are classified with regard to the perceived shaking; for this the Modified Mercalli scale is applied (Petersen et al., 2018).

In regard to the cryosphere, degradation of **permafrost** reduces the stability of rock walls, colluvial deposits, and sediments. Ice-filled joints are common in fractured bedrock under permafrost. In this way ice acts as cement and contributes to rock mass strength. If ice warms, this results in a higher disposition for rock falls

and rock avalanches (Draebing et al., 2014; Gruber and Haeberli, 2007; Hasler et al., 2012). Beside the disposition, permafrost degradation also contributes to the magnitude of mobilized material in rock walls (Krautblatter et al., 2013; Tapia Baldis and Trombotto Liaudat, 2019). In colluvial and glacial deposits, permafrost degradation results in an increased thickness of the active layer. This in turn augments the availability of loose material for debris flows (Damm and Felderer, 2013; Stoffel et al., 2014a; Tobler et al., 2015). Data on permafrost occurrence relies on the Permafrost Zonation Index Map (Gruber, 2012) and index values between 0 and 1 are classified following Boeckli et al. (2012).

From a hydrological perspective, the **stream order**, according to Strahler (1957), describes the position of a stream channel within the hierarchy of a river network. Associated with the stream order are specific patterns of geomorphic and hydrological processes. Allen et al. (2015), for example, demonstrated that a higher order stream feeding into Charobari lake, above Kedarnath, was a critical factor leading to rapid overflowing and catastrophic breaching of the lake during a period of heavy snowmelt and rainfall.

2.6 Amplifying effects

The reach (length) of process chains can be increased owing to the presence of favorable cryosphere and geomorphological conditions. Both **snow** and **ice** reduce the basal friction of rock avalanches and thus enlarges their reach. Entrained snow and ice can also reduce the friction within the moving mass (Sosio, 2015). This may also be the case for debris flows, where ice and snow entrained in the debris flow melts due to the heat that develops (Iverson, 1997). Thus, the shear stress exceeds the threshold given by the resistance to erosion. A larger volume can lead to an increased reach and to a higher impact (Evans et al., 2021; Huggel et al., 2005; McSaveney, 2002; Schneider et al., 2011; Sosio, 2015).

Likewise, the availability of **fine-grained loose material** in a travel path leads to process chains that exhibit a greater travel distance and higher velocity. This is due to (i) higher erodibility and as a result to (ii) higher volume and beside that to (iii) lower internal friction during movement (Pierson, 2005). Sources of this material are glacial, lacustrine and fluvial deposits, disaggregated rock, generated by seismic or volcanic impact as well as shattered rock in cases of grate fall height of rock falls or rock avalanches.

If slope processes such as slides, rock avalanches or debris flows are connected to river channels, **fluvial processes** can displace big volume of sediments over large distance. The distance depends on the gradient of the receiving river channel (Rickenmann et al., 2016). This leads to an enhanced reach of process chains if they include fluvial transport. High fluvial discharge can destabilize the riverbed and so mobilize large volumes of sediment thus increasing the length of the process chain (Cook et al., 2018). The presence of **lakes** can boost but also dampen the reach of process chains. Lakes dammed by moraines or landslides can release high volumes of water if the dams break, (i) caused by volume reduction by massive but gradual material input into the lake or (ii) by displacement waves, triggered instantaneously by slides or rock avalanches (Byers et al., 2019; Emmer et al., 2020; Konagai and Sattar, 2012). In bedrock dammed lakes, flood waves triggered by landslides can still trigger a GLOF, but full drainage of the lake is less likely. On the other hand, if the surface of a lake is large compared to the sediment input from debris flows or fluvial transport, and if dam freeboards are sufficient, this will dampen or even arrest a process chain.

2.7 Volume

The volume involved is an important parameter to assess the potential impact of a process chain. For the classification the **initial volume** and the **total volume mobilized** of a process chain are collected. Both the initial volume and the total volume can cover a large range from less than one million (e.g. ice or rockfall) to several tens of million cubic meters (e.g., massive ice or rock avalanche).

The ratio of the total relocated volume to the start volume or entrainment ratio within a process chain can also be very different between process chains and is indicative of the amplification processes occurring (Hungr and Evans, 2004). In some cases, both volumes are more or less equal, for instance when only a small part of the initial volume is involved in subsequent processes and no further material uptake occurs. This was the case in the Hattian Bala rock avalanche event (Konagai and Sattar, 2012). Conversely, in the 1970 Huascarán event the total volume involved in the process chain was 6.6 times higher ($58 \times 10^6 \text{ m}^3$) than the volume

of the triggering rock-/ice fall (Evans et al., 2009). For some cases of GLOF-debris flow process chains the entrainment ratio of the total volume mobilized to the initial volume was significantly higher. For example, the debris flow that occurred in Kichi Almaty catchment in the Northern Tian Shan on 15 July 1973 was initiated by a GLOF with a total volume of just $225 \times 10^3 \text{ m}^3$, yet the total volume of the debris flow was $3800 \times 10^3 \text{ m}^3$ (Petrakov et al., 2020; Yafyazova, 2007).

2.8 Trajectory characteristics

Relief characteristics are a further class of parameters for the classification of process chains. Relief controls the potential energy that is inherent in hazard processes. Hereinafter the relief parameters used in the classification are described.

In this study the **reach** (travel distance) is defined as the horizontal distance of a process chain along the trajectory. Depending on the processes involved in a process chain and the relief characteristic, the reach may have a large range (from a few to hundreds of km) and is therefore an important parameter to estimate potential impacts.

The affected area can further be defined by the **Fahrböschung** or **average slope**. This parameter means the average slope between the highest point of the starting area and the distal limit of the effects of a process chain. The horizontal distance is measured along the cascade trajectory. This parameter is widely used for the characterization of rock and/or ice avalanches (Alean, 1985; Deline et al., 2011; Geertsema et al., 2006; Schneider et al., 2011), but can also be used to characterize a process chain as a whole (Guthrie et al., 2012).

Finally, extensive low gradient areas along the path of a process chain can function as **retention areas**, where material is deposited temporarily or indefinitely (Rickenmann et al., 2016). Due to the low gradient, remobilization of the deposited material is limited; substantial loss of material in low gradient areas can lead to a reduced length of a process chain.

2.9 Climate change impacts

The impact of climate change on the current and future development of natural hazards and related process chains is essential for natural hazard assessment. The impact of climate change on process chains can be manifold. It can affect both the individual processes and the interaction between the processes. The effect can enhance or diminish the occurrence and scale of process chains. For example, atmospheric warming can increase the potential for ice avalanches due to the basal warming of hanging glaciers (Faillettaz et al., 2011; Huggel, 2009). However, if hanging glaciers have melted away this potential no longer exists (Evans et al., 2021). On the other hand new starting zones for rock avalanches are exposed (Allen et al., 2011; Fischer et al., 2006). Overall, as glaciers retreat and permafrost thaws, an increasing potential for process-chains involving rock or ice avalanches into expanding and more numerous glacial lakes is anticipated (Haeberli et al., 2017; Zheng et al., 2021a). Furthermore, changes in precipitation patterns can alter the disposition and triggering of slope processes (Stoffel et al., 2011). Paranunzio et al. (2016) and Allen and Huggel (2013) have shown that rockfall events can in many cases be associated with temperature anomalies, although deeper and larger volume failures are complicated by delayed responses to changes in atmospheric conditions (Evans et al., 2021). Two aspects are addressed in this study: (i) The **existing effect of climate change** on the event (i.e. due to effects of warming over the past century), and (ii) the possible **future influence of climate change** over the next up to the end of the century. As event descriptions in the literature typically provide only limited information regarding future evolution, we estimated the further development (glacier, glacier lakes) based on Google maps. Main criteria are the existence and shape of glaciers and the existence of glacier lakes. Climate projections for the end of this century are derived from the IPCC WG I Interactive Atlas (Iturbide et al., 2021).

3. Description of process chains

To characterize process chain events, we conducted a comprehensive literature review. This resulted in 51 events that occurred in high mountain regions and for which the majority of the parameters for characterization could be derived. Of these, 12 globally distributed events that are illustrative of the

characteristics of different types of process chains are selected and described in greater detail in the following paragraphs.

The events in the database cover all continents of the world except Africa and Antarctica (Table 2) and the latitude from 43.4° south to 54.4° North. In the database most events originate from the Alps, the Himalaya, the Andes and the Coast Ranges. This not only represents the occurrence of process chains in the regions but the availability of literature on these events that provides sufficient information to complete the database

Table 2: Spatial distribution of process chain events in the database

Continent	Glacier region	Events	with detailed description
Asia	Himalaya	10	3
	Hissar Alay	1	1
	Karakoram	1	0
	S and E Tibet	2	0
	Tien Shan	4	0
Europe	Alps	10	3
	Caucasus	3	1
North America	Coast Ranges	9	1
South America	Andes	9	3
Oceania	New Zealand	2	0
Total		50	12

3.1 Earthquake as triggering process

3.1.1 Huascaran 1970

The Cordillera Blanca in Peru is the most heavily glacierized tropical mountain range worldwide. It stands above the densely populated valley of the Callejón de Huaylas, the vertical drop exceeding 4000 m over a horizontal distance of approx. 20 km in some places. The risk of glacial disasters is therefore high, with most documented events attributed to GLOFs (Carey et al., 2012; Mergili et al., 2018b; Schneider et al., 2014). Two of the most notable disasters in recent history, however, evolved from rock-ice falls at the west face of Huascarán Norte (6654 m asl.) in 1962 and 1970. Both events have been extensively described and analyzed (e.g. Evans et al., 2009; Ghigliino Antunez, 1971; Mergili et al., 2018b). There was no obvious trigger for the 1962 event, whereas the 1970 event was directly caused by an earthquake that was also highly destructive by itself, creating a multi-hazard disaster situation (Evans et al., 2009).

Both initial falls dropped over a vertical distance of approximately 2 km before impacting a steep glacier. Glacier ice, firn and snow, and huge amounts of paraglacial debris were entrained, resulting in high-energy debris-ice avalanches (Figure 4). In 1962, an initial volume of $3 \times 10^6 \text{ m}^3$ (one third rock, two thirds ice) bulked up to $17 \times 10^6 \text{ m}^3$ of solid and fluid material. In 1970, an initial volume of $7.5 \times 10^6 \text{ m}^3$ (80% rock, 20% ice) increased to approx. $66 \times 10^6 \text{ m}^3$. All these values are rough estimates derived by Evans et al. (2009).

The 1962 event passed through the Shacsha Valley and spread over the debris cone of Ranrahirca, resulting in at least several hundreds of fatalities (Evans et al., 2009) (Figure 4a). The 1970 event, more energetic due to its larger volume, developed extremely dynamic behavior, including ballistic travel of particles over distances of kilometers and an estimated maximum velocity in exceedance of 100 m/s. The average velocity was in the range 50–85 m/s. Back-calculating this event with numerical simulation software required the decrease of friction parameters to almost zero in order to achieve empirically adequate results (Mergili et al., 2018b). As in 1962, most of the mass passed through the Shacsha Valley and spread over the debris fan of Ranrahirca. It converted into a distal mud flow/debris flood propagating all the way down to the Pacific Ocean at a distance of 180 km. The most notable feature of the 1970 event, however, was the fact that part

of the mass (an estimated volume of $3.6 \times 10^6 \text{ m}^3$) left the Shacsha Valley by overtopping a more than 100 m high ridge, the Cerro de Aira. The town of Yungay at the other side of this ridge was completely destroyed and buried in debris and ice. The number of fatalities was initially given with $>20,000$, a number which turned out to be unrealistically high in the re-analysis of Evans et al. (2009). The real number of fatalities might have been around 6,000 in this event. Few inhabitants of Yungay escaped the event, some of them by climbing on Cemetery Hill (Figure 4b).

The 1962 and 1970 events at Nevado Huascarán demonstrated the importance of threshold effects in high-mountain process chains: overtopping of Cerro de Aira in the 1970 event led to an increase in the number of fatalities by approximately one order of magnitude, compared to 1962. This phenomenon highlights the challenges of simulation-based hazard mapping, as relatively minor misestimates of initial conditions or uncertain flow parameters might lead to completely wrong predictions (Mergili et al., 2018b).

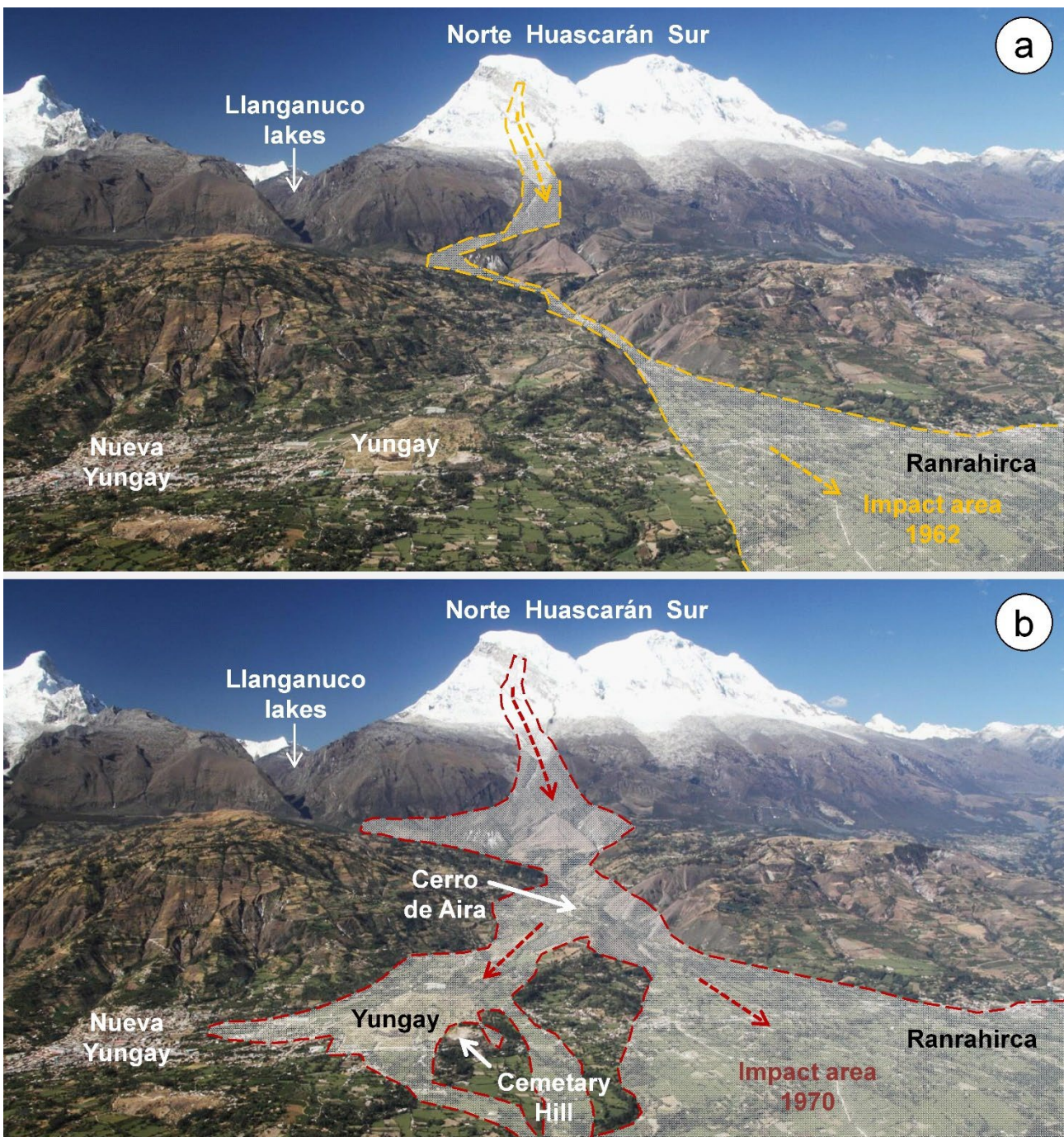


Figure 4. Impact areas of the 1962 and 1970 Huascarán events draped over a photograph taken from the opposite slope. (a) 1962 event; (b) 1970 event. Photo: M. Mergili, 20 July 2017. In both cases, the initial

rock/ice falls impacted the glacier at the base of the W face of Huascarán Norte. Entrainment of ice and, below, till, resulted in the evolution of avalanching flows of debris, mud, and ice. In the 1970 event, overtopping of Cerro de Aira resulted in the almost complete destruction of the town of Yungay. The town was rebuilt 1.5 km in NNW direction (Nueva Yungay, left side of Figure 4), but had grown towards the edge of the destroyed site by the 2010s.

3.1.2 Langtang 2015

On April 25, 2015, the Mw 7.8 Gorkha earthquake struck Nepal, causing thousands of landslides over a broad swath of the Lesser and Greater Himalaya in Nepal and Tibet (Collins and Jibson, 2015; Kargel et al., 2016; Roback et al., 2018; Shrestha et al., 2016). The most devastating mass movements hit Langtang Valley, north of Kathmandu. The valley had several small villages whose economic mainstay was logistical support of trekkers and mountaineers. About 350 people were killed or left missing in Langtang Valley. The worst event impacted directly on the village of Langtang (Kargel et al., 2016). Other mass movements also affected the valley (Kargel et al., 2016; Lacroix, 2016; Roback et al., 2018).

A careful study of the Langtang Valley landslides by Lacroix (2016) used the best available satellite imaging and derived topography. Those results show 160 landslides and avalanches in the Langtang Valley in the year between before/after SPOT stereo image sets. Nearly all of the mass movements are thought to have been co-seismic. Most were small and inconsequential, and most originated at low elevations just above the valley floor. However, the five largest mass movements clustered along the Langtang ridgeline (above 6800 m elevation) up to Langtang Lirung Peak (7200 m elevation); they coalesced and together destroyed Langtang village (Lacroix, 2016). Four of the five large events were likely co-seismic with the main shock. Digital Globe (now Maxar) images indicate that the final of these largest mass movements happened several weeks after the main shock (Kargel et al., 2016).

The largest events each started as snow and ice avalanches, with most of the initial mass comprised of snow derived from anomalously thick snowpack at the time of the earthquake (Fujita et al., 2017). The avalanches picked up rock mass and then went airborne over a cliff, freefalling more than a kilometer before crashing on the valley floor, producing powerful snow-ice-and-debris-laden air blasts (Figure 5). The wind leveled and scoured almost every structure in Langtang that was not buried under the avalanche. Thus, part of the village was buried; part was blown away. Burial depths, according to Lacroix (2016) reached 60 m, but most areas had a thinner snow-ice-rock avalanche cover of just a few meters, and many areas were scoured but not covered at all, as field photos show (Kargel et al., 2016). Blown-away buildings were generally constructed of stone slab. The landslide wind also flattened a small forest and stripped branches and leaves on the opposing valley wall, suggesting wind speeds comparable to an Enhanced Fujita Scale EF5 tornado ($>322 \text{ km hour}^{-1}$), according to Kargel et al. (2016). Three nearby settlements, Singdum, Mundu, and Kyangjin, were also damaged by avalanche air blasts.

“Before” and “after” photos of Langtang village and the valley taken by mountaineer and cinematographer David Breashears in 2012 and 2015, reported in Kargel et al. (2016), illustrate the destruction of Langtang. Just one hotel, though damaged, escaped complete destruction due to its unique location under a protective bedrock overhang.

Breashears’s photos showed that the deposit initially contained snow and ice in addition to rock debris. Landsat 8 thermal imaging on 30 April 2015 showed depressed temperatures of the debris surface apparently caused by melting ice. The ice-rock avalanche reached the Langtang River, but the stream soon incised it, so impoundment was minor.

Devastation in the air-blast zones indicates the huge energy involved. Kargel et al. (2016) made a guess at the Langtang landslide mass using an assumed thickness and estimated the energy release from the final freefall phase of descent as $\geq 3.2 \times 10^{13} \text{ J}$ (7.6-kiloton TNT equivalent), which begins to explain the devastation. However, Lacroix (2016) produced a measured thickness distribution and made a better volume estimation—about four times greater. Hence, the energy involved in the final freefall phase was roughly twice that of the Hiroshima atomic bomb explosion.

The conditions needed for a repetition of the Langtang disaster still prevail. The extreme snow depths prior to the disaster have been estimated to exceed a 100-year return period (Fujita et al., 2017) although such events may become more frequent at high elevation under a wetter future climate. Nonetheless the simultaneity and large sizes of multiple avalanches probably (but not definitively) require a seismic trigger, while weakened peri- and para-glacial slopes provide an abundant source of rock and debris that can be entrained into a mass of snow and ice.

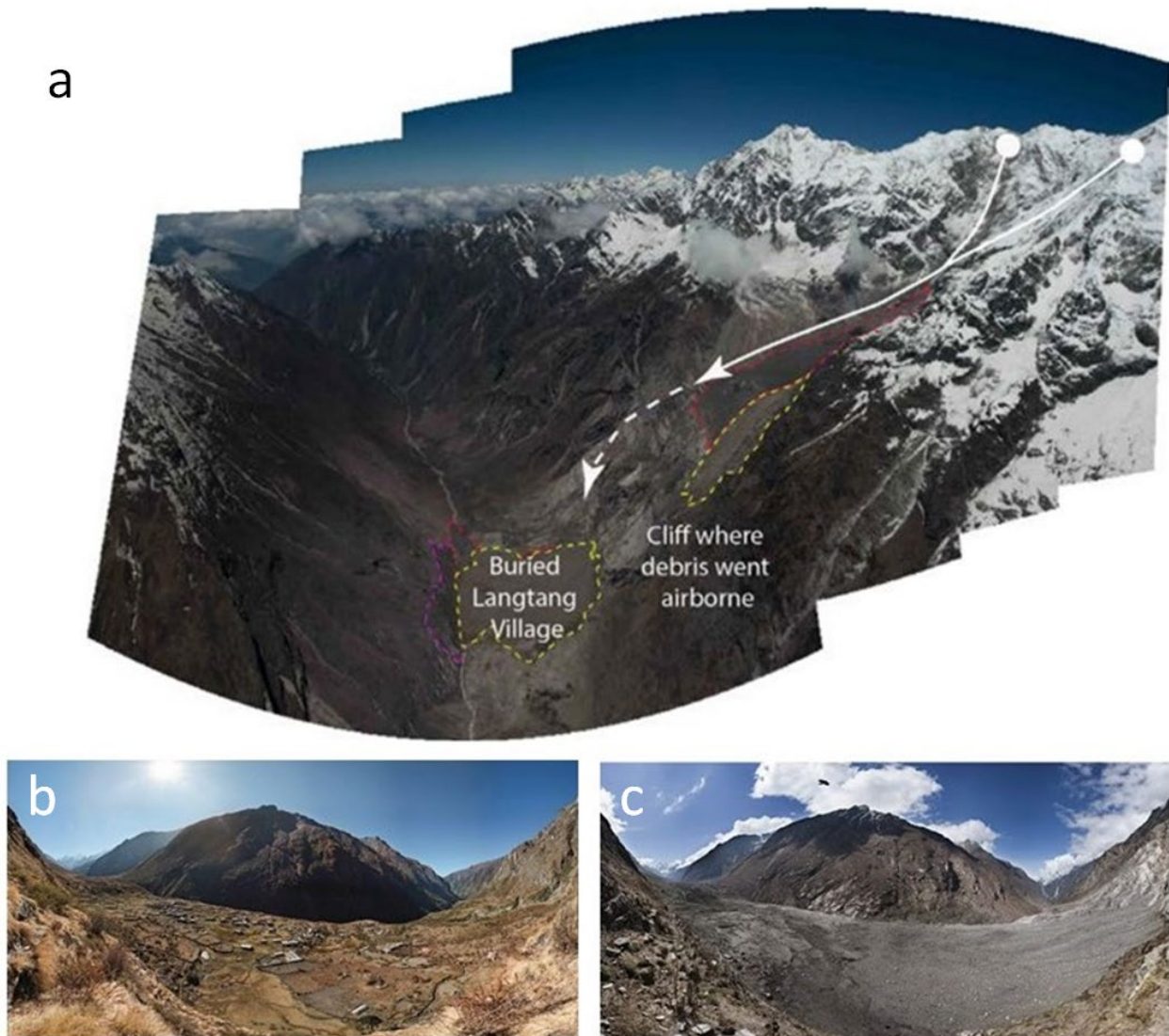


Figure 5. (a) The source areas and flow paths of the two Langtang mass movement process chains (white arrow, dashed where airborne). The red dashed line indicates the extent of the first slide, the yellow dashed line indicates extent of second slide, and the purple dashed line indicates extent of debris run-up. Dramatic “before” (b) and “after” (c) images of Langtang Village obtained in 2012 and 2015. All images are from David Breashears/GlacierWorks (used with permission). First appearance in (Kargel et al., 2016).

3.2 Volcanic eruption as triggering process

3.2.1 Nevado del Ruiz, Cordillera Central, Colombia 1985

Nevado del Ruiz is the northernmost glaciated volcano of the Andean chain. It reaches an elevation of 5320m asl and is a composite stratovolcano with a flat summit and a glacial ice cap. At 9:09 p.m on November 13, 1985, Nevado del Ruiz ejected volcanic particles more than 30 kilometres into the atmosphere (Pierson et

al., 1990; Voight, 1990). The total mass of the erupted material was 35×10^6 tonnes (that is only 3% of the amount that erupted from Mount St. Helens in 1980). The eruption reached 3 on the 8-stage Volcanic Explosivity Index, giving it a classification of 'moderate'. Despite the relatively modest size and short duration of the eruption, the devastating lahar of water, mud and debris travelling more than 100 km downstream led to one of the deadliest volcanic disasters in history (Huggel et al., 2007).

The key to this event was the interaction between volcanic activity and the snow and ice of the glaciated upper slopes of Nevado del Ruiz (Pierson et al., 1990). While the 1985 eruption lasted only 20 to 90 minutes, it contributed to a reduction in the glaciated area of the summit by 16% from around 25 to around 20.8 square kilometres (Thouret et al., 2007). In terms of volume, the overall loss of snow and ice was estimated to be $60 \times 10^6 \text{ m}^3$, which was about 10% of the pre-eruption total (Thouret et al., 2007). The most significant loss of snow and ice occurred where high-energy pyroclastic flows violently scoured or removed the snow and fractured ice that detached from steep-sided glaciers. In contrast, the loss was lower on glaciers with gentle slopes, where tephra was passively deposited, even though the temperature of the deposit exceeded 500°C initially. This has been seen also on other glaciated volcanoes, with melting resulting from violent pyroclastic flows estimated to be at least 10 times greater than melting under static depositions (Seynova et al., 2017). Other eruption-induced effects observed at Nevado del Ruiz included tunnel formation at the margins of the glacier. A striking pattern of parallel gullies emerging from these tunnels was the result of internal drainage within the glacier, which, once established, enhanced the transfer of heat and meltwater. During the eruption, these drainage tunnels collected pyroclastic material and increased in size, allowing hotter meltwater to be drained towards the margins of the glacier. It is thought that this influx of warm meltwater generated by the eruption enhanced melting at the sides of the glacier and probably led to the detachment of glacier ice from the surrounding bedrock, leading to further instability and ice avalanches that contributed additional mass to the downstream lahars.

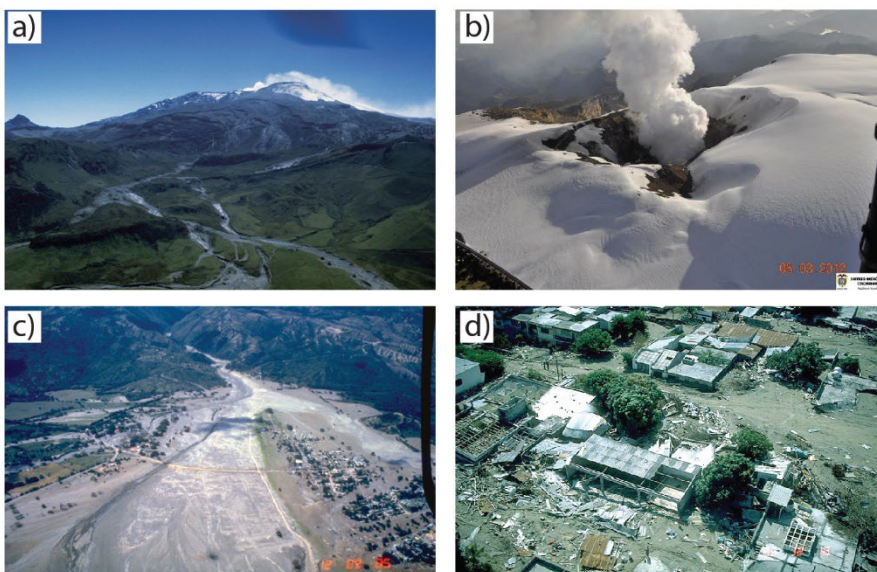


Figure 6. Images of Nevado del Ruiz showing (a) lahar paths descending from the upper slopes (date unknown), and (b) the summit crater and glaciers in June 2012. Images (c) and (d) taken in December 1985 show the devastation in the town of Armero. Source of photos are USGS (a, c, and d) (<https://www.usgs.gov/>), and Geological Service of Colombia (b).

Watery flows and avalanches originating from the glaciated summit area of the volcano rapidly transformed into devastating lahars following entrainment of both volcanic and glacial sediment within the downstream river valleys (Pierson et al., 1990). Some of this sediment would have contained water, and surface water from rain that fell throughout the evening of the eruptions would have further added to the volume of the lahars. Two to three main waves of mud and debris were reported, with depths of up to 30 metres (Voight, 1990). The total volume of lahars reaching downstream areas was around $90 \times 10^6 \text{ m}^3$. Peak velocities ranged from 5 – 15 metres per second, and a peak discharge of $48,000 \text{ m}^3/\text{s}$ was recorded at a distance of 9 km

downstream from the source. It took slightly over 1 hour for the lahars to travel 50 km downstream wiping out several villages, while the town of Armero was reached in a little over 2 hours. Most of the devastation was focused in Armero, where up to 75% of the residents were killed following the arrival of the lahars shortly before midnight. The most distant areas affected by the lahars, more than 100 km away from the source, were reached in about 4 hours (Huggel et al., 2007; Pierson et al., 1990).

3.3 Falls as initial processes

3.3.1 Cengalo-Bondasca, Switzerland, 2011 and 2017

At Pizzo Cengalo, a 3369 m high summit located at the upper end of the Bondasca Valley (Canton of Grisons, Switzerland), two massive rock slope failures occurred on its NE face. A first event was recorded in December 2011, a second event took place in August 2017 (Walter et al., 2020), with both developing into rock avalanches. Assessment after the first event showed that the start zone was largely covered by a thick permafrost ice layer (Wilhelm et al., 2019).

Despite the quite comparable initial conditions and comparable starting zone elevations, distinct differences exist between the process chains that developed as a result of these two rock slope failures. According to Baer et al. (2017), the 2011 rock slope failure mobilized $1.5 - 1.7 \times 10^6 \text{ m}^3$ of rock material at an altitude of 3100 m asl; the rock masses travelled down to 2200 m asl in the form of a rock avalanche and were deposited in the upper part of the Bondasca Valley. As the event occurred in winter, the rock avalanche entrained substantial amounts of snow with an estimated water equivalent of the entrained snow of $7 - 15 \times 10^4 \text{ m}^3$. In this case, snowmelt in spring increased the water saturation of the rock avalanche deposits, leading to the triggering of four debris flows in summer 2012 with the biggest event in August 2012 reaching the village of Bondo (Baer et al., 2017).

Ice slabs in the detachment zone provide clear evidence of the critical role of permafrost in the starting zone of the process chain. Also, debris flows were not triggered directly by the rock avalanche, but the rock avalanche increased the availability of material in the starting zone of debris flows and thus increased the disposition for them to occur. The disposition was amplified further by the snow that was entrained by the rock avalanche.

During the second event in August 2017, $c. 3 \times 10^6 \text{ m}^3$ of rock detached below the starting zone of the 2011 rock avalanche (Mergili et al., 2020a). On its way down the rock avalanche entrained $c. 0.6 \times 10^6 \text{ m}^3$ of glacier ice. The sudden addition of melted ice favored the immediate conversion of part of the rock avalanche into a debris flow (Figure 7) which reached the village of Bondo. Six additional surges were observed the same day and obviously developed out of the freshly deposited, saturated rock avalanche deposit. Two more debris flows developed in the days following the initial process chain, leaving a total of $5 - 8 \times 10^5 \text{ m}^3$ of material in the area of Bondo. In addition to the liquefaction of parts of the rock avalanche material by the melted ice, Walter et al. (2020) suggested that much water was also stored in the deposits of the 2011 rock avalanche that were overrun by the 2017 event and that the dynamic loading of sediments could have resulted in excessive pore pressure, therefore triggering the debris flows immediately after the rock avalanche (Mergili et al., 2020a; Walter et al., 2020).



Figure 7. Overview of the upper Bondasca valley. The rock avalanche started in the north-east face of Piz Cengalo. A large part of the material was deposited in the uppermost part of the valley, where a part of the material instantaneously transformed to a debris flow that run down to Bondo village at the valley mouth. (Photo: Andreas Badrutt/AWN)

By contrast to the December 2011 event, the August 2017 rock avalanche resulted in an immediate triggering of debris flows. Both events had starting zones in permafrost, even if only small ice patches were visible in the starting zone of the 2017 rock slope failure, with many wet patches in the back scarp. In both cases, a majority of the entrained rock avalanche material was retained in the upper part of the Bondasca Valley, whereas the narrow gorge in the lower part of the valley system promoted sediment transport by debris flows.

Climate change will likely enhance the occurrence of such process chains as a result of the anticipated degradation of permafrost. By contrast, the gradual disappearance of glaciers is not expected to alter the situation and/or process dynamics in this specific case. Even if opinions diverge between experts, it is possible that the entrained glacier ice neither led to an increased runout distance nor was it responsible for the immediate triggering of debris flows (Walter et al., 2020).

3.3.2 Kolka, Republic of North Ossetia–Alania, 2002

In the evening of 20 September 2002, a complex catastrophic mass movement occurred in the Genaldon Valley, Caucasus Mountains, Republic of North Ossetia–Alania, Russian Federation. The Kolka glacier snout with a volume of more than $100 \times 10^6 \text{ m}^3$ (Kääb et al., 2021), detached from the bed and travelled 19 km downstream. A narrow gorge stopped the ice mass but a debris flow with a volume of $3\text{--}5 \times 10^6 \text{ m}^3$ (Evans et al., 2009) travelled 17 km farther down to stop just 2 km above the settlement of Gizel with a population of c. 5000 people. A total of 135 people perished (Kortiev et al., 2009). The event has been described and analysed in many papers, although processes involved are debated (Drobyshev, 2006; Evans et al., 2009; Haeberli et al., 2004; Huggel et al., 2005; Kääb et al., 2021; Kotlyakov et al., 2004).

According to initial studies, a massive rock slope failure occurred on the slope of Mt. Dzhimarai-Khokh, falling onto the surface of Kolka glacier, leading to its instantaneous detachment (e.g., Haeberli et al., 2004; Huggel

et al., 2005). However, later assessments of satellite images and eyewitness reports evidenced that abnormal slope failures already started to occur from the northern flank of Mt. Dzhimarai-Khokh during summer 2002 and were probably triggered by a low-magnitude earthquake on July, 14, 2002 with an epicenter near Mt. Dzhimarai-Khokh (Drobyshev, 2006; Evans et al., 2009). The volume of rock and ice that were falling onto the glacier were estimated at about $15 \times 10^6 \text{ m}^3$. During this period of mass-movement activity, the glacier bulged and became heavily crevassed, developing a differential vertical displacement and partial dislocation of the Kolka Glacier ice mass indicating its response to ice and rock debris loading (Evans et al., 2009; Käab et al., 2021). It is possible that this overloading of the Kolka glacier might have disrupted internal drainage of the glacier, thereby leading to the development of excess water pressures at its base (Evans et al., 2009). High geothermal fluxes, the impact energy of rock and ice falls, as well as a positive precipitation anomaly might have further contributed to excess water underneath the glacier as well (Evans et al., 2009; Kotlyakov et al., 2004). The basal shear stress is hypothesized to have increased until it exceeded a frictional threshold given by the glacier bed material, topography, and hydraulic conditions (Käab et al., 2021).

The flow velocity of the mass reached 65-80 m/s during the first 19 km and reduced significantly thereafter (up to 10-20 m/s) when the mass was transformed into a debris flow. In addition to immediate partial transformation of the glacier detachment into a debris flow, the ice masses that were deposited in the Karmadon depression dammed a tributary river. A number of lakes formed with $3 \times 10^6 \text{ m}^3$ of water stored in the largest lake (Popovnin et al., 2003). Saniba village was partially flooded and the threat of an outburst flood was significant. Luckily, lake drainage was slow, also thanks to the relatively low temperatures at the end of October.

3.3.3 Seti River, Nepal, 2012

On May 5, 2012, a flash flood crashed out of an intermontane basin, the Sabche Cirque (Figure 8), nestled between the Annapurna peaks north of Pokhara (Nepal's second largest city). Conditions were partly cloudy and dry (Dwivedi and Neupane, 2013). Flowing from this high basin, the flood reached small villages and Pokhara's northern outskirts, where damages and casualties occurred on the lowest terraces and in the Seti riverbed (Figure 8). More than 70 people were killed (Nibanupudi et al., 2015); homes, bridges, and agricultural land were destroyed. Casualties included children recreating on a nearly dry riverbed, gravel workers, tourists, and villagers in their homes, shops, and farms on the lowest terrace. Location details determined life or death (Figure 9 (E)).

Satellite imagery, resident videos, and post-event air- and ground-based inspections constrain the process chain, while leaving some elements unclear. An air tour plane's pilot and video camera caught early glimpses of a turbulent "brown cloud" within the Sabche Cirque. Simultaneous seismic data (Dwivedi and Neupane, 2013) indicated that a large avalanche of ice and rock began while the brown cloud was billowing and collapsing, then continued for 70 minutes. Half an hour later, the mass movement at Kharapani (20 km from the source) had transformed to a flood-like debris flow, then further downstream, it became a hyperconcentrated slurry flood. Satellite and airborne images revealed that the debris field (Figure 8 (B)) traces toward the Annapurna ridgeline— seen also in an airborne photo by Dixit (2014). A missing ridgeline cornice disappeared, narrowly bracketed around the time of the disaster, suggesting that an ice avalanche initiated near 6900 m (Figure 9 (A)). The process chain left an ice-rock avalanche field $\sim 2500 \text{ m}$ lower (Figure 9 (B)); layered above that—emplaced by the same overall mass movement—a darker, maybe rockier landslide is visible in a Landsat 7 image (Figure 8 (B)).

Maxar images (Google Earth) reveal stripped alpine vegetation, and field photos show a downed forest of large trees blown over with root balls ripped out. Maxar also shows movement of some large boulders—up to 30 m across—during a 1-year interval between "before" and "after" images (Figure 8 (E), (F)); and formation of erosional rills (2-5 m wide) likely due to prompt mud runoff on landslide-slammed surfaces (Figure 8 (F)). The mass movement involved somewhere around $15 \times 10^6 \text{ m}^3$ of rock and ice (Petley, 2012).

Evolving flow vectors are difficult to trace. In Figure 8 (B) the flowlines are conceptual over different phases of the mass movement. To obtain the distribution of rock, ice, and mud, and the directions of downed trees and pattern of mud-plastering of boulders, much material must have collapsed from a debris cloud during the mass movement until it transitioned to a surface-based debris-flow and slurry flood.

Residents' and travelers' mobile-phone videos, some still widely available on the internet, give important constraints on the avalanche/debris flow processes and properties. Where the mass flow reached the Seti barrage (north side of Pokhara), the dimensions of built structures and flow tracing of trees and other floating debris seen in an eyewitness video allowed a flow discharge estimation of $2.5 \times 10^5 \text{ m}^3$ of water and suspended or floating debris and ice during the first couple of minutes after the flood reached that site (Kargel, 2014). The leading edge of the flood transported huge masses of large floating tree trunks and branches, which apparently were derived from the avalanche-blown forest (Figure 9 (C)). The violence of the event in the lower forested part of the Sabche Cirque is evident from the upturning of tree root balls, complete defoliation, and removal of most branches from 1-m-diameter tree trunks (Figure 9D). Below roughly 3500 m elevation, protruding objects such as boulders and vegetation, where not displaced, were plastered on one side by a calcium carbonate and phyllosilicate-rich mud. The mud plaster— typically 2 cm thick, plus and minus, may total $\sim 4 \times 10^5 \text{ m}^3$ over the plastered area of the Sabche Cirque. Hence, at that elevation, there already was abundant liquid water. The debris flow flood starting from Kharapani (elevation 1250 m asl) and lower was made of similar mud, but millions of cubic meters of it with more water, and some large pieces of ice, according to eyewitnesses.

The first news reports (The Hindu, 2012) labelled this event a GLOF. Satellite imagery made immediately clear that no significant glacial lake existed in the Seti basin. The lack of a big lake required a search for liquid water sources: possibly wet snow, supraglacial ponds, landslide-dammed lakes hidden in gorges, water in subglacial lakes or caverns, and water produced by conversion of gravitational potential energy to kinetic energy and then heat to melt ice. Preconditioning by filling of a landslide-impounded lake in a deep glacier-fed river gorge may have been important. Conceptually, all of these sources might have contributed to transform the event from an initial avalanche of ice and rock, into a far-reaching flood (Kargel et al., 2014).

The rich details available for Chamoli event (Shugar et al., 2021) provides potentially crucial insights into the Seti flood. In both cases, the initial collapsing mass involved mainly solid material (ice and rock), but by the time it reached lower elevations the mass transfer involved mainly liquid water and suspended debris. In retrospect, these events may have been quite similar. By contrast, the Langtang event had a much lower relative amount of liquid water in the deposited mass. The Seti and Chamoli events each may have started as ice-and-debris avalanches, then as kinetic energy was gained during collapse, the mass accelerated. With so much vertical fall distance, much of the ice mass melted, and debris flows and slurry floods developed by the time these events reached populated areas. The Langtang event similarly involved a high elevation drop, and much snow and ice mass must have melted. However, as was shown for the well-characterized Chamoli event, there exists a critical ratio of ice to mass (a different ratio for differing fall distances) whereby liquid water fraction reaches the maximum (where almost all the ice melts); if there is too much ice in the collapsing mass, much ice remains frozen, and the flow and depositional dynamics are different than when all of the ice melts.

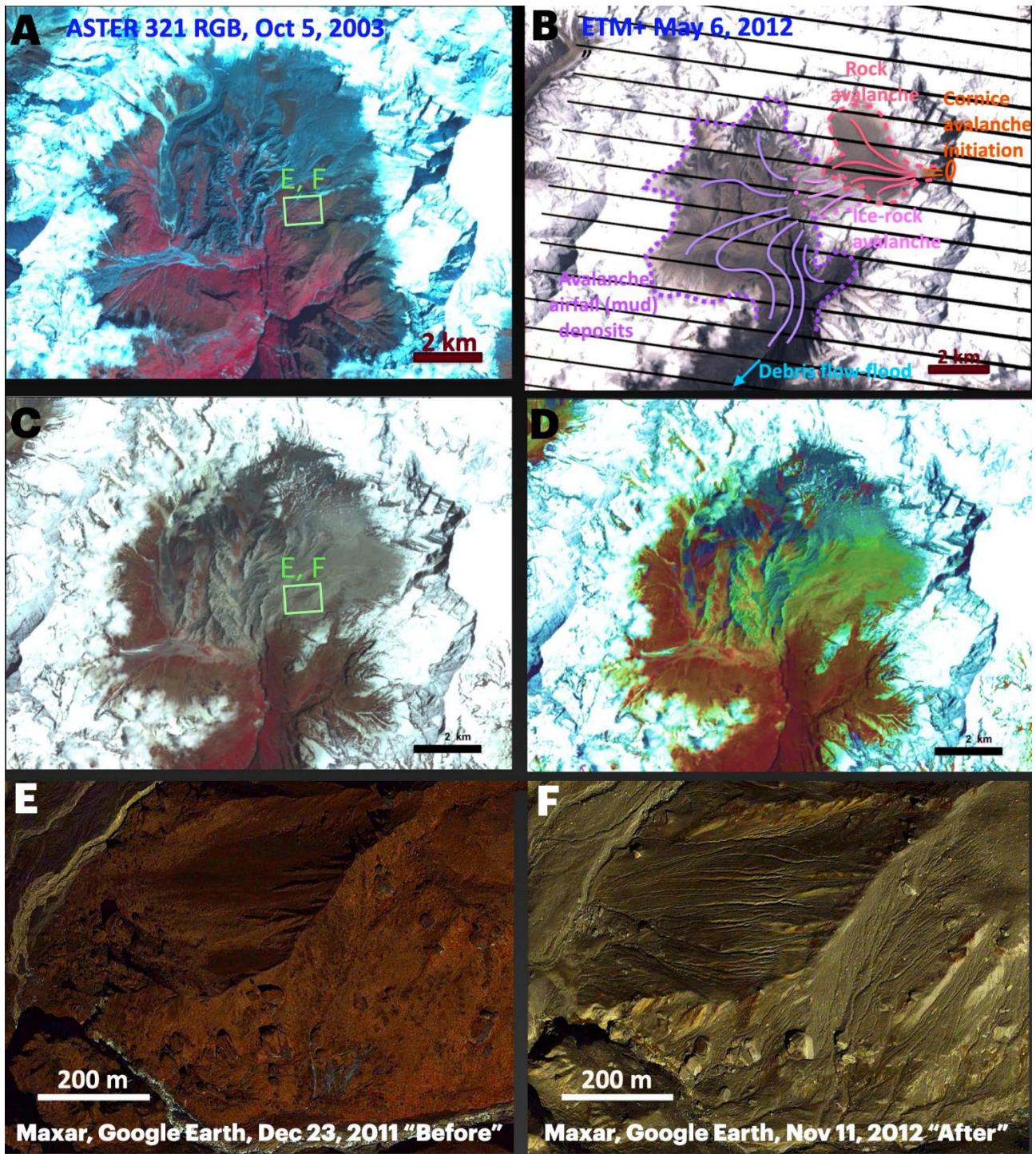


Figure 8. Sabche Cirque source of the 2012 mass movement. (A) ASTER 321-RGB, saturated false color, Oct 5, 2003, nine years before the disaster. (B) Landsat 7 ETM+ pan-321-RGB, 1 day after the disaster, showing debris- and rock-ice-mantled zones. Flow lines are conceptual. (C) ASTER 321 RGB, May 22, 2012, 17 days after the disaster, shows a widespread debris mantle across the lower Sabche Cirque. (D) Color saturation of image in (C) to accentuate areas most affected by the mass movement. (E), (F) Color-saturated Maxar images (footprint in panels (A), (C)) show “before” and “after” details.

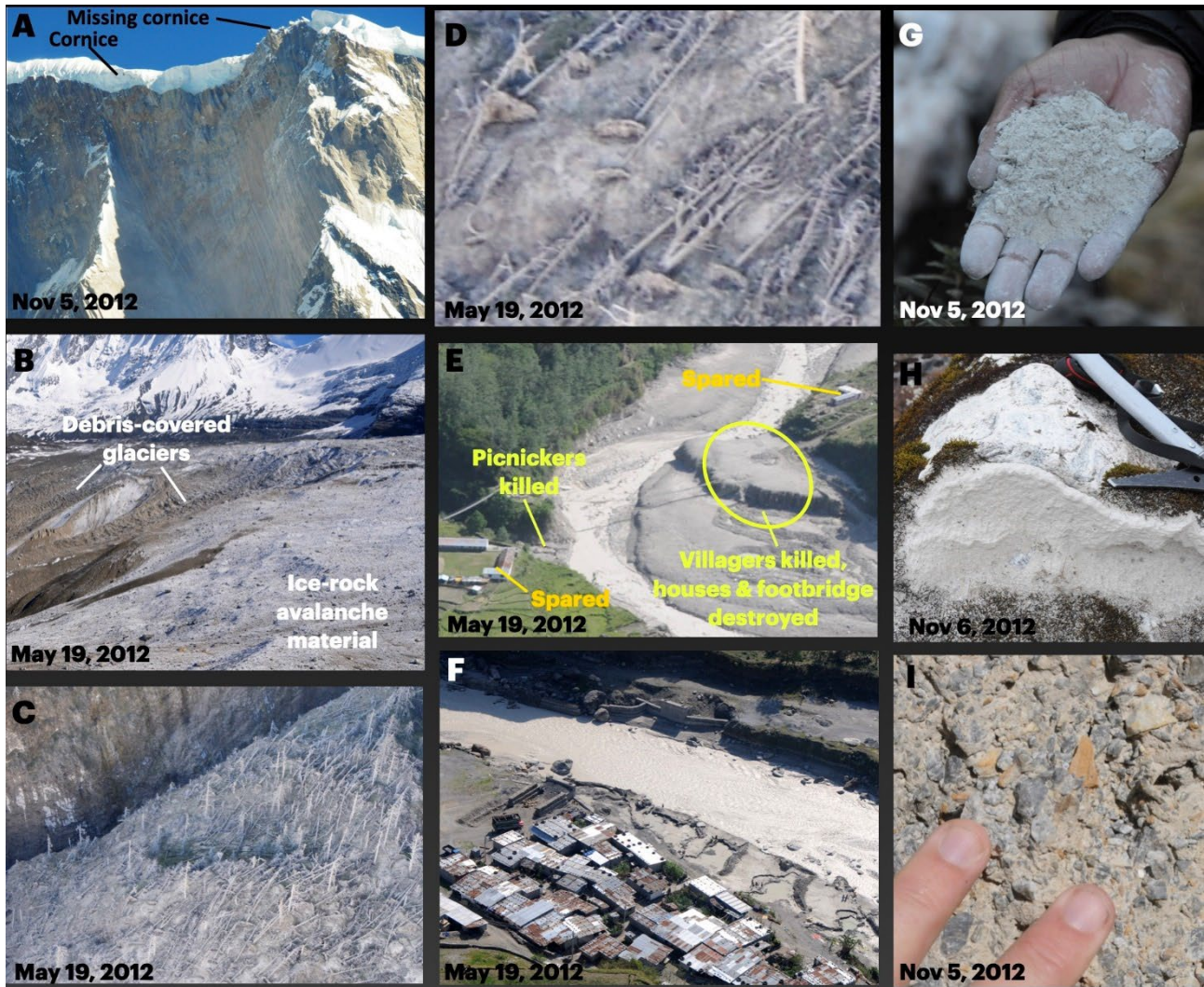


Figure 9. Ground and air views of the 2012 Seti mass movement site. (A) A 200-m-long missing cornice of snow and ice is a likely initiation point for an ice avalanche. (B) Ice-rock avalanche deposit two weeks after the event. (C) Defoliated, blown-down forest, coated with dried mud emplaced by the avalanche wind. (D) Blow-up of (C) shows upturned root balls of trees up to 20 m long/tall; trunks are 1 m wide. (E) Kharapani village, 27 km flow distance and 5700 m below the cornice source. Remnants of the village survived on terraces on both banks ~25 m above river level. Houses, shops, agricultural land, a bridge, and all humans and animals on a lower terrace were destroyed. (F) A densely populated neighborhood on Pokhara's northern outskirts, narrowly surviving, was bathed in mud. (G) Avalanche-wind-blown calcite and phyllosilicate mud, typically 2 cm thick (talc powder-like consistency when dry), formed crusts on about 20 km² of the Sabche Cirque. Mineralogically and texturally similar mud— decimeters to meters of it— was deposited directly by the debris flow as it approached Pokhara. (I) Vast amounts of poorly consolidated sediment from silt to boulder size carbonate and calc-silicate lithologies are contained within the Sabche Cirque. Photos by J. Kargel.

3.4 Slides as initial processes

3.4.1 Phuktal River, Zaskar Himalaya, India, 2014

On December 31, 2014, a large landslide ($2.4\text{--}2.6 \times 10^6 \text{ m}^3$) blocked the Phuktal river (also known as Tsarap river) in what was then the state of Jammu and Kashmir, Northern India, leading to the formation of a 17.2 km long lake (Martha et al., 2017). Subsequent breaching of the lake dam 127 days later on May 7, 2015, resulted in flash flooding, leading to extensive damage to the bridges, culverts, buildings and land downstream. While the evacuation of 3000 people in the 90 km reach downstream of the lake prevented loss of life, the event is representative of the type of cascading process chain associated with the formation and breaching of a landslide dammed lake (LLOF). The description below primarily draws on the remote sensing

based analyses undertaken by Martha et al. (2017), while some direct field observations have been reported by the Indian National Disaster Management Authority (NMDA).

The landslide into the Phuktal river originated as a translational movement from within the tectonically active Zaskar synclinorium, which comprises of nappes and several imbricate thrusts (Fuchs and Linner, 1995). The lithology of the area consists of a weak sedimentary sequence (carbonate, limestone, shale, and sandstone) resting on top of the Higher Himalayan Crystalline rocks. At least three older landslide dammed lakes are observed within 10 km of the 2014 site, highlighting the propensity for these processes to occur in the region (Martha et al., 2017).

The 2014 debris landslide initiated from an elevation of around 4100–4400 m asl, sliding a length of around 600–800 meters into the river valley below where the flow was obstructed by the adjacent valley wall. Distinct tension cracks were observed above the crown of the landslide, where maximum slope angles are up to 45°. Pre- and post-landslide terrain modelling revealed the landslide deposit extended over a width of 630 meters across the valley, had an area of around $9 \times 10^4 \text{ m}^2$, with a maximum height of the dam being 69 meters (Martha et al., 2017). The landslide dam was classified as being of type III (after Costa and Schuster, 1988), whereby the depositing material was located both upstream and downstream of the initial point of impact into the valley. Analyses of two distinct depositional lobes on the downstream side of the dam were interpreted as consisting of a fine-grained initial slide of talus and scree, overlaid by a secondary, near-simultaneous slide of larger blocky material originating from further up the slope. Given the lack of significant rainfall or any seismic activity, there seems no obvious trigger for this event. The long-term undercutting by the Phuktal river likely played a role in destabilizing the steep, and geologically unfavorably structured slopes.

Following the damming of the river, the width of the lake near the blockage increased to a maximum of 160 m by March 2015, with the lake volume estimated at up to $30 \times 10^6 \text{ m}^3$. Subsequent blasting and dredging efforts coordinated by NDMA led to the creation of a 2 x 2m channel through the dam, allowing surface water to flow. However, the channel proved insufficient and unstable, and with the increase in outflow resulting from snow and ice-melt in early May, the dam catastrophically breached (Martha et al., 2017).

3.4.2 Meager Creek

Long complex process chains are also initiated on rock slopes in glacierized dissected Quaternary volcanic centers, such as the Mount Meager Volcanic Complex (Garibaldi Volcanic Belt) in southwestern British Columbia (Friele et al., 2008; Jordan and Slaymaker, 1991). Here we describe three examples from within the Meager Creek watershed that occurred over an approximate elevation range of 2250 m (2625 to 375 m asl). On July 22, 1975 a complex series of landslide events took place at Devastation Glacier near Pemberton, British Columbia when approximately $13 \times 10^6 \text{ m}^3$ of altered Quaternary volcanic rock and glacier ice slid from the west flank of Pylon Peak within the Mount Meager volcanic complex (Figure 10; Petrakov et al., 2020). The rockslide formed a long complex process chain as it quickly transformed into a high-velocity debris flow, consisting of glacial ice and disaggregated pyroclastic rocks, which continued down Devastation Creek valley. The overall length of the flow path was 7 km and its vertical height was 1220 m, yielding a Fahrböschung of 10°. Stability analysis of the initial 1975 failure (Evans, unpublished data) suggests that the 1975 rockslide was the result of a complex history of glacial erosion, loading and unloading of the toe of the slide mass caused by the Little Ice Age advance and subsequent retreat of Devastation Glacier (Figure 10). In early August 2010 a mass flow occurred in Capricorn Creek, a tributary to the main Meager Creek (Guthrie et al., 2012). It involved initial failure of the western flank of Mount Meager in Pleistocene rhyodacitic volcanic rock which mobilised additional volcanic material below; rapid evacuation of the entire flank ensued and the initial rock slope failure was transformed into a massive high-velocity ice-rock debris flow (Figure 11 (A), (B); Guthrie et al., 2012; Roberti et al., 2018; Roberti et al., 2017). The disintegrating mass travelled down Capricorn Creek at an average velocity of 64 m/s, exhibiting marked super-elevation in bends, to the intersection of Meager Creek, 7.8 km from the source. At Meager Creek the debris impacted the south side of Meager valley causing a runup of 270 m above the valley floor (Iverson et al., 2016) and the deflection of the landslide debris both upstream (for 3.7 km), and downstream into the Lillooet River valley (for 4.9 km) where it blocked the Lillooet River (Figure 11 (B)) for some hours, ca. 13 km from the landslide source (Figure 11 (B)). Deposition at the Capricorn-Meager confluence also dammed Meager Creek for about 19 hours creating a lake 1.5 km long.

The volume of the initial displaced mass from the flank of Mount Meager was estimated to be $53 \times 10^6 \text{ m}^3$ (Roberti et al., 2018), the height of the path (H) to be 2183 m and the total length of the path (L) to be 12.7 km. This yields $H/L = 0.17$ and a Fahrböschung of 9.8° (Guthrie et al., 2012). Initial failure involved a slope that had been debutressed by 20th century glacial retreat (Holm et al., 2004; Roberti et al., 2018).



Figure 10. Vertical aerial photograph of source area of July 22, 1975 Devastation Glacier mass flow, Mount Meager Volcanic Complex (Evans et al., 2021). The 1975 mass flow originated in altered Quaternary pyroclastic rocks which had undergone significant pre-failure subglacial deformation as a result of downwasting of Devastation Glacier at the foot of the slope (note crevasse patterns around the head of the landslide scar). The mass involved in the initial failure (volume $\sim 13 \times 10^6 \text{ m}^3$ including rock and ice) disintegrated during movement forming a high velocity debris flow that travelled 7 km down valley (to the right of photograph). [National Air Photo Library A37245-113]. An earlier debris flow (est. total volume $1.2 \times 10^6 \text{ m}^3$) had taken place in Capricorn Creek in July 1998 (Bovis and Jakob, 2000) and involved slopes that would form the source of the 2010 mass flow described above. In this event, initial failure took place in a periglacial slope consisting of volcanic colluvium which had recently been debutressed by glacial retreat. The debris flow blocked Meager Creek and formed an 800 m long landslide-dammed lake; the lake began to drain naturally after a spillway formed subsequent to overtopping several days after damming.

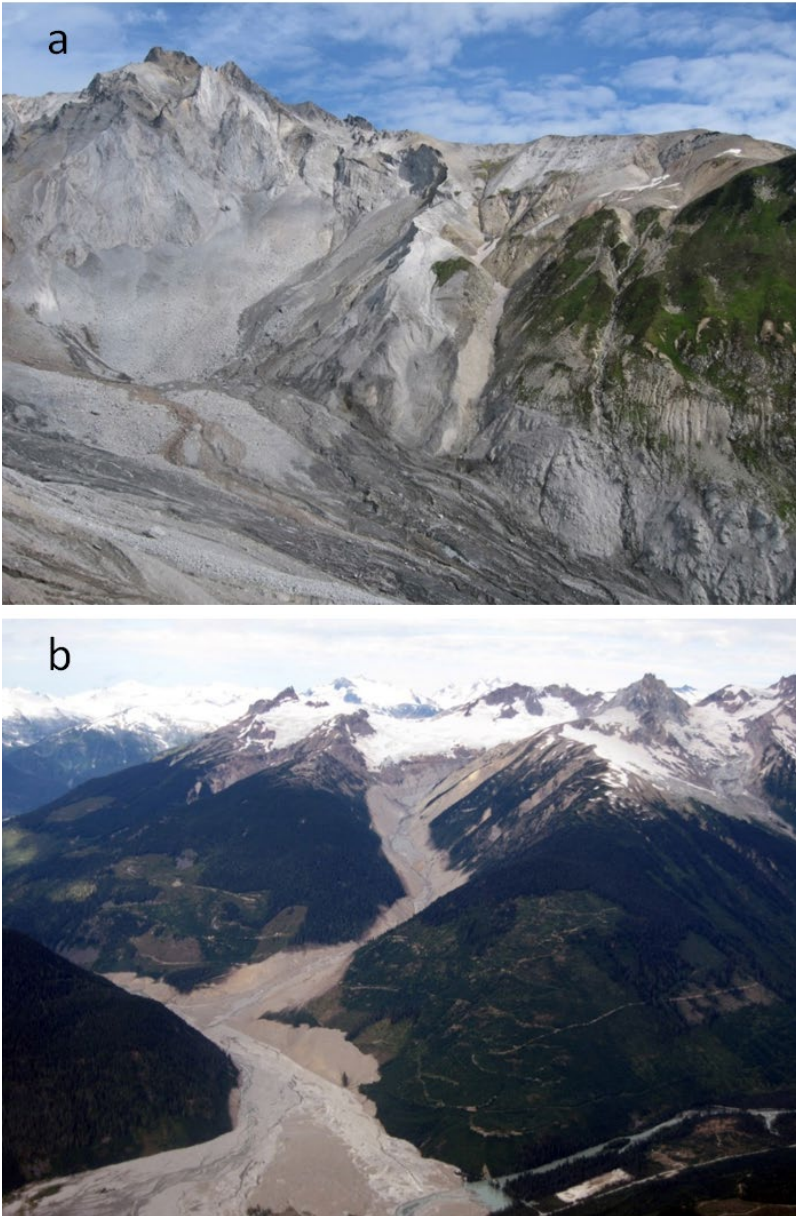


Figure 11. (a): Source area of the August 6, 2010 mass flow on the west flank of Mount Meager, in the Mount Meager Volcanic Complex, Coast Mountains, British Columbia (Guthrie et al., 2012). The initial rockslide (volume $\sim 53 \times 10^6 \text{ m}^3$; Roberti et al., 2018) developed into a high-velocity mass flow. (b): Oblique aerial photograph of the 2010 mass flow (view to the north) which ran 7.8 km down Capricorn Creek to enter Meager Creek. At the confluence, some debris ran 3.7 km upstream and most of the debris ran 4.9 km downstream to enter the Lillooet River valley (foreground), temporarily blocking its braided channels. The remainder of the debris formed a transient blockage of Meager Creek (Guthrie et al., 2012), forming a 1.5 km long lake. Photographs taken on August 29, 2010.

The three examples from the Quaternary Mount Meager Volcanic Complex show that in glacierized dissected volcanic centers steep topographic gradients combine with geomechanically weak materials and glacier retreat to create conditions for large-scale mass failure that frequently form long complex process chains. Initial failure is driven by glacier ice-loss and pre-failure slope deformation (Bovis, 1990; Holm et al., 2004) that progressively weakens the moving rock mass until catastrophic failure ensues (Roberti et al., 2018). During motion the initial failure volume is increased by entrainment of material in the path of the flow. Mass flows in this complex can dam rivers and create transient debris-dammed lakes which represent temporary stored energy fundamental to understanding complex process chains in this geomorphic environment.

3.5 Flows as initial processes

3.5.1 Gastern valley, Switzerland, 2011

The Gastern Valley is the uppermost part of the Kander River catchment (Bernese Oberland, Switzerland). It is affected by steep relief and permafrost degradation, resulting in a high intensity of hazard processes. On October 10, 2011, an extraordinary event hit this region involving several debris flow channels in which about $8 \times 10^5 \text{ m}^3$ of material was eroded and deposited in the valley bottom. It is noteworthy that the main part of the material was eroded from the higher parts of the cones, something that obviously did not occur in the last few centuries or even millennia. The material from these channels blocked the receiving Kander River at several places (Figure 12 (a)). Just below the uppermost blockage the Kander River shows massive widening and degradation. The next flatter stretch was blocked by deposits of a debris flow from the Märbegggrabe (about $3 \times 10^5 \text{ m}^3$). Behind this, most of the eroded material was deposited. Large deposits of fine material show that for some time a lake existed (Figure 12 (c)). The vast cone of the Märbegggrabe was not eroded but overflowed. Relieved from sediment the Kander degraded its riverbed in the next steeper stretch again (Figure 12 (d)). The eroded material was then deposited in the following flatter stretch. Here, meandering led to lateral erosion (Figure 12 (e)). The sum of these processes led to a reshaping of the landscape of the upper Gastern valley.

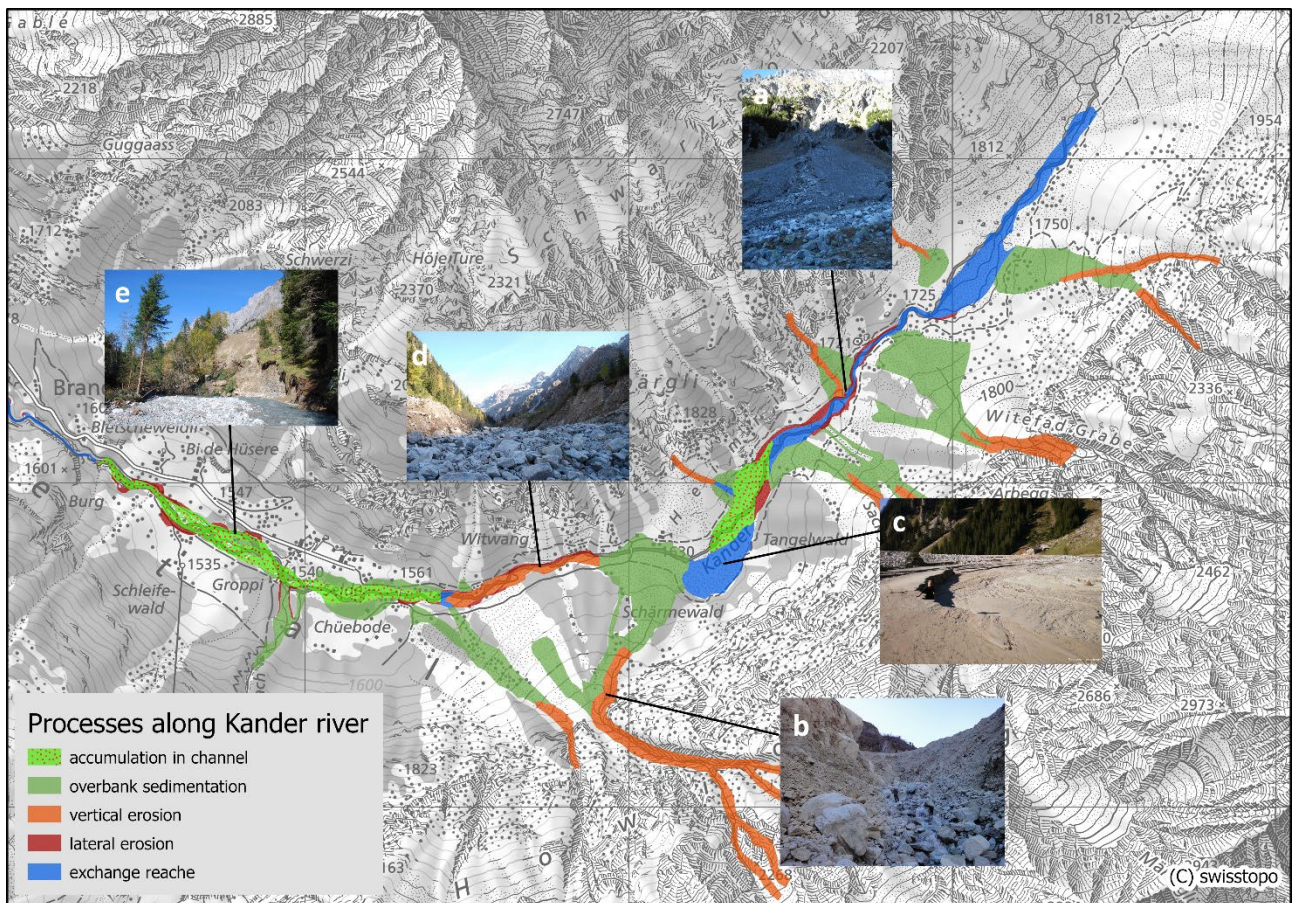


Figure 12. Process overview along Kander river: (a) place of uppermost blockage, (b) erosion at Märbegggrabe apex, (c) large deposits of fine material behind Märbegggrabe cone, (d) massive channel degradation below Märbegggrabe blockage, (e) lateral erosion along meandering stretch. (Photos: c) Berggasthaus Heimritz, all others Emch + Berger AG)

Not only the changes in landscape but also the triggering of these processes was extraordinary. During three days before the event, heavy snowfall far down into the valleys occurred. At 2000 m asl, about 50 cm snow depth was measured, at 2500 m asl about 100 cm. In the afternoon of October 9, the temperature rose rapidly. This was caused by an atmospheric river that brought very warm air and a lot of humidity into the area. Together with strong winds this led to fast moisture penetration into the snowpack (Badoux et al.,

2013). There are indications that as a result, snow slides were released from the steep rock faces and that a lot of snow accumulated in the area of the steep gullies in the cirques. This is confirmed by modelling the possible snow slides applying the GIS based mass conserving approach proposed by Gruber (2007).

Shortly before midnight rainfall started whereupon the zero-degree level was at about 3000 m asl. Simulation results from a study carried out for this event indicate that for about 5 hours the liquid water was almost completely retained in the thick cold snowpack (Mani et al., 2014). Würzer et al. (2016) show that in cases where initial snow cover conditions are mostly cold and dry, water retention in snow cover is considerably higher than in conditions where snow cover is isothermal as is the case in spring. Increasing saturation of the snow cover leads to compaction and to destruction of the initial snow matrix with the result that storage capacity decreases (Wever et al., 2014). The consequence of this is that even more water is released from snow cover. Figure 13 (a) shows this effect: from 4 AM the curve of water available for runoff (WAR) becomes steeper and increasingly faster than the precipitation at the IMIS (Intercantonal Measurement and Information System) station Fisi. Simulation results show that roughly 10 mm of water was released every hour from the snow cover between 7 AM and 1 PM (Mani et al., 2014).

Eyewitnesses say that the first debris flow mixed with snow in the Märbegggrabe occurred at about 9 a.m., followed by many more till about 1 p.m. (Figure 13 (b)) Within this time roughly $3 \times 10^5 \text{ m}^3$ of material were deposited on the cone (Figure 13 (c)). In the Märbegggrabe catchment the WAR sum over this period is $5 \times 10^4 \text{ m}^3$ what results in an extremely high bulk density of 2.4 kN/m^3 . This suggests that the surges should have stopped on the steep terrain. However, the surges extended beyond the existing cone. The slope of the cone diminished from 15.3° to 14.8° . The hypothesis for this is that the debris flows not only consisted of debris and water but also entrained snow. This can lead to a twofold effect: (i) the incorporated snow reduces the friction and, as a result, leads to a greater reach; and (ii) thermal effects in the debris flow as described by Iverson (1997) add additional water to the debris flow which means that the power of erosion is kept high (Hungr et al., 2005) down to the apex where erosion cross section of 600 m^2 were observed and half of the total debris flow volume was eroded (Figure 12 (b)).

Badoux et al. (2013) show that rain-on-snow events in fall, as seen in this case, are not common at higher elevation. Such events show a different, more complex behavior compared to rain-on-snow events in spring. With increasing temperatures related to global warming such events may occur more frequently as a deep snowpack will still exist at higher elevations, while rainfall up to high elevations may become more frequent (CH2018, 2018).

Further effects of climate warming that were relevant are the glacier retreat and the permafrost degradation. Most of the starting zone of the debris flows in the Gastern valley were either until recently covered by firn or glacier ice or are in the region of permafrost degradation. Comparable situations are widespread in the Alps (Figure 13 (d)).

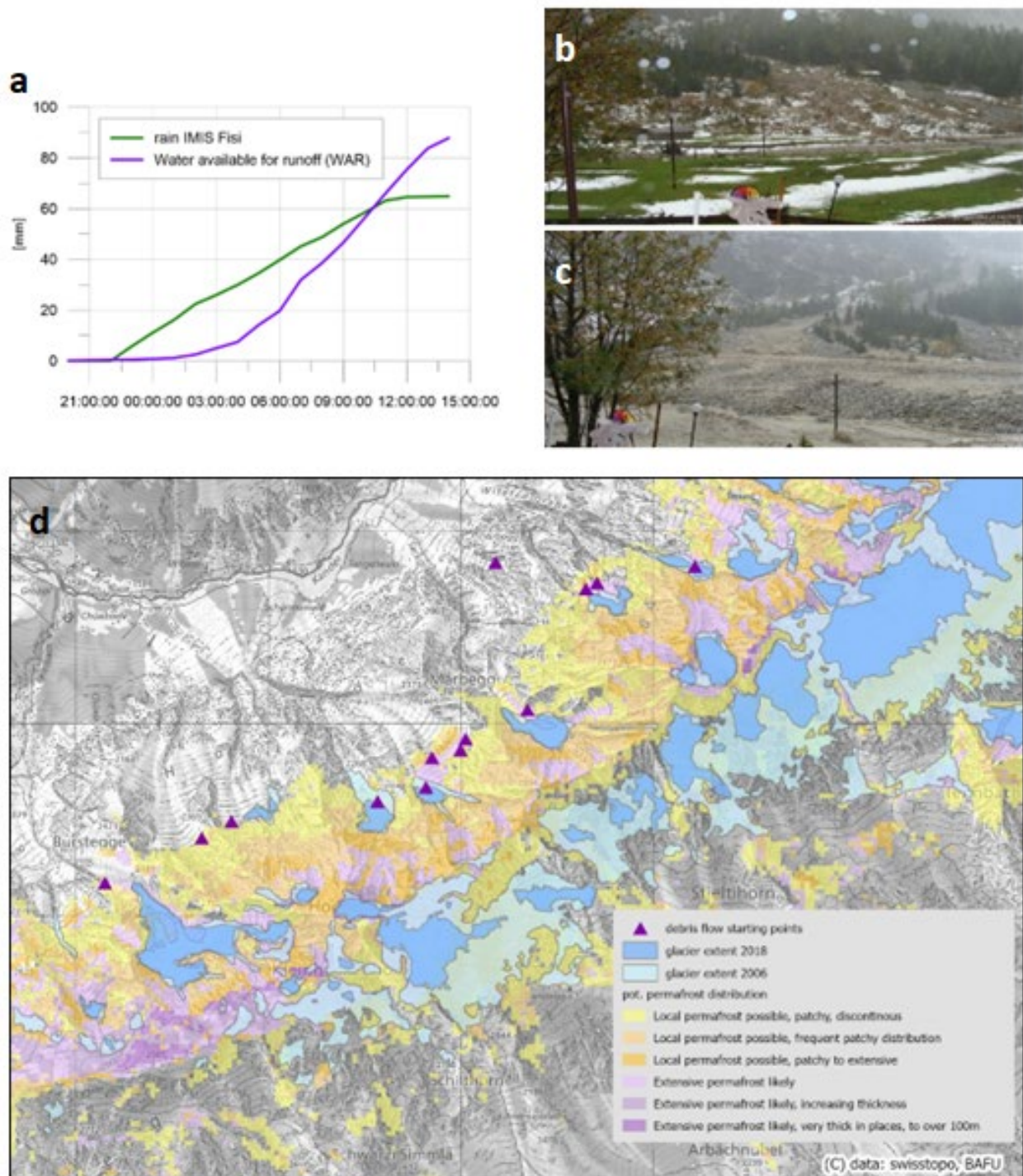


Figure 13. Process properties in the debris flow channels: (a) accumulated rainfall at IMIS station Fisi (2155 m asl) and WAR in the Märbeegggrabe catchment, (b) Märbeegggrabe cone at the beginning of the event, (c) Märbeegggrabe cone at the final phase of the event. (photos: Berggasthaus Heimritz), (d) debris flow starting points related to glacier retreat and permafrost degradation.

3.5.2 Giétro, Switzerland, 1818

On June 16, 1818 in the Bagnes Valley (Valais, Switzerland) the most significant GLOF in Switzerland during the last centuries occurred. It is also one of the world's most documented GLOFs (Ancy et al., 2019). Already

in the 16th and 17th century at least three flood events occurred, two of them very likely related to GLOFs (Raymond et al., 2003).

The climate cooling provoked by the Tambora eruption in April 1815 (Brönnimann and Krämer, 2016) accelerated the glacial advance. In the Bagnes Valley this had the consequence that the glacier front of the Giétro glacier came to lie on the escarpment above the valley and the activity of ice avalanches increased. Subsequently a regenerated glacier developed in the valley. Initially, the Drance River found its path underneath the ice dam, but creeping ice caused the passage to shrink progressively (Ancey et al., 2019). In spring 1818 the regenerated glacier grew rapidly, reaching a volume of about $10 \times 10^6 \text{ m}^3$ (Lambiel et al., 2020). The ice dam was 600 +/- 100 m wide at its base and 90 m high on the lowest part, opposite of the Giétro glacier (Ancey et al., 2019). This resulted in a blockage of the Drance River and a lake developed behind the ice dam (Figure 14). By early May 1818 the estimated volume of the lake reached $5 \times 10^6 \text{ m}^3$ and it was continuing to fill quickly with water resulting from snowmelt. From 10 May to 13 June 1818, the lake's depth increased by 22 m (Ancey et al., 2019).

This was perceived by the local population as the runoff in the Drance River became vanishing small in late April 1818. They informed the authority of the Canton Valais which evaluated the risk posed by the lake and to propose countermeasures. Authorities feared that the lake surface would reach the top of the ice dam and spill over it, so it was decided to dig a tunnel 23 m below the top of the ice dam through which the water would flow, when it reaches the tunnel. Thermal and mechanical erosion would then lower down the tunnel floor which would gradually empty the lake. The tunnel was finished on June 13 after about one month of work (Ancey et al., 2019).

In the following days, about $10 \times 10^6 \text{ m}^3$ were released through the tunnel and the water level decreased by c. 14.6 meters. However, strong erosion at the base of the ice dam as well as water infiltration through the ice and sediment below the dam provoked a dam failure during which $18 \times 10^6 \text{ m}^3$ of water were released within only 30 minutes.

The resulting flood was reconstructed by compiling both historical sources and geomorphological observations (Lambiel et al., 2020). Ancey et al. (2019) used numerical models to analyze the drainage of the lake and the propagation of the flood down the Drance Valley. The calculated peak discharge was $14'500 \text{ m}^3/\text{s}$ and the frontal velocity 5 to 6 m/s (Ancey et al., 2019). 1.5 hours after the dam break the flood reached the town Martigny, 33 km away from Giétro, at the confluence with the Rhone River. Here the peak discharge was about 3500 to 5000 m^3/s . Five hours later the flood reached Lake Geneva, about 40 km away from Martigny.

In the uppermost part of the course the water level was about 8 m above the upper edge of the 30 and 25 meters deep gorges (Lambiel et al., 2020). At Champsec, 11 km below the ice dam and Le Chable, 15 km below the ice dam, the flood simulation of Ancey et al. (2019) results in a flow depth of 13 m while the geomorphological analysis resulted in 6 m flow depth (Lambiel et al., 2020). A flow depth of 2 to 3 m was calculated for Martigny (Ancey et al., 2019). The 1818 Giétro flood ranks among the most intense recorded floods for this range of volume, regardless of the failure scenario (Ancey et al., 2019).

The extreme flood led to massive material displacements along the flow path. The DEM-analysis of Lambiel et al. (2020) shows large deposition areas at three wider sections along the Drance River. In narrower sections, lateral erosion was dominant. Large boulders were transported about 11 km downwards (Lambiel et al., 2020). The high intensity of these processes led to extensive damage. Hundreds of buildings were destroyed and 34 people died (Lambiel et al., 2020).

This event occurred during a period when glaciers advanced. Thereby the snout of the Giétro glacier became unstable as it became positioned on a steep slope. This led to an ice dammed lake that consisted of a regenerated glacier produced by avalanching ice (Lambiel et al., 2020), what is rather uncommon today, but was more likely during the Little Ice Age, when glaciers advanced. Nevertheless, unstable glacier tongues are not limited to advancing glaciers. Glacial recession can cause glaciers to recede to terminate on steep relief and their tongues become unstable. This was the case, for example, with the Allalin glacier catastrophe that

occurred in 1965 (Faillettaz et al., 2012). So, climate warming may create new situations where glacier tongues become unstable, resulting in new ice dammed lake – at least as long as glaciers still exist.



Figure 14. Lake Mauvoisin, blocked by ice avalanches from Giétro glacier in spring 1818 (Bridel, 1818). A glacier advance was the reason that the glacier front of the Giétro glacier came to lie on the escarpment above the valley and the activity of ice avalanches increased. Strong erosion led on June 16 to a failure of the dam and $18 \times 10^6 \text{ m}^3$ of water were released within only 30 minutes.

3.6 GLOFS as initial processes

3.6.1 Tronador, Argentina, 2009

Mount Tronador (3480 m asl) is the highest peak in Nahuel Huapi National Park and straddles the border between Chile and Argentina in northern Patagonia. Its summit is covered by an ice cap from which eleven outlet glaciers (64 km^2) flow into several valleys and down to 950 m asl. On the south-eastern flank of Mount Tronador, Ventisquero Negro – meaning black glacier due to a thick debris layer covering large portions of its ice – flow into Rio Manso valley (Villalba et al., 1997). Ventisquero Negro is constrained by a massive terminal moraine with a fork-like shape, forming the Rio Manso outlet at its lowermost point (Figure 15).



Figure 15. In the overview, flow type of the 2009 GLOF at Tronador (Argentina), inundated area, the moraine breach, the ice core and actual and former lake outline are illustrated, and the positions of pictures (A–F) are indicated. In addition, a longitudinal profile of the study reach and three cross-sections of the breach are provided. Pictures (A), (B) and (E) were taken shortly after the GLOF from a helicopter and show (A) the moraine breach, (B) the emptied lake and (E) the flooded area, respectively (Club Andino Bariloche, used with permission). The other pictures were taken during the field campaign and illustrate (C) the buried ice core, (D) debris flow deposits close to the moraine and (F) trees transported along the flow path. Figure reproduced with permission from Worni et al. (2012)

On 21 May 2009, the Ventisquero Negro terminal moraine breached to produce a lake outburst flood devastating the Rio Manso Valley. Over a period of six days prior to the GLOF, the nearby (16 km) Lake Mascardi meteorological station recorded unusually heavy rainfall (170 mm), whereas daily temperatures remained at their long-term average ($\bar{\varnothing}$ 7°C). Both the length and the intensity (50 mm in the 48 h preceding the GLOF) of the rainfall event were among the highest reported for the station (Worni et al., 2012). According to that study, these rainfalls would have increased the level and outflow of the glacier lake. As a further consequence, ice blocks originating from glacier calving were uplifted and subsequently floated towards the outlet. The increasing lake level and lake outflow most likely induced the moraine failure, as other triggering mechanisms could be excluded due to the absence of traces of mass-wasting events impacting the lake. Worni et al. (2012) also presented alternative scenarios that could have led to dam failure and breach formation at Ventisquero Negro: According to the authors it is also possible (i) the unusually high lake level could have helped stranded ice blocks to drift toward the outlet where they plugged the outlet, ponding the lake to an even higher level and increasing water pressure further to abruptly wash away the ice blocks and exceed the critical shear stress for erosion. As an alternative trigger, Worni et al. (2012) consider that (ii) the rising water level of the lake could have resulted in increased hydrostatic pressure on the dam, which ultimately could have led to instability of the ice core abutting the moraine through an uplift caused by the hydrostatic gradient, by partially breaking apart, or by gradual melting as a result of water infiltration.

Using field evidence and the dynamic dam-break model BASEMENT (Faeh et al., 2011), Worni et al. (2012) modeled the breach trigger mechanism, breaching and lake emptying processes as well as the dynamics of the outburst flood. They demonstrate that the lake volume of c. $10 \times 10^6 \text{ m}^3$ was released within 3 hours, resulting in high-discharge (c. $4100 \text{ m}^3/\text{s}$) debris flows and hyperconcentrated flows as the escaping water entrained large volumes of clastic material.

Levees with boulders of up to 6 m in diameter indicate that the outflowing water entrained moraine sediment to form a debris flow over a distance of c. 350 m downstream of the breach mark, from where the GLOF flowed for 150 m as a sediment-laden flow. The surge again evolved into a debris flow to deposit material on relatively flat terrain (c. 2°). Maximum grain sizes and levee heights decrease with increasing flow distance and terminal lobes are found c. 1000 m below the breach. Total approximate debris-flow volume was assessed at c. $25 \times 10^4 \text{ m}^3$, corresponding roughly with the volume of eroded moraine material. The GLOF propagated downstream as a hyperconcentrated flow to become a stream flow before entering Mascardi Lake. Over a distance of 10 km the outburst flood changed the flood plain morphology significantly by eroding entire forest stands and destroyed the bridge and parts of the road to Pampa Linda, while a camp ground and houses were partly flooded. Downstream of Pampa Linda the channel of Rio Manso was able to accommodate most of the released lake water.

3.6.2 Shakhimardan, Kyrgyzstan, 1998

On July 8, 1998, the deadliest GLOF in Central Asia for at least the last 100 years occurred in the Shakhimardan catchment, Kyrgyzstan. Most of the >100 victims were, however, killed in the Uzbek enclave of Shakhimardan, i.e. in the downstream part of this transboundary catchment. Due to political tensions, access to the site was impossible and a detailed assessment of the disaster was realized just in recent years. There were no published reports on the event, so almost all data is taken from (Petraikov et al., 2020).

The lake at the origin of the Shakhimardan event appeared in the 1960s, reached its maximum area with $32.2 \pm 0.7 \times 10^3 \text{ m}^2$ in 1976 and drained periodically, without causing damage to downstream areas. The total area of the lake before the 1998 disaster was estimated at $20 \pm 1.2 \times 10^3 \text{ m}^2$, the volume of the lake was assessed as $120 - 133 \times 10^3 \text{ m}^3$.

The Shakhimardan event started with a GLOF which then triggered a suite of chain reactions. The GLOF was triggered by a heat wave after a period of relatively cold weather. Most probably, the englacial drainage system did not adapt to rapidly increasing ablation and the lake has been overfilled. The GLOF transformed quickly into a debris flow dominated by coarse-grained components and travelled for approximately 17 km down the valley before the flow transformed into a debris flood between 17 and 37 km downstream. Farther downstream, and over ~60 km away from the source, field evidence points to a transformation of the debris flood into a flash flood.

The rapid transformation of the GLOF into a debris flow started at the lower end of the moraine complex where the GLOF was forced to pass through a narrow river section due to the presence of two rock glacier lobes; as a result, intense erosion roughly estimated to $100 \text{ m}^3/\text{m}$ occurred at this segment of the channel. Erosion zones are mostly located in the headwaters where bed and bank erosion was favored by steeper slope angles in the main channel with a mean weighted channel angle in the erosion zones of 6.7° . This value is significantly lower comparatively to international literature where debris-flow erosion is described to be important for cases in which channel gradients exceed 8° (e.g., Huggel et al., 2004; O'Connor et al., 2001). Due to considerable entrainment of material along its path, the resulting volume of accumulated debris was estimated as $0.80 \times 10^6 \text{ m}^3$. This value does not include sediments transported out of the study zone by the flash flood. Water was added to the flow by numerous tributaries with significant meltwater discharge as well as by entrainment of water-saturated soils. Debris flow discharge at a distance ca. 10 km from the source was assessed as $600 \text{ m}^3/\text{s}$.

Transformation of the debris flow to a debris flood happened within a very flat (1.2°) and long (about 2 km) section of the valley bottom, after the confluence with Ikedavan and Akbek rivers. Mean channel angle along the debris flood path was 2.2° . Flood discharge reduced due to sediment deposition and wave flattening. In

Shakhimardan it has been assessed as 150-200 m³/s. Further downstream the debris flood transformed into a flash flood, and no significant depositions were found in the lower Shakhimardan settlement.

Transformation of a GLOF to debris flow or debris floods is typical for Central Asia including Kazakhstan (Medeu et al., 2016; Yafyazova, 2007), Kyrgyzstan (Erokhin et al., 2018; Narama et al., 2018; Narama et al., 2010; Zaginaev et al., 2019), and Tajikistan (Mergili and Schneider, 2011) as they move down steep terrain covered with abundant loose sediments. The volume of initial outbursts could increase up to 17 times during the stage of debris flow as happened in July, 1973 during the GLOF and disastrous consequent debris flow in the Malaya Almatinka river near city of Almaty (Yafyazova, 2011). The average slope from the GLOF source to the Medeo dam where debris flow has been stopped was 8.8° which is 1.5 times higher than for the Shakhimardan event with an entrainment ratio of 8. Typical regional entrainment ratio for chain GLOF – debris flow is significantly smaller (Erokhin et al., 2018; Medeu et al., 2016).

Shakhimardan event thus might be considered as a “worst-case”, especially taking into account the extremely low channel angle of the debris flow path and the whole process chain.

3.7 Summary

The 12 comprehensively described examples were selected to illustrate typical characteristics of process chains. The selection provides an overview of different process chains, and is not representative of the frequency of the different types. The examples cover all triggering processes, the threshold failure as well as all geomorphic processes either as initial or as subsequent processes, as shown in Figure 16. Examples also cover all GTN-Regions which are represented in the database except Karakoram, Tibet and New Zealand, and the starting zones cover a range of altitude from 900 to 7000 m asl. Eight process chains only link one initial with one subsequent process, while four have two or more subsequent processes. Thereby, it should be noted that fluvial processes comprise multiple processes as hyperconcentrated flow, debris flood or fluvial sediment transport. 10 of the process chains described in detail show a direct linking of the initial and the subsequent processes while three showed a delayed reaction. Six of these events claimed victims, and in four cases more than 100 fatalities. This shows the threat posed by such events in the absence of any significant warning time.



Figure 16. Interaction diagrams for the process chain events with detailed description (cf. Chapter 3)

4. Characteristics and key parameters of process chains: towards a classification scheme

Characteristics and parameters of process chains were analysed, based on the classification concept described in chapter 2, for a total of 51 events for which information was either available in the literature or

derived from globally available datasets. The information is stored in a database that is available as supplementary material.

4.1 Processes involved and process interaction

When analyzing the full dataset of 51 case studies and looking first at the reason why process chains occurred, we realize that initial processes most frequently result from **threshold failure** and not due to the occurrence of a distinct **triggering process** (Table 3). This means that the long lasting, gradual loss of stability of rock or loose material - induced by e.g. weathering, permafrost degradation or seismicity - is more frequent than any other factor. As could be expected, heavy precipitation are a crucial trigger of process chains and the second most common trigger.

If all 51 events in the database are taken into account, rock avalanches are the most frequent **initial process**, followed by GLOFs (Table 3). Rock avalanches are the most frequent initial process in the Alps and in the Coast Range, while GLOFs are most frequent in Tien Shan. For slides as well as rock-/ice-avalanches, no distinct hot spots exist. The Andes and the Himalaya show the highest variety of initial processes.

Table 3: Frequency of triggering and initial processes. The total of 55 events result from 4 cases with a combination of precipitation and snow/icemelt as triggering process. *Threshold failure is not a triggering process in itself, but rather the absence of a distinct process.

Initial process	Triggering process						Total
	Volcano	Earthquake	Precipitation	Snow-/icemelt	Threshold failure*	no information	
Debris flow	0	0	1	0	1	0	2
Glacial surge	0	0	0	0	2	0	2
GLOF	0	0	5	4	2	3	14
Ice avalanche	0	1	0	0	3	1	5
Lahar	1	0	0	0	0	0	1
Slide	1	0	1	1	2	2	7
Rock avalanche	0	1	0	1	9	1	12
Rock-/ice avalanche	0	0	0	0	5	1	6
Rock-/ice fall	0	1	0	0	1	0	2
Rockfall	0	0	1	0	0	0	1
Rockslide	0	0	1	1	1	0	3
Total	2	3	9	7	26	8	55

From the 51 case studies analyzed, debris flows are the most frequent **subsequent process**, followed by debris floods (Figure 17 (a)). GLOFs and river blockings are also of greater importance whereupon the latter is not a true slope process, but its result and an important element of many process chains. From a regional perspective, most debris flows occur in the Alps, in the Coast Range, the Andes and the Himalayas. The distribution of the debris floods is comparable. GLOFs as a subsequent process occur most frequently in the Andes. The blocking of a receiving river is most documented in the Alps, the Coast Range and in the Himalaya.

Process chains initiated by rock avalanches show the largest number of subsequent processes. Debris flows, debris floods and blockings of receiving rivers are the most frequent subsequent processes (Figure 17 (a)). GLOFs initiate the second largest number of subsequent processes. Here, debris flows and debris floods are the most common subsequent processes. Slides as initial processes are mainly followed by GLOFs and debris floods, rock-/ice-avalanches by GLOFs, debris flows and debris floods. Process chains initialised by ice-avalanches mostly involve GLOFs.

The process linking of initial processes with the first subsequent process is summarized in Figure 17 (b). Direct interactions occur in most cases listed in the database – the only exceptions found are glacial surges and some rockfall events. By contrast, all GLOF events show a direct triggering of the subsequent process, mostly

as a result of the high discharge of GLOFs compared to rainfall induced floods, abundance of loose unconsolidated moraine in the outflow area, and their considerable erosive forces (Cenderelli and Wohl, 2001; Cook et al., 2018). Ice avalanches and rock-/ice-avalanches show a high proportion of direct triggering of subsequent processes as well; here, we ascribe the direct triggering to the melting of ice, which in turn leads to the liquefaction of the mass, and far reach of these initial processes.

A delayed linking is much less frequent. Most often it occurs in the case of rock avalanches/rockslides. A reason for this is that deposits of rock avalanches consist of coarse debris and thus show higher stability, thereby preventing direct failure of the valley blocking dam (Dunning et al., 2005; Dunning and Armitage, 2011). However, rockslide dam failure most often occurs within days of formation (Evans et al., 2011) and forms an important part of rockslide process chains.

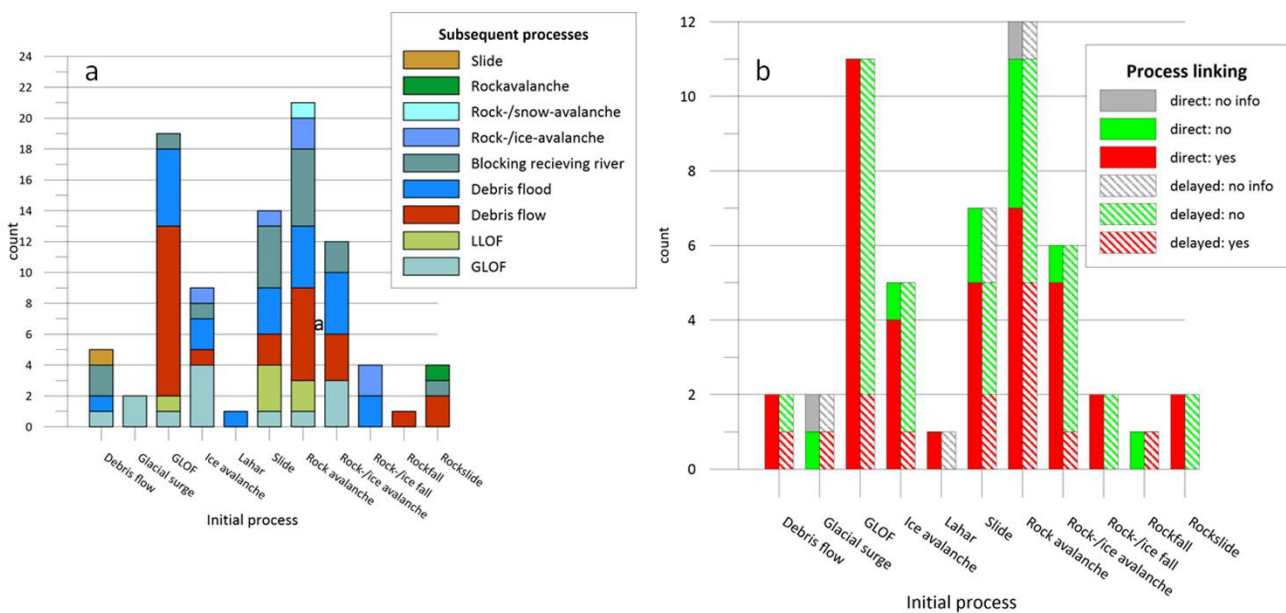


Figure 17. Subsequent processes related to the initial process (a) and type of process linking in process chains by initial process (b) based on the 51 events in the database.

4.2 Starting zone parameters

More than 50% of the events in the database have their starting zone in the range where permafrost is probable (mostly in the PZI classes “cold” or “in nearly all conditions”, Table 4). In the Tien Shan region, where all starting zones are in probable permafrost area, median and maximum elevations of the starting zones are located at about 3500 m and 3900 m, respectively, and therefore well above the lower limit of present-day permafrost in this region (about 2800 m according to Gruber (2012)). This means that even with continued global warming and rising of the permafrost boundary, permafrost will still be an important factor in the starting zones of process chains by the end of the century and beyond. This is also true for the Himalaya and the Karakoram whereupon for the latter only one event is represented in the database. On the other hand, smaller differences between local maximum elevation and elevation of the starting zones are seen for the Andes, the Alps, the Caucasus and for New Zealand.

A striking feature is the high proportion of rock- and rock-/ice-avalanches starting zones outside or in the lowest category of permafrost (55%) (Figure 18 (b)). Smaller rock instabilities that respond more directly to warming of the active layer of permafrost (e.g. Gruber et al., 2004) are unlikely to involve sufficient volumes to generate process chains. Looking at threshold failure, the most important reason for landslide-generated process chains, roughly 60% of the starting zones of all initial processes are within the zone where permafrost is probable, which means that also in the starting zones of other initial processes such as slides or GLOFs, permafrost is present (Figure 18 (a)). Almost all of the starting zones with threshold failure as the triggering process are also in the range of strong to violent seismicity, what is expected in most mountain regions.

Regarding **lithology**, acid plutonic rocks are most frequently (15) present in the starting zone of the initial processes (not considering ice avalanches and glacial surges). They make up the majority in the case studies with rock avalanches, rock-/ice falls and GLOFs. With 35%, their occurrence is far out of proportion with the global distribution of 5.6%. Since acid plutonic rocks are more likely to be stable and weathering-resistant, seismicity and permafrost is rather the reason for an increased disposition for slope failure. Another explanation could be that this lithology produces steeper slopes, more prone to large catastrophic failures than a weaker lithology from which smaller, more frequent instabilities may originate.

Table 4: Permafrost occurrence according to a global model (Gruber, 2012) and elevation of starting zones by region. The large grid cell (ca. 1km) of the permafrost model may not capture local presence of permafrost in some situations.

Region	Permafrost [number]				Elevation [m asl]		
	no	only in very cold cond.	mostly in cold cond.	in nearly all cond.	maximum	median starting zone	maximum starting zone
Himalaya	3	1	4	2	8849	4675	7000
Hissar Alay			1		4643	3800	3800
Karakoram			1		8611	4800	4800
S and E Tibet	1		1		7253	4122	4444
Tien Shan			3	1	7439	3400	3600
Alps	2	4	3	1	4809	2840	3870
Caucasus			1	2	5642	4400	4780
Coast Range	2	1	6		4019	2300	2620
Andes	5	3	1		6962	5230	6600
New Zealand	2				3754	2295	2460
Total	15	9	21	6			

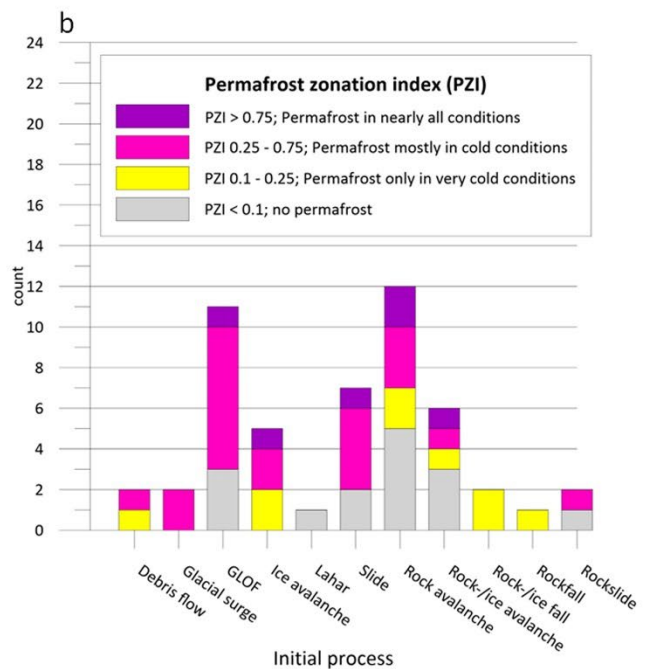
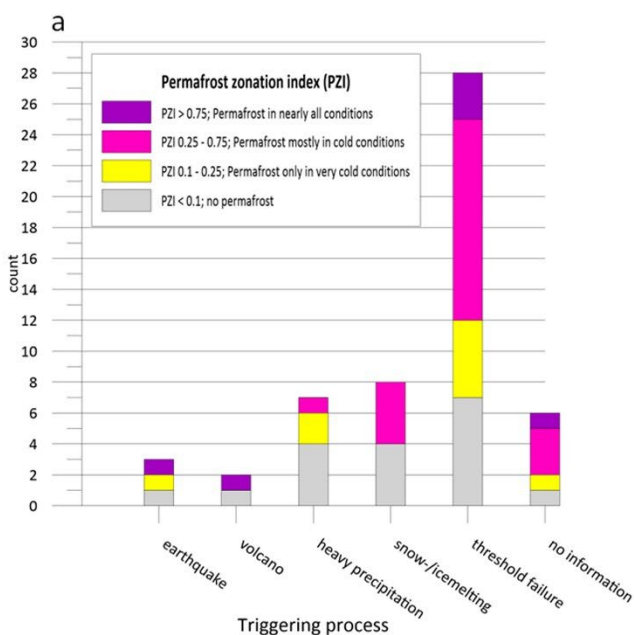


Figure 18. Permafrost zonation index (PZI) by triggering process, including threshold failures (a) and initial process (b). Less than 10% of the starting zones of process chains in the database lie outside of the permafrost area. About 50% lie in the range where permafrost is probable. Related to the triggering processes most of the events which were triggered by threshold failure lie within permafrost area.

The **local elevation range (LER)** is used here as a proxy for the potential energy involved in the process chains and evaluated within a radius of 500 and 1000 meters (Figure 19) (LER within a radius of 5000 m shows no clear pattern and fades into background). Rock- and/or ice-falls and rock- and/or ice avalanches are associated with the highest LER500 median, with values over 600 meters, while the lowest values are associated with glacial surges. In between are the sliding processes, lahars, GLOFs and debris flows. This is in line with the process characteristics but for some processes (e.g lahars or rockfalls) there are only few entries in the database. Rock-/ice-avalanches show by far the largest range between minimum and maximum LER500, with about 1200 meters. The LER1000 median values show a comparable pattern. Again rock-/ice-avalanches, rock-/ice-falls, rockfalls show the highest values with 1000 and more meters. In addition, rockslides and debris flows show comparable values. On the other hand, rock avalanches show a median value that is slightly lower. Again, glacial surges and lahars have the lowest median values. Rock-/ice-avalanches show the largest range of LER1000 values with about 1800 meters, followed by GLOFs with about 1100 meters.

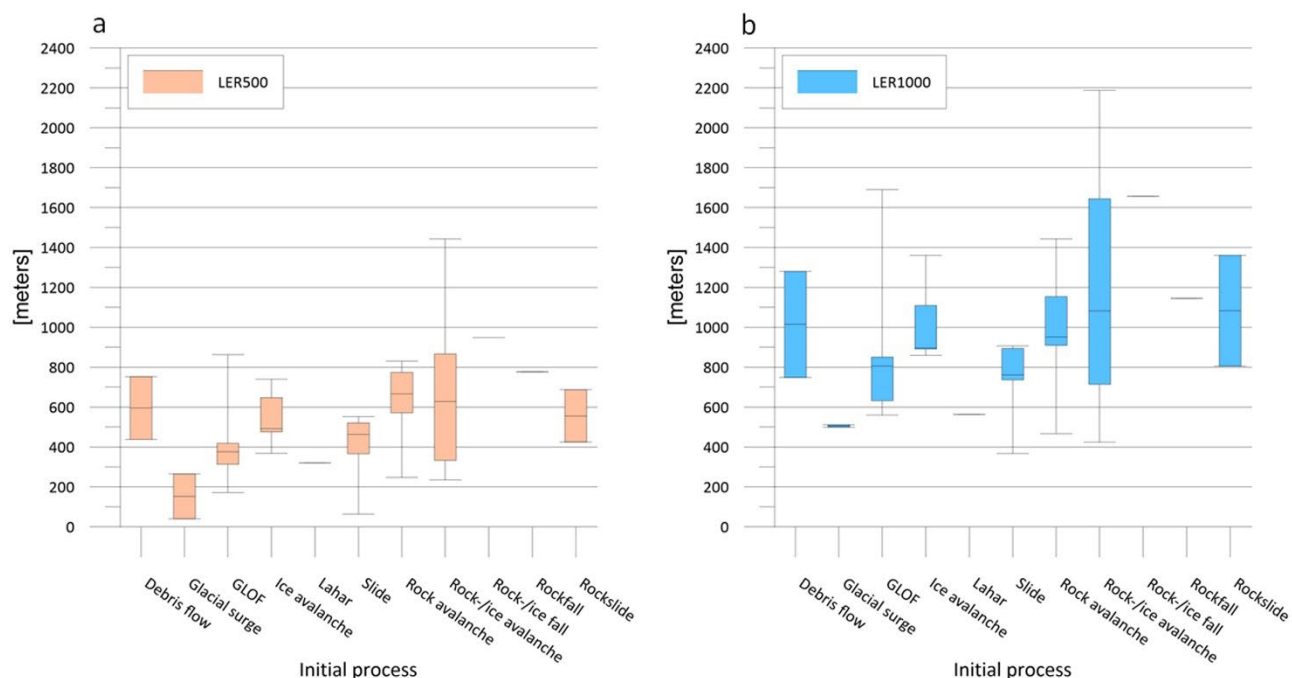


Figure 19. Local elevation range for 500 m radius (LER500, (a)) and 1000 m radius (LER1000, (b)) by initial process. The box represents the range between the lower and the upper quartile, the whiskers the minimal and maximal value.

4.3 Amplification effects

Snow entrainment or the reduction of friction caused by snow is only a relevant factor in 11 cases, mostly in the Alps and the Coast Range and most cases are related to rock avalanches and rockslides (Table 5). **Ice entrainment** plays a role in 17 events, mainly for rock avalanches and rock-/ice-avalanches but also for slides. However, in many cases, information on snow entrainment is not available.

For the availability of **fine-grained loose material**, which contains a relevant ratio of grain size less than or equal to sand and what is relevant for the reach of debris flows and debris floods (Pierson, 2005), three sub-parameters are combined in this study, namely (i) fine grained material along the path trajectory (visual detection of fluvial or lacustrine sediments from satellite images), (ii) highly fractured deposits of rock avalanches and rock-/ice-avalanches if LER500 exceeds 600 m, assuming that high fall energy pulverizes part of the mass; and (iii) disaggregated rock caused by seismicity if seismicity classified as severe or violent. If at

least one of these sub-parameters is true, the existence of fine-grained loose material is assumed. This is the case for 40 events and occurs most frequently in the case of GLOFs, slides and rock-ice avalanches.

Fluvial processes have an amplification effect in 27 events as they can transport high volume of sediments over long distance. Notably, however, only 4 of 10 GLOF events included fluvial processes in their process chain. Much more frequent are debris flows as subsequent process. Again, this amplification effect applies to less than half of the process chains that are triggered by rock avalanches, while it is important for slides and rock-/ ice avalanches. **Lakes formed by natural dams and bedrock** play a role along the process chain trajectory in 27 cases. This includes obviously all GLOF events as well as all glacial surges, most ice avalanches and 3 out of 7 slides. In 25 cases, lakes have amplifying effects as the failure or overtopping of their dams lead to flood waves downstream from the dam site. For the other cases lakes can have a damping effect, if sediments of debris floods or debris flows are trapped.

Table 5: Amplification effects related to initial processes (ND: no data available)

Process	Snow entrainment			Ice entrainment			Fine grained material			Fluvial Processes			Lakes involved		
	yes	no	ND	yes	no	ND	yes	no	ND	yes	no	ND	yes	no	ND
Debris flow	1	1	0	0	2	0	2	0	0	2	0	0	1	1	0
Glacial surge	0	1	1	0	1	1	2	0	0	1	0	1	2	0	0
GLOF	0	10	0	0	10	0	9	2	0	5	5	1	11	0	0
Ice avalanche	0	4	1	0	4	1	3	2	0	4	1	0	4	1	0
Lahar	1	0	0	1	0	0	1	0	0	0	0	1	0	1	0
Slide	1	6	0	3	4	0	6	1	0	5	2	0	3	4	0
Rock avalanche	5	6	1	5	6	1	6	6	0	4	7	1	3	9	0
Rock-/ice avalanche	0	0	6	4	0	2	6	0	0	4	0	2	4	2	0
Rock-/ice fall	0	0	2	2	0	0	2	0	0	2	0	0	0	2	0
Rockfall	1	0	0	0	1	0	1	0	0	1	0	0	0	1	0
Rockslide	2	0	0	2	0	0	2	0	0	0	2	0	0	2	0

4.4 Volume

Volume data are not available for all events in the database. Information is missing for 8 events for initial volume, and almost for half of the events for total volume. The largest initial volume for the analyzed events is for lahars (Nevado del Ruiz) with $90 \times 10^6 \text{ m}^3$ (Figure 20 (a)). This is followed by rock-/ice-avalanches with a maximum value of $50 \times 10^6 \text{ m}^3$. and a median value of about $18 \times 10^6 \text{ m}^3$. For the other processes the initial volume lies below $10 \times 10^6 \text{ m}^3$. Lowest values are for debris flows, GLOFs and rockfalls. For the events with values for the total volume (including the volume of entrained material), rock avalanches show the highest value ($135 \times 10^6 \text{ m}^3$, Kolka event, Figure 20 (b)). Except for lahars all other total volumes are below $20 \times 10^6 \text{ m}^3$. Where both initial and total volumes are available, the ratio between the two values can be calculated. Here, the highest values result for GLOFs. For the event in the Klattasine Creek (Coast Range) the ratio is 750, for the Zharsay Issyk 180. For the other events the ratio is below 20.

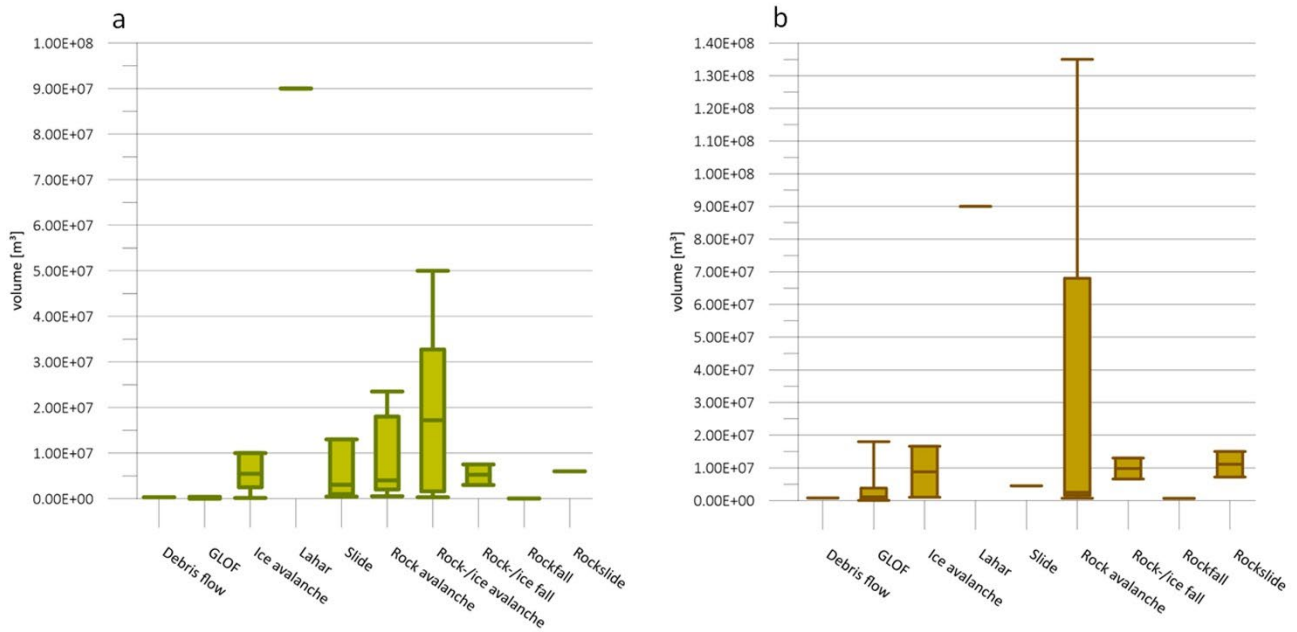


Figure 20. Initial volume (a) and total volume (b) related to initial process

In order to look for possible controls of volumes involved in process chains, we analyzed the respective role of triggering processes and thermal state of the ground on the size of events. As shown in Figure 21 (a), volcanic processes and earthquakes tend to trigger the largest initial volumes, both in terms of maximum and median values. A high maximum value can also be observed in the case of threshold failures, while their median value is in the range of the remaining triggering processes with rather low initial volumes. Concerning the role of permafrost, the largest overall initial volume has been recorded from a zone without permafrost (lahar, Nevado del Ruiz) whilst median and 75% values of volumes increase as the likelihood of permafrost increases (Figure 21 (b)). This could potentially be indicative of deep permafrost thaw destabilizing large rock volumes, as, for example, was recently suggested for the Chamoli disaster in Northern India, that falls in the “mostly in cold conditions” class (Shugar et al. 2021).

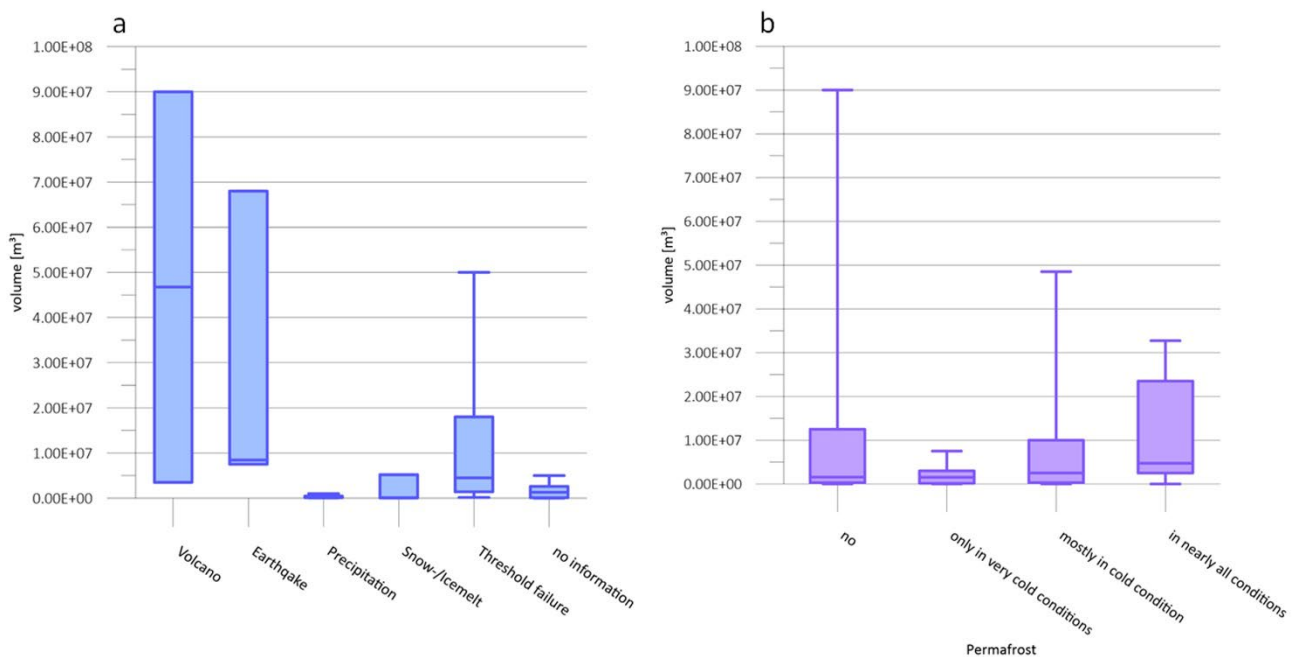


Figure 21. Initial volume related to triggering process (including threshold failure) (a) and permafrost occurrence (b)

4.5 Trajectory characteristics

We used reach and the average slope for the characterization of the path of the process chains, in 35 of the 51 events in the database for which this information is available. In other cases, the reach cannot be reliably determined, particularly where there is no distinct endpoint, and the process rather gradually attenuates downstream. Figure 22 shows the expected relation whereby high values of average slope are achieved for short reaches. By contrast, long reaches lead to low values of average slope, which is self-evident from topographic limits. For better readability, the Yarlung Tsangpo event with a reach of 460 km is omitted.

The distinction between process chains with and without snow or ice entrainment shows no difference in the average slope (Figure 22 (a)). Surprisingly, the maximum reach of process chains with snow or ice entrainment seems to be shorter when compared to the maximum reach of these processes in the absence of entrainment. This is not in correspondence with events and processes described e.g. by Evans and Clague (1999), McSaveney (2002), Sosio (2015) and Evans et al. (2021). Even if process chains with fluvial processes are excluded there is no clear evidence of larger reaches for process chains with snow or ice entrainment. This is also the case if we look only at fall processes without subsequent fluvial processes. But here the reason for this is that all cases except for one include entrainment of ice and/or snow.

The presence of fine-grained material along a process chain can lead to long reaches (Figure 22 (b)). The reach of events with no relevant sources of fine-grained material is smaller than 20 km in all cases except for the event with the largest reach (Nostetuko Lake, Coast Range; 115 km). The reach of 6 events with fine grained material involved lies between 30 and 80 km.

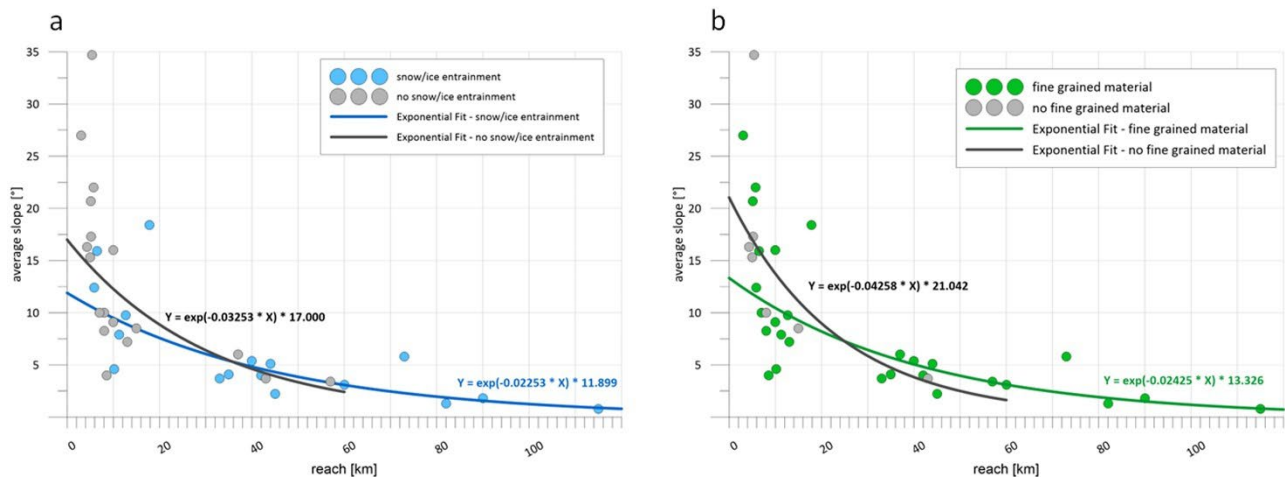


Figure 22. Reach and average reach slope classified by snow and/or ice entrainment (a) and presence of fine-grained material (b). In both cases the exponent differs quite clearly between the cases with and without the impact of entrainment and fine-grained material respectively. This means that the average slope is steeper and reach is shorter without the entrainment or presence of fine-grained material.

Process chains that include fluvial processes or lakes show larger reaches and tend to result in lower average slope (Figure 23). The average reach of process chains with fluvial processes is 36.4 km, compared to 14.3 km without fluvial processes. Comparable values result for process chains with and without lakes involved (36.1 and 13.1 km, respectively). Hence, fluvial processes, lakes, and associated outburst events have the potential to transform mountain hazards into far-reaching downstream disasters. The process chains with or without large retention areas do not show a distinct difference in reach (not shown). Likewise, we do not observe any significant trends between initial and total volume or reach of process chains (Figure 24 (a)).

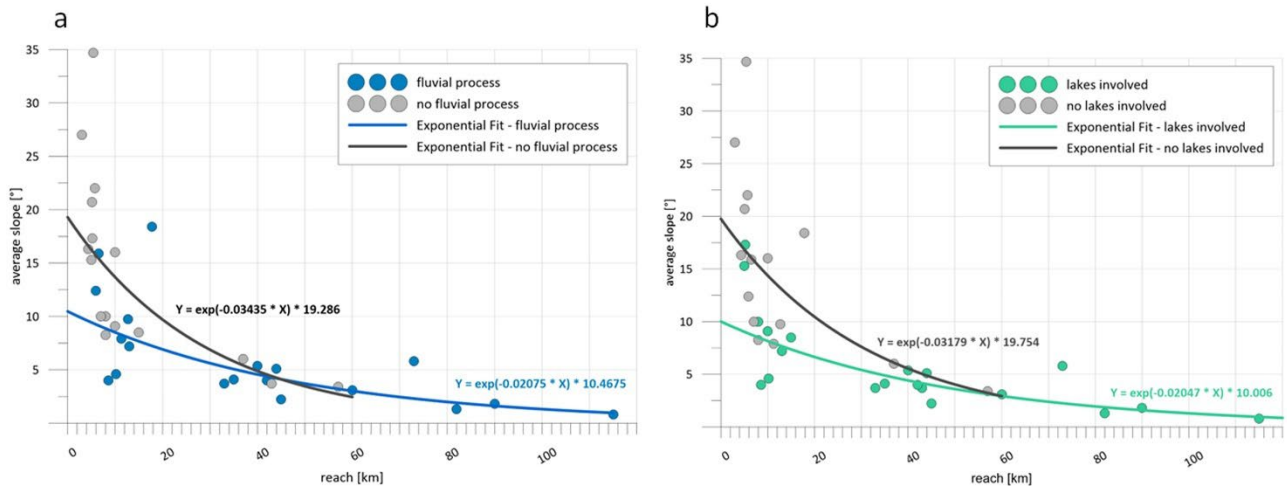


Figure 23. Reach and average slope classified by occurrence of fluvial processes (a) and lakes involved (b) in process chains. In both cases the exponent differs quite clearly between the cases with and without the impact of fluvial processes and lakes involvement respectively. This means that the average slope is steeper and reach is shorter without the impact.

The Yarlung Tsangpo rock-/ice-avalanche event in Tibet (2018) shows an exceptional reach of 460 km, owing to the subsequent outburst of the temporary dammed lake. All other values involving lakes in this study are below 120 km. Most events with a reach of more than 50 km include fluvial processes as (one of) the subsequent process(es). This suggests that initial processes do not exert a key control on the reach of a process chain, and more important is the potential for the initial event to intersect with large fluvial systems and/or lead to secondary lake formation. This is supported by the fact that reaches show a negative trend related to the LER values for all radius (500, 1000 and 5000 m) (Figure 24 (b)), thereby suggesting that LER is an indication for potential energy of the initial process, but not for the whole process chain.

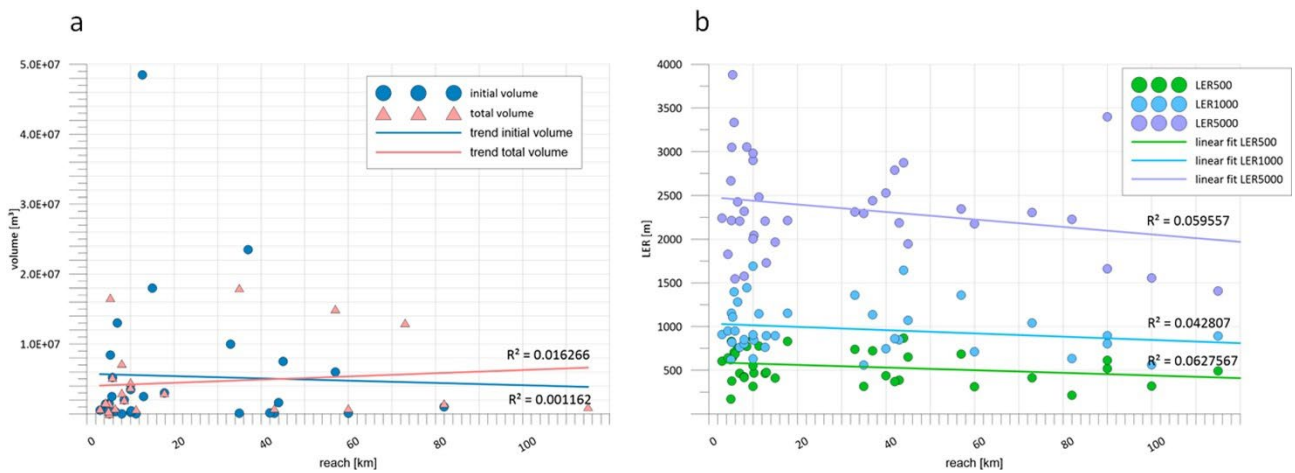


Figure 24. Reach related to initial and total volume respectively (a) and to LER (radius 500, 1000 and 5000 m) (b). Trends are weak and coefficients of determination are general low.

4.6 Potential climate change impact

Only sparse and often qualitative information is usually available in the literature on the role of climate change on past process chains, and even less information exists on how changing climatic conditions and the related glacier retreat and thawing of permafrost could change the frequency of occurrence, magnitude and/or triggers of process chains by the end of the 21st century. Therefore, we combined here different rules to derive the potential role of climate change in these cases and to assess their future occurrence. These rules are specific to the triggers and initial processes affected by climate change and thus consider the permafrost zonation index (PZI), occurrence of glaciers along the process trajectories, observed changes in

precipitation (Sun et al., 2021) and projected changes by the end of this century (Iturbide et al., 2021). For the latter, we analyzed changes of annual precipitation sums (PSUM), changes in the highest 1-day (Rx1d) and 5-day (RX5d) precipitation totals for the Representative Concentration Pathway (RCP) 8.5. The applied rules are shown in Table 6 together with their likely impacts on triggering, initial and subsequent processes.

Table 6: Rules to derive climate change impact on triggering, initial and subsequent processes

	process	impact on event	impact in future
triggering process	heavy precipitation	precipitation → amplification	$\Delta Rx1d$ or $Rx5d \geq 10\%$ → amplification $\Delta Rx1d$ or $Rx5d > -5\%$ - $< 10\%$ → indifferent $\Delta Rx1d$ or $Rx5d \leq -5\%$ → diminishing
	snow or ice melt	PZI → indifferent glacier → indifferent precipitation → indifferent	PZI > 25 → amplification glacier → diminishing (at high altitude amplification) $\Delta Rx1d$ or $Rx5d \geq 10\%$ → amplification $\Delta Rx1d$ or $Rx5d > -5\%$ - $< 10\%$ → indifferent $\Delta Rx1d$ or $Rx5d \leq -5\%$ → diminishing
	threshold failure	PZI → indifferent glacier → indifferent precipitation → indifferent	PZI > 25 → amplification glacier → indifferent $\Delta Rx1d$ or $Rx5d \geq 10\%$ → amplification $\Delta Rx1d$ or $Rx5d > -5\%$ - $< 10\%$ → indifferent $\Delta Rx1d$ or $Rx5d \leq -5\%$ → diminishing
initial or subsequent processes	rockfall, rock avalanches, rock/ice avalanches	PZI > 0 → amplification glacier → amplification precipitation → indifferent	PZI > 25 → amplification glacier → amplification $\Delta Rx1d$ or $Rx5d \geq 10\%$ → amplification $\Delta Rx1d$ or $Rx5d > -5\%$ - $< 10\%$ → indifferent $\Delta Rx1d$ or $Rx5d \leq -5\%$ → diminishing
	snow and ice avalanche	PZI > 0 → amplification glacier → indifferent precipitation → indifferent	PZI > 25 → amplification glacier → diminishing (at high altitude amplification) $\Delta Rx1d$ or $Rx5d \geq 10\%$ → amplification $\Delta Rx1d$ or $Rx5d > -5\%$ - $< 10\%$ → indifferent $\Delta Rx1d$ or $Rx5d \leq -5\%$ → diminishing
	debris flow	PZI > 0 → amplification glacier → indifferent precipitation → indifferent	PZI > 25 → amplification glacier → amplification $\Delta Rx1d$ or $Rx5d \geq 10\%$ → amplification $\Delta Rx1d$ or $Rx5d > -5\%$ - $< 10\%$ → indifferent $\Delta Rx1d$ or $Rx5d \leq -5\%$ → diminishing
	glacial surge	PZI indifferent glacier → indifferent precipitation → indifferent	PZI indifferent glacier → amplification precipitation → indifferent
	lahar	PZI indifferent glacier → indifferent precipitation → indifferent	PZI indifferent glacier → diminishing precipitation → indifferent
	Slide, rockslide	PZI > 0 → amplification glacier → amplification precipitation → indifferent	PZI > 25 → amplification glacier → amplification $\Delta PSUM \geq 10\%$ → amplification $\Delta PSUM > -5\%$ - $< 10\%$ → indifferent $\Delta PSUM \leq -5\%$ → diminishing
	flood, debris flood	PZI → indifferent glacier → indifferent precipitation → indifferent	PZI indifferent glacier → amplification $\Delta Rx1d$ or $Rx5d \geq 10\%$ → amplification $\Delta Rx1d$ or $Rx5d > -5\%$ - $< 10\%$ → indifferent $\Delta Rx1d$ or $Rx5d \leq -5\%$ → diminishing
	GLOF	PZI > 0 → amplification glacier → amplification precipitation → indifferent	PZI > 25 → amplification glacier → amplification $\Delta Rx1d$ or $Rx5d \geq 10\%$ → amplification $\Delta Rx1d$ or $Rx5d > -5\%$ - $< 10\%$ → indifferent $\Delta Rx1d$ or $Rx5d \leq -5\%$ → diminishing

Using these rules and existing information from the literature, we assess the impacts of climate change on triggering and initial processes, both for the time the event occurred in reality and for a future situation, i.e., towards the end of the century.

Most process chains in the database are related to threshold failures. In most of these cases (21), climate change has had an amplifying effect; the fact that a majority of the threshold failures had their starting zones in permafrost areas also supposes that a direct impact of climate change on the triggering process can be assumed as likely. Due to more intense precipitation, 5 process chain events show an amplifying effect. In total, 26 triggering processes show an amplifying effect of climate change, while 18 events show an indifferent effect (Figure 25 (a)).

In the future, for 30 events an amplifying effect is assumed, for 4 a diminishing effect and for 10 events the effect is indifferent (Figure 25 (b)). The diminishing cases are related to glacier retreat and to the decrease of heavy rainfall in the southern part of the Andes. However, glacial retreat can lead to glacier tongues terminating on steep relief where they become unstable and can trigger new process chains. Furthermore, debutressing as a result of glacier retreat can destabilize slopes.

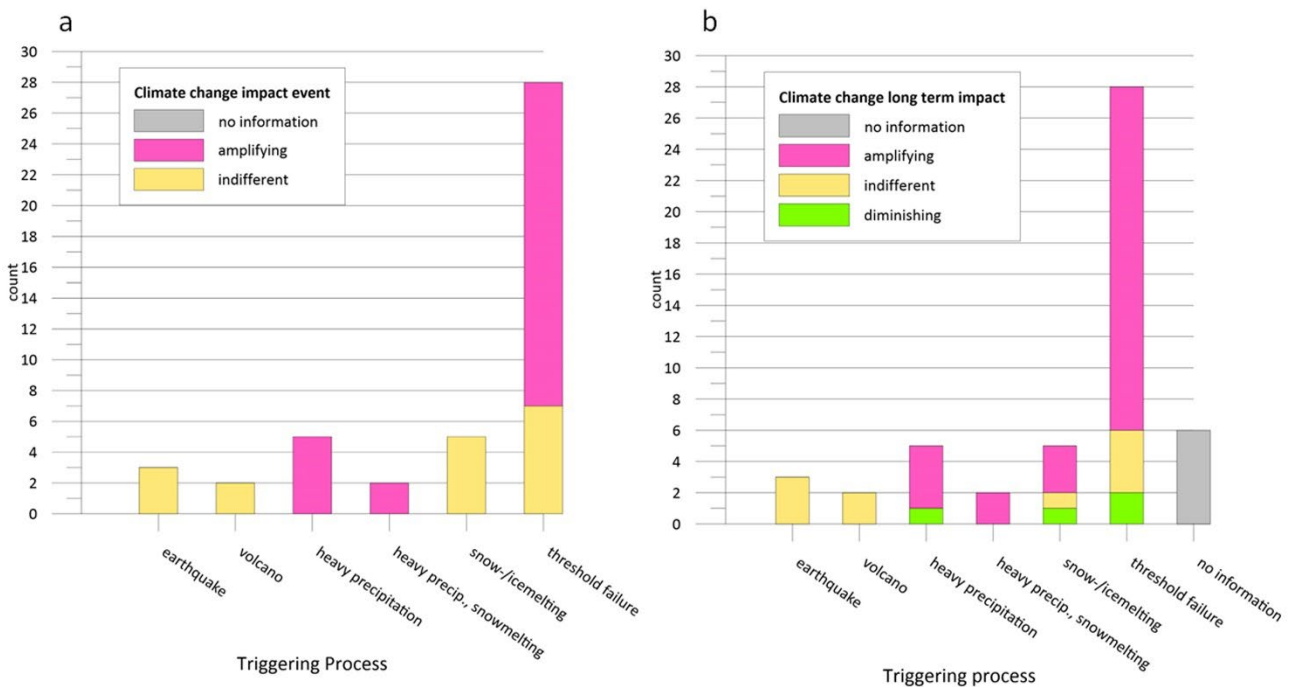


Figure 25. Climate change impact on the events that have occurred (a) and for the long term (b), related to the triggering process (including threshold failure).

The impact of climate change on initial processes is shown in Figure 26, indicating that more than 80% of these processes show an amplifying effect from climate change (Figure 26, (a)). In the case of GLOF events, an amplifying effect can be assumed to apply in all cases, except in the case of GLOFs relating to glacial surges. GLOFs from moraine dammed lakes as an initial process are per se typically closely associated with climate change because lake development is intimately coupled with glacial retreat (Harrison et al., 2018). Amplifying effects are also strong for ice avalanches, rock avalanches and rock/ice avalanches, in line with findings number of previous work (e.g. Allen and Huggel, 2013; Bessette-Kirton and Coe, 2020; Fischer et al., 2013; Gruber and Haeberli, 2007; Stoffel and Huggel, 2012). Only in 8 out of the 51 process chain events analyzed, climate change may have played an indifferent role.

When looking at the development until the end of the 21st century, the picture becomes something different (Figure 26 (b)). Whereas in 70% of all cases, further climate change is anticipated to have an amplifying effect on future processes, we observe some changes with respect to future GLOFs at the sites at which such events have occurred in the past. Indeed, only in 3 out of the 11 cases, we project an amplifying effect of climate change. The diminishing effect can be attributed to the reduction of the water volume stored in a dam that

was incised by the event or even eroded down to the bedrock so that only small impact waves can occur in the future. There are other cases where the lake was emptied during a GLOF and no further lake can develop. At the same time, however, ample evidence exists that the ongoing climate warming and glacier wasting will lead to the formation of myriads of new lakes across all mountain chains of the globe, which could eventually become sources of new GLOFs (e.g. Ahmed et al., 2021; Emmer et al., 2022; Mal et al., 2021; Zheng et al., 2021a). These new lakes may be more exposed to ice-rock avalanches, as they grow closer towards steep mountain headwalls characterized by degrading permafrost (Haeberli et al., 2017). Downwasting of glaciers and expansion of lakes can also directly destabilize adjacent lateral moraines, and expose the lake to new threats. This was illustrated, for example, in the 2021 GLOF from Jinwuco in Tibet, where the triggering slide from the side hit the terminal part of the lake, in an area that was covered by the glacier only a few years before (Zheng et al. 2021b).

Ice avalanches may diminish as a result of climate change in four out of five cases because many hanging glaciers will significantly retreat or completely disappear due to global warming, with the result that ice avalanches will no longer be possible. However, in the meantime, we may not rule out the possibility of a temporarily increasing likelihood for such events to occur as the warming could still destabilize the increasingly smaller, yet still-existing hanging glacier (e.g. Faillettaz et al., 2015). The evaluation of the database shows that slides, rock and rock/ice avalanches are again strongly associated with amplifying effects of climate change, due to the possible role of permafrost both in gradual weakening, and in enhancing the initial process.

For the process chains initiated by lahars, future climate change is considered to be indifferent. On the one hand a reduced ice volume on glacier-clad volcanoes means that water generated by the melting of ice during an eruption will be less and the potential for large-scale lahars will decrease. On the other hand, more intense rainfall will increase the potential for large-scale lahars.

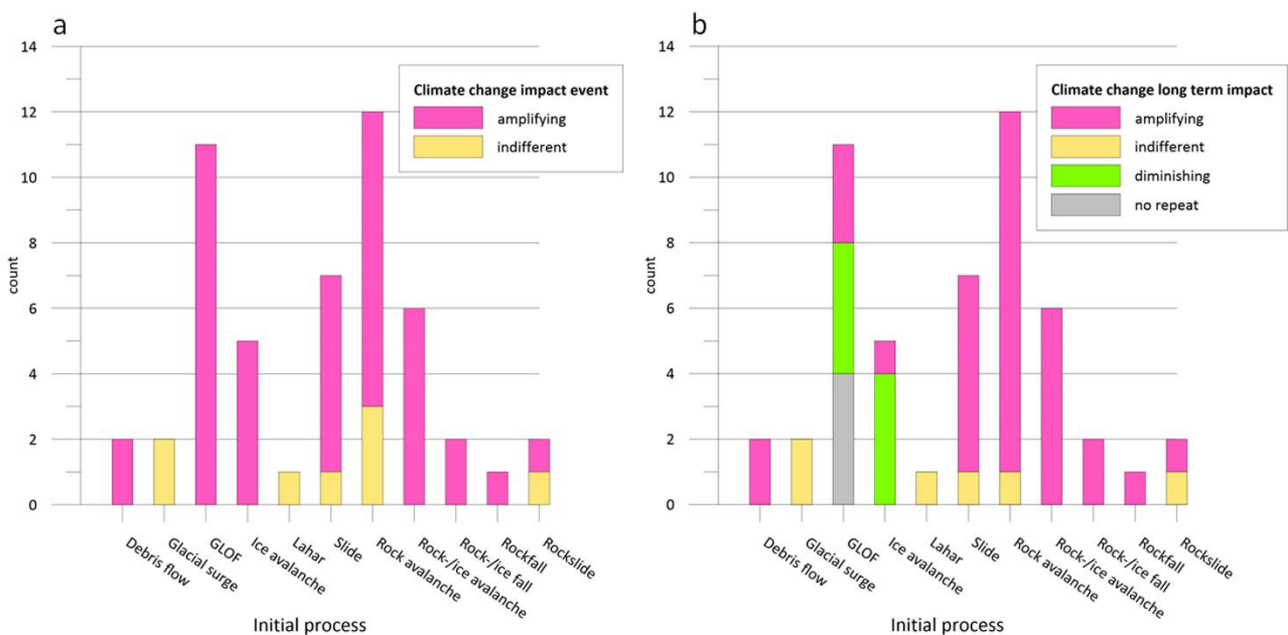


Figure 26. Climate change impact on the events that occurred (left) and for the long term (right), related to the initial process.

4.7 Kedarnath 2013 and Chamoli 2021 as idealized process chains

Based on the case studies (chapter 3) and classification scheme (chapter 4), two idealized process chain models emerge.

- 1) Catastrophic water release events (floods, lahars, GLOFs) commonly associated with an external trigger (heavy rainfall, snowmelt, volcanic eruption), that directly transform into debris flows and mudflows following immediate entrainment of loose debris and sediment.

- 2) Catastrophic mass movement events (typically rock-/ice avalanches) where there is often no discernable trigger, and numerous phase changes occur downstream from debris flows through to floods. GLOFS may be initiated as a direct secondary process, while delayed secondary events can be associated with valley blocking and lake formation.

Below we illustrate these idealized process chains, with reference to two well documented examples occurring within the same geographical context, in the Indian Himalayan state of Uttarakhand.

The catastrophic water release from a small lake ($0.4 \times 10^6 \text{ m}^3$) dammed at the side of Chorabari Glacier, just 1.2 km upstream from the village of Kedarnath, was triggered by extremely heavy rainfall which overwhelmed the limited capacity of the seasonal lake (Das et al., 2015; Singh et al., 2014). Unusually rapid snow-melt during the month preceding the early onset of the monsoon rainfall, and a limited amount of debris eroded from the surrounding slopes likely also contribute to high water levels in the lake (Allen et al., 2015). Early morning on June 17, the combined volume of melt-water, runoff and debris accumulating in the lake led to catastrophic breaching and erosion of the lateral moraine of the glacier, producing a devastating debris flow. Debris from the surface of the glacier and within steep channels ($>20^\circ$) upstream of the villages provided an additional source of volume (Allen et al., 2015). Kedarnath was destroyed, and as the debris flow transformed downstream into a hyperconcentrated flow and flood along the Mandakini river, further villages were damaged, and access into the valley was cut off. Unlike typical proglacial lakes that are in contact with their glacier, the size of Charobari lake dammed at the side of the glacier had remained essentially stable over many decades (Dobhal et al., 2013a). However, climate warming and associated lowering of the adjacent glacier has increased the height of the moraine dam, and removed lateral support, with 15 meters of vertical ice loss observed from 2003 to 2010 alone, and up to 0.072 km^2 of loose, steep moraine has been uncovered by glacial retreat over the past half-century (Dobhal et al., 2013b). In addition, climate change was assessed to have increased the probability of the rainfall event that ultimately triggered the process chain (Singh et al., 2014). Hence, climate change had both increased likelihood of the lake breaching over time, and amplified the volume of erodible debris within the downstream path (Allen et al., 2015). Given the full depth of the breach that occurred, the lake cannot refill, meaning a repeat event from this source cannot occur. However, climate change is increasing the threat of a similar cascade process initiating from supraglacial lakes that are enlarging on the tongue of Chorabari glacier.



Figure 27. Images of the 2013 Kedarnath disaster showing the location of Chorabari lake (black arrow (a)), from which it breached the lateral moraine of the adjacent glacier (inset image), transforming quickly into a catastrophic debris flow that destroyed the village of Kedarnath (b). Further downstream, the resulting flood inundated further villages and destroyed roads (c). Top images from Vaibhav Kaul, with inset image from Daniel Grossman, and bottom images from The Indian Express.

The catastrophic mass movement from the 5500 m Ronti Peak, in Chamoli district of Uttarakhand, February 7 2021, initiated as a $26.9 \times 10^6 \text{ m}^3$ failure of mostly rock (80%) and glacial ice (20%) (Bhardwaj and Sam, 2022). Melting of this ice from frictional heating as the flow descended over a local elevation range of $> 3000 \text{ m}$ (to the hydropower dam at Tapovan) was essential to the downstream evolution of the flow, transforming the rock and ice avalanche into a highly mobile debris flow. Along the valley floor, within what Zhang et al. (2022) refer to as the dynamic entrainment zone, colluvium (likely saturated), fluvial sediments, and fresh snow would have added to the initial mass of the flow. At the confluence of the Ronti Gad and Rishiganga rivers, significant deposition of sediment formed a 46 meter high dam, leading to formation of an 800 m long lake (Kropáček et al., 2021). Although this was initially a concern for authorities, lake outflow stabilized and began to exceed inflow with a few weeks, such that a secondary LLOF was avoided. Upon reaching the wider and lower gradient Dhauliganga river, the sediment load of the debris flow reduced, and a devastating flood continued downstream to destroy the Tapovan hydropower station, where most of the 204 fatalities and missing persons are located. The flood attenuated further downstream, but increased turbidity observed at Kanpur on the Ganges River some 2.5 weeks later, around 900 km from the source, are testimony to the extreme scale of this event (Shugar et al., 2021).

While several studies have focused on meteorological conditions prior to the rock and ice collapse (e.g. Sidique et al., 2022; Srivastava et al., 2022), there is no compelling evidence to suggest any direct external

triggering. Rather, analyses suggests that long term regional climate and related cryospheric change combined with unfavorable geological structure and extremely steep topography were the main predisposing factors (Shugar et al., 2021). Retrospective analyses of optical satellite imagery has revealed that the failure block moved 20 – 30 meters horizontally between 2016 and 2021, opening up a large fracture with a depth of up to 150 meters, but with no acceleration in velocity immediately prior to collapse (van Wyk de Vries et al., 2021). While the north facing failure zone is expected to contain cold permafrost, the presence of a glacier at the surface, and heat fluxes from the adjacent ice-free south face, likely led to local thermal anomalies (Shugar et al., 2021). Increasing ground temperatures and associated permafrost degradation over time, enhanced by meltwater entering the large fracture, could have gradually reduced the strength of the frozen rock mass until a critical threshold was reached. Additional weight associated with the loading of winter snow into the widened fracture is a possible, but highly speculative final contributing factor (van Wyk de Vries et al., 2021).

Importantly, both example cases illustrate that potential would have existed for monitoring and early warning, and hence, reduction in societal impacts could have been possible. In the case of a catastrophic water release as occurred at Kedarnath, early warning systems would typically be two-fold, monitoring the water source (e.g. lake level), and prediction or forecasts based on the external triggering factors (e.g. heavy rainfall). In combination, this can enable a warning time in the order of days to hours. As has been demonstrated in the case of Chamoli, process chains initiating as a catastrophic mass movement are typically more difficult to predict temporally, given the lack of any direct trigger in many cases (threshold failure), and challenges in real time monitoring of slope movement on high mountain faces. However, satellite-based monitoring to detect slope movement years to months before a critical threshold is reached enables problem zones to be identified, and instrumentation can then be positioned downstream to signal the initiation of any secondary hazards. Given a considerably reduced warning time, estimated at 10 – 20 minutes in the case of Chamoli (Shugar et al., 2021) effective risk management in such cases critically depends on downstream hazard mapping, and well-planned response strategies.

5. Conclusions

This first comprehensive compilation of geomorphic process chain events in high-mountain regions shows the diversity and complexity of such phenomena, but also their widespread occurrence across all major mountainous regions worldwide. The 51 process chain events assembled in the database cover High Mountain Asia, the European Alps and the Caucasus, North and South America and New Zealand. From the analysis of the broad characterization of the events the following key findings can be derived:

1. Process chains show a big diversity of processes involved but initialize as slope instability or water release events. Most slope processes according to the classification in Chapter 2 are associated with process chains, with the most frequent being rock and ice avalanches or a combination of both as well as slides. In addition, many events associated with water release are listed in the database. They occur in most mountain regions of the Earth.
2. Falls and slides have the highest relevance as initial process in process chains. As subsequent processes flow processes are most represented.
3. There is often no discernable trigger of a process chain, and the initial process is most frequently classified as a threshold failure. This is especially true for rock- and rock-/ice-avalanches. We ascribe this to intense weathering, glacial debulking, and permafrost degradation in cryosphere environments and to the seismic weakening in areas with high seismic activity. But we also understand that process chains triggered by volcanic eruptions may be underrepresented in this database where the focus was clearly on high mountain regions.
4. A look at the starting areas of the process chains shows clear regional differences. In the Asian mountains the median elevation is well below the maximum elevation of the mountains (<3000 m). In the other regions the difference is less than 2000 m. Seismic activity is obviously lower in the Alps and in the Coast Range than in tectonically active Asian, South American and New Zealand mountains.

5. We distinguish initial volume and total volume of process chains. In most cases, the initial zone of process chains lies in an area where permafrost occurs, and the total volume of events typically is larger from zones where permafrost is more extensive. The largest initial volumes are related to volcanic and earthquake triggering. For the initial processes the largest volumes are observed for lahars, rock or rock ice avalanches, rockfalls and slides. Surprisingly, our findings suggest that the initial volume does not influence the total volume or travel distance.
6. High relative relief is an important precondition for the occurrence of landslide-generated process chains, whereupon the range of LER values remains very wide. High relative relief is generally associated with first order watersheds.
7. An instantaneous linking of initial and subsequent processes occurs much more frequently than a delayed linking, making these processes difficult to predict, fast and often devastating. However, an exception to this is the occurrence of river damming by landslides and the formation of landslide dammed lakes which may fail after some time forming delayed distal components of landslide-generated process chains. Indeed, the blocking of receiving rivers with subsequent breaching and debris flows and/or debris floods is an important element of process chains.
8. We do not find a significant effect of ice and/or snow entrainment on larger travel reach; the assumption of such an effect cannot be confirmed through the evaluation of the events in the database. A reason for this may be that this effect is masked by other factors or that this effect only influences the initial process but not the entire process chain. However, we have to consider uncertainties in the definition of the reach. Length of process chains rarely exceed 120 km.
9. Longer process chains occur if fluvial processes are part of a process chain or when lakes exist along the trajectory of a process chain giving rise to instantaneous or delayed water release. But in some cases, lakes can reduce the reach if they retain sediments or high volume of water and thus cause flood waves to flatten out.
10. The presence of fine-grained material along the path leads to a larger reach of process chains. This may be due to buoyancy effect, which causes the sediments to be transported over longer distance. Thereby it must be taken into account that it is difficult to determine the reach of process chains in the case of pure water discharge if direct observations are lacking.
11. Climate change has had an amplification effect on the occurrence, scale, travel distance and velocity in the majority of the analyzed process chains mainly by the melting of mountain permafrost, glacier retreat, and changes in rainfall patterns. Amplifying can be effective on the triggering process as well as initial and subsequent processes. The impact of future climate change is not one-directional. In some cases, it can be still amplifying, in other cases the effect is to diminish process chains. An important implication of climate change is that we can expect an increase in the reach of events in the future, as glacial environments transform into paraglacial and fluvial environments. The impact can also change over time as shown for the ice avalanches.

The results of this study provide comprehensive information about the determining factors of the processes involved in mountain process chains. They therefore represent an important contribution to natural hazard assessments of process chains. Recent events like the Chamoli (Shugar et al., 2021) or Melamchi (Maharjan et al., 2021) disasters show that process chains have a high destructive potential on settlements and infrastructure in mountain regions. Despite their devastating nature, we realize that very limited information often exists on these events and that insights remain limited or established by proxy, presumably as their starting zones are often located in remote areas to which access is difficult. In view of the potentially high destruction caused by these process chains and the risk that they pose to mountain communities, it would be extremely valuable if future process chain events were documented in greater detail, and in line with the parameters described in this study.

Acknowledgement

Joel Fiddes for providing the Google Earth Engine script to calculate local elevation ranges (LER).

Open Research

The data that supports the research reported in this manuscript is available in the Supplementary Information (SI) file. The same file also contains all the information used to perform calculations.

References

1992. Agenda 21. <<https://sustainabledevelopment.un.org/outcomedocuments/agenda21>> (accessed 6 May 2020).
- Ahmed, R., Wani, G.F., Ahmad, S.T., Sahana, M., Singh, H., Ahmed, P., 2021. A Review of Glacial Lake Expansion and Associated Glacial Lake Outburst Floods in the Himalayan Region. *Earth Syst Environ* 5, 695–708. <https://doi.org/10.1007/s41748-021-00230-9>.
- Alean, J., 1985. Ice Avalanches: Some Empirical Information about their Formation and Reach. *J. Glaciol.* 31, 324–333. <https://doi.org/10.3189/S0022143000006663>.
- Allen, S., Frey, H., Haeberli, W., Huggel, C., Chiarle, M., Geertsema, M., 2022. Assessment principles for glacier and permafrost hazards in mountain regions, in: *Oxford Research Encyclopedia of Natural Hazard Science*.
- Allen, S., Huggel, C., 2013. Extremely warm temperatures as a potential cause of recent high mountain rockfall. *Global and Planetary Change* 107, 59–69. <https://doi.org/10.1016/j.gloplacha.2013.04.007>.
- Allen, S.K., Cox, S.C., Owens, I.F., 2011. Rock avalanches and other landslides in the central Southern Alps of New Zealand: a regional study considering possible climate change impacts. *Landslides* 8, 33–48. <https://doi.org/10.1007/s10346-010-0222-z>.
- Allen, S.K., Rastner, P., Arora, M., Huggel, C., Stoffel, M., 2015. Lake outburst and debris flow disaster at Kedarnath, June 2013: hydrometeorological triggering and topographic predisposition. *Landslides* 13, 1479–1491. <https://doi.org/10.1007/s10346-015-0584-3>.
- Ancey, C., Bardou, E., Funk, M., Huss, M., Werder, M.A., Trewthella, T., 2019. Hydraulic Reconstruction of the 1818 Giétro Glacial Lake Outburst Flood. *Water Resour. Res.* 55, 8840–8863. <https://doi.org/10.1029/2019WR025274>.
- Arias, P.A., Coppola, E., Jones, Richard G., Krinner, Gerhard, 2021. IPCC AR6 WG1 Technical Summary.
- Badoux, A., Hofer, M., Jonas, T., 2013. Hydrometeorologische Analyse des Hochwasserereignisses vom 10. Oktober 2011. Birmensdorf, Swiss Federal Institute for Forest, Snow and Landscape Research WSL.
- Baer, P., Huggel, C., McArdell, B.W., Frank, F., 2017. Changing debris flow activity after sudden sediment input: a case study from the Swiss Alps. *Geology Today* 33, 216–223. <https://doi.org/10.1111/gto.12211>.
- Ballesteros-Cánovas, J.A., Trappmann, D., Madrigal-González, J., Eckert, N., Stoffel, M., 2018. Climate warming enhances snow avalanche risk in the Western Himalayas. *Proceedings of the National Academy of Sciences of the United States of America* 115, 3410–3415. <https://doi.org/10.1073/pnas.1716913115>.
- Barla, G., Barla, M., 2001. Investigation and modelling of the Brenva Glacier rock avalanche on the Mount Blanc Range, in: *Proceedings of the ISRM Regional Symposium Eurock 2001, Espoo, Finlandia. 3-7 giugno 2001*, pp. 35–40.
- Becker, J.S., Johnston, D.M., Paton, D., Hancox, G.T., Davies, T.R., McSaveney, M.J., Manville, V.R., 2007. Response to landslide dam failure emergencies: issues resulting from the October 1999 Mount Adams landslide and dam-break flood in the Poerua River, Westland, New Zealand. *Natural hazards review* 8, 35–42.
- Beniston, M., Farinotti, D., Stoffel, M., Andreassen, L.M., Coppola, E., Eckert, N., Fantini, A., Giacona, F., Hauck, C., Huss, M., Huwald, H., Lehning, M., López-Moreno, J.-I., Magnusson, J., Marty, C., Morán-Tejeda, E., Morin, S., Naaim, M., Provenzale, A., Rabatel, A., Six, D., Stötter, J., Strasser, U., Terzago, S.,

- Vincent, C., 2018. The European mountain cryosphere: a review of its current state, trends, and future challenges. *The Cryosphere* 12, 759–794. <https://doi.org/10.5194/tc-12-759-2018>.
- Beniston, M., Stoffel, M., 2016. Rain-on-snow events, floods and climate change in the Alps: Events may increase with warming up to 4°C and decrease thereafter. *The Science of the total environment* 571, 228–236. <https://doi.org/10.1016/j.scitotenv.2016.07.146>.
- Bessette-Kirton, E.K., Coe, J.A., 2020. A 36-Year Record of Rock Avalanches in the Saint Elias Mountains of Alaska, With Implications for Future Hazards. *Front. Earth Sci.* 8, 293. <https://doi.org/10.3389/feart.2020.00293>.
- Bhardwaj, A., Sam, L., 2022. Reconstruction and Characterisation of Past and the Most Recent Slope Failure Events at the 2021 Rock-Ice Avalanche Site in Chamoli, Indian Himalaya. *Remote Sensing* 14, 949. <https://doi.org/10.3390/rs14040949>.
- Boeckli, L., Brenning, A., Gruber, S., Noetzli, J., 2012. Permafrost distribution in the European Alps: calculation and evaluation of an index map and summary statistics. *The Cryosphere* 6, 807–820. <https://doi.org/10.5194/tc-6-807-2012>.
- Boulton, N., Stead, D., Schwab, J., Geertsema, M., 2006. The Zymoetz River rock avalanche, June 2002, British Columbia, Canada. *Engineering Geology* 83, 76–93. <https://doi.org/10.1016/j.enggeo.2005.06.038>.
- Bovis, M.J., 1990. Rock-slope deformation at affliction creek, southern Coast Mountains, British Columbia. *Can. J. Earth Sci.* 27, 243–254.
- Bridel, P.-S., 1818. Course à l'éboulement du glacier de Gétroz et au lac de Mauvoisine, au fond de la vallée de Bagnes, 16 mai 1818, Vevey.
- Brönnimann, S., Krämer, D., 2016. Tambora und das "Jahr ohne Sommer" 1816: Klima, Mensch und Gesellschaft : a perspective on earth and human systems science = Tambora and the "year without summer" of 1816. *Geographica Bernensia Geographisches Institut der Universität Bern Schweiz, Bern*, 48 pp.
- Bründl, M., Bartelt, P., Schweizer, J., Keiler, M., Glade, T., 2010. Review and future challenges in snow avalanche risk analysis, in: Alcantara-Ayala, I., Goudie, A.S. (Eds.), *Geomorphological Hazards and Disaster Prevention*. Cambridge University Press, Cambridge, pp. 49–62.
- Byers, A.C., Rounce, D.R., Shugar, D.H., Lala, J.M., Byers, E.A., Regmi, D., 2019. A rockfall-induced glacial lake outburst flood, Upper Barun Valley, Nepal. *Landslides* 16, 533–549. <https://doi.org/10.1007/s10346-018-1079-9>.
- Carey, M., Huggel, C., Bury, J., Portocarrero, C., Haeberli, W., 2012. An integrated socio-environmental framework for glacier hazard management and climate change adaptation: lessons from Lake 513, Cordillera Blanca, Peru. *Climatic Change* 112, 733–767. <https://doi.org/10.1007/s10584-011-0249-8>.
- Carrega, P., Michelot, N., 2021. Une catastrophe hors norme d'origine météorologique le 2 octobre 2020 dans les montagnes des Alpes-Maritimes. *physio-geo*, 1–70. <https://doi.org/10.4000/physio-geo.12370>.
- Castebrunet, H., Eckert, N., Giraud, G., Durand, Y., Morin, S., 2014. Projected changes of snow conditions and avalanche activity in a warming climate: the French Alps over the 2020–2050 and 2070–2100 periods. *The Cryosphere* 8, 1673–1697. <https://doi.org/10.5194/tc-8-1673-2014>.
- Cenderelli, D.A., Wohl, E.E., 2001. Peak discharge estimates of glacial-lake outburst floods and "normal" climatic floods in the Mount Everest region, Nepal. *Geomorphology* 40, 57–90. [https://doi.org/10.1016/S0169-555X\(01\)00037-X](https://doi.org/10.1016/S0169-555X(01)00037-X).
- CH2018, C., 2018. Climate scenarios for Switzerland. National Centre for Climate Services Zurich.
- Chen, C., Zhang, L., Xiao, T., He, J., 2020. Barrier lake bursting and flood routing in the Yarlung Tsangpo Grand Canyon in October 2018. *Journal of Hydrology* 583, 124603. <https://doi.org/10.1016/j.jhydrol.2020.124603>.
- Chernomorets, S., Savernyuk, E., Petrakov, D., Dokukin, M., Gotsiridze, G., Gavardashvili, G., Drobyshev, V., Tutubalina, O.V., Zaporozhchenko, E., Kamenev, N., Kamenev, V., Kääh, A., Kargel, J., Huggel, C. (Eds.),

2016. The Devdorak ice-rock avalanche and consequent debris flow from the slope of Mt. Kazbek (Caucasus, Georgia) in 2014.
- Chernomorets, S.S., Petrakov, D.A., Aleynikov, A.A., Bekkiev, M.Y., Viskhadzhieva, K.S., Dokukin, M., Kalov, R.K., Kidyaeva, V.M., Krylenko, V.V., Krylenko, I.V., Krylenko, I.N., Rets, E.P., Savernyuk, E.A., Smirnov, A.M., 2018. The outburst of Bashkara glacier lake (Central Caucasus, Russia). On September 1, 2017. EC XXII. [https://doi.org/10.21782/EC2541-9994-2018-2\(61-70\)](https://doi.org/10.21782/EC2541-9994-2018-2(61-70)).
- Clague, J.J., Evans, S.G., 2000. A review of catastrophic drainage of moraine-dammed lakes in British Columbia. *Quaternary Science Reviews* 19, 1763–1783. [https://doi.org/10.1016/S0277-3791\(00\)00090-1](https://doi.org/10.1016/S0277-3791(00)00090-1).
- Clague, J.J., Evans, S.G., Blown, I.G., 1985. A debris flow triggered by the breaching of a moraine-dammed lake, Klattasine Creek, British Columbia. *Can. J. Earth Sci.* 22, 1492–1502. <https://doi.org/10.1139/e85-155>.
- Collins, B.D., Jibson, R.W., 2015. Assessment of existing and potential landslide hazards resulting from the April 25, 2015 Gorkha, Nepal earthquake sequence, Open-File Report 2015 ...
- Cook, K.L., Andermann, C., Gimbert, F., Adhikari, B.R., Hovius, N., 2018. Glacial lake outburst floods as drivers of fluvial erosion in the Himalaya. *Science (New York, N.Y.)* 362, 53–57. <https://doi.org/10.1126/science.aat4981>.
- Costa, J.E., Schuster, R.L., 1988. The formation and failure of natural dams. *Geological society of America bulletin* 100, 1054–1068.
- Damm, B., Felderer, A., 2013. Impact of atmospheric warming on permafrost degradation and debris flow initiation: A case study from the eastern European Alps. *E&G Quaternary Sci. J.* 62, 136–149. <https://doi.org/10.3285/eg.62.2.05>.
- Das, S., Kar, N.S., Bandyopadhyay, S., 2015. Glacial lake outburst flood at Kedarnath, Indian Himalaya: a study using digital elevation models and satellite images. *Nat Hazards* 77, 769–786.
- Deline, P., 2001. Recent Brenva rock avalanches (Valley of Aosta): new chapter in an old story. *Supplemento Geografia Fisica e Dinamica Quaternaria* 5, 55–63.
- Deline, P., 2003. Les grands écroulements rocheux de 1920 et de 1997 sur le glacier de la Brenva (massif du Mont-Blanc) : un vecteur géomorphologique pour la reconstitution de l'histoire holocène d'un bassin glaciaire de la haute montagne alpine. *edyte* 1, 169–182. <https://doi.org/10.3406/edyte.2003.873>.
- Deline, P., 2009. Interactions between rock avalanches and glaciers in the Mont Blanc massif during the late Holocene. *Quaternary Science Reviews* 28, 1070–1083. <https://doi.org/10.1016/j.quascirev.2008.09.025>.
- Deline, P., Alberto, W., Broccolato, M., Hungr, O., Noetzi, J., Ravanel, L., Tamburini, A., 2011. The December 2008 Crammont rock avalanche, Mont Blanc massif area, Italy. *Nat. Hazards Earth Syst. Sci.* 11, 3307–3318. <https://doi.org/10.5194/nhess-11-3307-2011>.
- Dixit, K., 2014. Anatomy of a Himalayan tsunami. <http://archive.nepalitimes.com/article/nation/Anatom-of-a-Himalayan-tsunami,1330>.
- Dobhal, D.P., Gupta, A.K., Manish, M., Khandelwal, D.D., 2013a. Kedarnath disaster: Facts and plausible causes. *Current Science* 105, 171–174.
- Dobhal, D.P., Mehta, M., Srivastava, D., 2013b. Influence of debris cover on terminus retreat and mass changes of Chorabari Glacier, Garhwal region, central Himalaya, India. *J. Glaciol.* 59, 961–971.
- Draebing, D., Krautblatter, M., Dikau, R., 2014. Interaction of thermal and mechanical processes in steep permafrost rock walls: A conceptual approach. *Geomorphology* 226, 226–235. <https://doi.org/10.1016/j.geomorph.2014.08.009>.
- Drobyshev, V.N., 2006. Glacial catastrophe of 20 September 2002 in North Osetia. *Russ. J. Earth Sci.* 8, 1–25. <https://doi.org/10.2205/2006ES000207>.
- Duhart, P., Sepúlveda, V., Garrido, N., Mella, M., Quiroz, D., Fernández, J., Moreno, H., Hermosilla, G., 2019. Santa lucía landslide disaster, chaitén-chile, the: origin and effects.

- Dunning, S.A., Armitage, P.J., 2011. The grain-size distribution of rock-avalanche deposits: implications for natural dam stability, in: *Natural and artificial rockslide dams*. Springer, pp. 479–498.
- Dunning, S.A., Mitchell, W.A., Rosser, N.J., Petley, D.N., 2007. The Hattian Bala rock avalanche and associated landslides triggered by the Kashmir Earthquake of 8 October 2005. *Engineering Geology* 93, 130–144. <https://doi.org/10.1016/j.enggeo.2007.07.003>.
- Dunning, S.A., Petley, D.N., Rosser, N.J., Strom, A.L., 2005. The morphology and sedimentology of valley confined rock-avalanche deposits and their effect on potential dam hazard, in: *Landslide risk management*. CRC Press, pp. 701–712.
- Durga Rao, K. H. V., Rao, Venkateshwar Rao, V., Dadhwal, V.K., Diwakar, P.G., 2014. Kedarnath flash floods: a hydrological and hydraulic simulation study. *Current Science*, 598–603.
- Dwivedi, S., Neupane, Y., 2013. Cause and mechanism of the Seti River flood, 5th May 2012, western Nepal. *Journal of Nepal Geological Society* 46. <https://doi.org/10.3126/jngs.v46i0.31576>.
- Emch+Berger AG, 2011. Ereignisdokumentation Hochwasser 10. Oktober 2011 Kander: Angaben für LLE.
- Emmer, A., 2016. Glacier Retreat and Glacial Lake Outburst Floods (GLOFs), in: Cutter, S.L. (Ed.), *Oxford research encyclopedias*. Oxford University Press, Oxford.
- Emmer, A., Harrison, S., Mergili, M., Allen, S., Frey, H., Huggel, C., 2020. 70 years of lake evolution and glacial lake outburst floods in the Cordillera Blanca (Peru) and implications for the future. *Geomorphology* 365, 107178. <https://doi.org/10.1016/j.geomorph.2020.107178>.
- Emmer, A., Vilímek, V., Klimeš, J., Cochachin, A., 2014. Glacier retreat, lakes development and associated natural hazards in Cordillera Blanca, Peru, in: *Landslides in cold regions in the context of climate change*. Springer, pp. 231–252.
- Emmer, A., Wood, J.L., Cook, S.J., Harrison, S., Wilson, R., Diaz-Moreno, A., Reynolds, J.M., Torres, J.C., Yarleque, C., Mergili, M., Jara, H.W., Bennett, G., Caballero, A., Glasser, N.F., Melgarejo, E., Riveros, C., Shannon, S., Turpo, E., Tinoco, T., Torres, L., Garay, D., Villafane, H., Garrido, H., Martinez, C., Apaza, N., Araujo, J., Poma, C., 2022. 160 glacial lake outburst floods (GLOFs) across the Tropical Andes since the Little Ice Age. *Global and Planetary Change* 208, 103722. <https://doi.org/10.1016/j.gloplacha.2021.103722>.
- Erokhin, S.A., Zaginaev, V.V., Meleshko, A.A., Ruiz-Villanueva, V., Petrakov, D.A., Chernomorets, S.S., Viskhadzhieva, K.S., Tutubalina, O.V., Stoffel, M., 2018. Debris flows triggered from non-stationary glacier lake outbursts: the case of the Teztor Lake complex (Northern Tian Shan, Kyrgyzstan). *Landslides* 15, 83–98. <https://doi.org/10.1007/s10346-017-0862-3>.
- Evans, S.G., Bishop, N.F., Fidel Smoll, L., Valderrama Murillo, P., Delaney, K.B., Oliver-Smith, A., 2009. A re-examination of the mechanism and human impact of catastrophic mass flows originating on Nevado Huascarán, Cordillera Blanca, Peru in 1962 and 1970. *Engineering Geology* 108, 96–118. <https://doi.org/10.1016/j.enggeo.2009.06.020>.
- Evans, S.G., Clague, J.J., 1994. Recent climatic change and catastrophic geomorphic processes in mountain environments. *Geomorphology*, 107–128.
- Evans, S.G., Clague, J.J., 1999. Rock avalanches on glaciers in the Coast and St. Elias Mountains, British Columbia, in: *Slope stability and landslides, 1999*, 115-123.
- Evans, S.G., Clague, J.J., Woodsworth, G.J., Hungr, O., 1989. The Pandemonium Creek rock avalanche, British Columbia. *Can. Geotech. J.* 26, 427–446. <https://doi.org/10.1139/t89-056>.
- Evans, S.G., Delaney, K.B., Hermanns, R.L., Strom, A., Scarascia-Mugnozza, G., 2011. The formation and behaviour of natural and artificial rockslide dams; implications for engineering performance and hazard management, in: *Natural and artificial rockslide dams*. Springer, pp. 1–75.
- Evans, S.G., Delaney, K.B., Rana, N.M., 2021. The occurrence and mechanism of catastrophic mass flows in the mountain cryosphere, in: Haerberli, W., Whiteman, C.A., Shroder, J.F. (Eds.), *Snow and ice-related hazards, risks, and disasters*. Elsevier, Amsterdam, pp. 541–596.

- Evans, S.G., Mugnozsa, G.S., Strom, A.L., Hermanns, R.L., Ischuk, A., Vinnichenko, S., 2006. Landslides from massive rock slope failure and associated phenomena, in: *Landslides from massive rock slope failure*. Springer, pp. 3–52.
- Faeh, R., Mueller, R., Rousselot, P., Veprek, R., Vetsch, D., Volz, C., Vonwiller, L., Farshi, D., 2011. BASEMENT–Basic Simulation Environment for Computation of Environmental Flow and Natural Hazard Simulation, VAW, ETH Zurich. <https://basement.ethz.ch/>.
- Faillietaz, J., Funk, M., Sornette, D., 2012. Instabilities on Alpine temperate glaciers: new insights arising from the numerical modelling of Allalingsletscher (Valais, Switzerland). *Nat. Hazards Earth Syst. Sci.* 12, 2977–2991. <https://doi.org/10.5194/nhess-12-2977-2012>.
- Faillietaz, J., Funk, M., Vincent, C., 2015. Avalanching glacier instabilities: Review on processes and early warning perspectives. *Rev. Geophys.* 53, 203–224. <https://doi.org/10.1002/2014RG000466>.
- Faillietaz, J., Sornette, D., Funk, M., 2011. Numerical modeling of a gravity-driven instability of a cold hanging glacier: reanalysis of the 1895 break-off of Altelsletscher, Switzerland. *J. Glaciol.* 57, 817–831. <https://doi.org/10.3189/002214311798043852>.
- Fan, X., Scaringi, G., Korup, O., West, A.J., Westen, C.J., Tanyas, H., Hovius, N., Hales, T.C., Jibson, R.W., Allstadt, K.E., Zhang, L., Evans, S.G., Xu, C., Li, G., Pei, X., Xu, Q., Huang, R., 2019. Earthquake-Induced Chains of Geologic Hazards: Patterns, Mechanisms, and Impacts. *Rev. Geophys.* 57, 421–503. <https://doi.org/10.1029/2018RG000626>.
- Farinotti, D., Round, V., Huss, M., Compagno, L., Zekollari, H., 2019. Large hydropower and water-storage potential in future glacier-free basins. *Nature* 575, 341–344.
- Ferrari, F., Giacomini, A., Thoeni, K., 2016. Qualitative Rockfall Hazard Assessment: A Comprehensive Review of Current Practices. *Rock Mech Rock Eng* 49, 2865–2922. <https://doi.org/10.1007/s00603-016-0918-z>.
- Field, C.B., Barros, V., Stocker, T.F., Dahe, Q., 2012. *Managing the Risks of Extreme Events and Disasters to Advance Climate Change Adaptation: Special Report of the Intergovernmental Panel on Climate Change*, 1st ed. Cambridge University Press, New York, 594 pp.
- Fischer, L., Huggel, C., Käab, A., Haeberli, W., 2013. Slope failures and erosion rates on a glacierized high-mountain face under climatic changes. *Earth Surf. Process. Landforms* 38, 836–846. <https://doi.org/10.1002/esp.3355>.
- Fischer, L., Käab, A., Huggel, C., Noetzli, J., 2006. Geology, glacier retreat and permafrost degradation as controlling factors of slope instabilities in a high-mountain rock wall: the Monte Rosa east face. *Nat. Hazards Earth Syst. Sci.*, 761–772.
- Fölmli, C., Schlunegger, F., Herwegh, M., 2015. Murgänge und Felsstürze im Gebiet Ritzlihorn-Spreitgraben, Guttannen BE : Analyse der Felskonditionierung und des Mur- und Sturzkegels. <https://doi.org/10.5169/seals-632525>.
- Frank, F., Huggel, C., McArdeell, B.W., Vieli, A., 2019. Landslides and increased debris-flow activity: A systematic comparison of six catchments in Switzerland. *Earth Surf. Process. Landforms* 44, 699–712. <https://doi.org/10.1002/esp.4524>.
- Freudiger, D., Kohn, I., Stahl, K., Weiler, M., 2014. Large-scale analysis of changing frequencies of rain-on-snow events with flood-generation potential. *Hydrol. Earth Syst. Sci.* 18, 2695–2709. <https://doi.org/10.5194/hess-18-2695-2014>.
- Friele, P., Jakob, M., Clague, J., 2008. Hazard and risk from large landslides from Mount Meager volcano, British Columbia, Canada. *Georisk: Assessment and Management of Risk for Engineered Systems and Geohazards* 2, 48–64. <https://doi.org/10.1080/17499510801958711>.
- Friele, P., Millard, T.H., Mitchell, A., Allstadt, K.E., Menounos, B., Geertsema, M., Clague, J.J., 2020. Observations on the May 2019 Joffre Peak landslides, British Columbia. *Landslides* 17, 913–930. <https://doi.org/10.1007/s10346-019-01332-2>.
- Fuchs, G., Linner, M., 1995. Geological traverse across the western Himalaya—a contribution to the geology of eastern Ladakh, Lahul, and Chamba. *Jahrbuch der Geologischen Bundesanstalt* 138, 665–685.

- Fujita, K., Inoue, H., Izumi, T., Yamaguchi, S., Sadakane, A., Sunako, S., Nishimura, K., Immerzeel, W.W., Shea, J.M., Kayastha, R.B., Sawagaki, T., Breashears, D.F., Yagi, H., Sakai, A., 2017. Anomalous winter-snow-amplified earthquake-induced disaster of the 2015 Langtang avalanche in Nepal. *Nat. Hazards Earth Syst. Sci.* 17, 749–764. <https://doi.org/10.5194/nhess-17-749-2017>.
- GAPHAZ, 2017. Assessment of Glacier and Permafrost Hazards in Mountain Regions. Technical Guidance Document: Prepared by Allen, S., Frey, H., Huggel, C. et al. Standing Group on Glacier and Permafrost Hazards in Mountains (GAPHAZ) of the International Association of Cryospheric Sciences (IACS) and the International Permafrost Association (IPA). Zurich, Switzerland / Lima, Peru.
- Gärtner-Roer, I., Nussbaumer, S.U., Hüsler, F., Zemp, M., 2019. Worldwide Assessment of National Glacier Monitoring and Future Perspectives. *Mountain Research and Development* 39. <https://doi.org/10.1659/MRD-JOURNAL-D-19-00021.1>.
- Geertsema, M., Clague, J.J., Schwab, J.W., Evans, S.G., 2006. An overview of recent large catastrophic landslides in northern British Columbia, Canada. *Engineering Geology* 83, 120–143. <https://doi.org/10.1016/j.enggeo.2005.06.028>.
- Geertsema, M., Menounos, B., Bullard, G., Carrivick, J.L., Clague, J.J., Dai, C., Donati, D., Ekstrom, G., Jackson, J.M., Lynett, P., Pichierri, M., Pon, A., Shugar, D.H., Stead, D., Del Bel Belluz, J., Friele, P., Giesbrecht, I., Heathfield, D., Millard, T., Nasonova, S., Schaeffer, A.J., Ward, B.C., Blaney, D., Blaney, E., Brillon, C., Bunn, C., Floyd, W., Higman, B., Hughes, K.E., McInnes, W., Mukherjee, K., Sharp, M.A., 2022. The 28 November 2020 Landslide, Tsunami, and Outburst Flood – A Hazard Cascade Associated With Rapid Deglaciation at Elliot Creek, British Columbia, Canada. *Geophys. Res. Lett.* 49. <https://doi.org/10.1029/2021GL096716>.
- Geertsema, M., Menounos, B., Shugar, D., Millard, T., Ward, B., Ekstrom, G., Clague, J., Lynett, P., Friele, P., Schaeffer, A., Jackson, J., Higman, B., Dai, C., Brillon, C., Heathfield, D., Bullard, G., Giesbrecht, I., Hughes, K., 2021. A landslide-generated tsunami and outburst flood at Elliot Creek, coastal British Columbia. *EGU General Assembly Conference Abstracts*, EGU21-9148.
- Ghiglino Antunez, L., 1971. Alud de Yungay y Ranrahirca del 31 de Mayo de 1970. *Revista Peruana de Andinismo y Glaciología* 9, 84–88.
- Giacona, F., Eckert, N., Corona, C., Mainieri, R., Morin, S., Stoffel, M., Martin, B., Naaim, M., 2021. Upslope migration of snow avalanches in a warming climate. *Proceedings of the National Academy of Sciences of the United States of America* 118. <https://doi.org/10.1073/pnas.2107306118>.
- Gilbert, A., Leinss, S., Kargel, J., Käab, A., Gascoïn, S., Leonard, G., Berthier, E., Karki, A., Yao, T., 2018. Mechanisms leading to the 2016 giant twin glacier collapses, Aru Range, Tibet. *The Cryosphere* 12, 2883–2900. <https://doi.org/10.5194/tc-12-2883-2018>.
- Gill, J.C., Malamud, B.D., 2014. Reviewing and visualizing the interactions of natural hazards. *Rev. Geophys.* 52, 680–722. <https://doi.org/10.1002/2013RG000445>.
- Gill, J.C., Malamud, B.D., 2016. Hazard interactions and interaction networks (cascades) within multi-hazard methodologies. *Earth Syst. Dynam.* 7, 659–679. <https://doi.org/10.5194/esd-7-659-2016>.
- Gischig, V., Preisig, G., Eberhardt, E., 2016. Numerical Investigation of Seismically Induced Rock Mass Fatigue as a Mechanism Contributing to the Progressive Failure of Deep-Seated Landslides. *Rock Mech Rock Eng* 49, 2457–2478. <https://doi.org/10.1007/s00603-015-0821-z>.
- Global Terrestrial Network For Glaciers, 2017. GTN-G Glacier Regions (GlacReg).
- Gnyawali, K.R., Xing, A., Zhuang, Y., 2020. Dynamic analysis of the multi-staged ice–rock debris avalanche in the Langtang valley triggered by the 2015 Gorkha earthquake, Nepal. *Engineering Geology* 265, 105440.
- Gobiet, A., Kotlarski, S., Beniston, M., Heinrich, G., Rajczak, J., Stoffel, M., 2014. 21st century climate change in the European Alps—a review. *The Science of the total environment* 493, 1138–1151. <https://doi.org/10.1016/j.scitotenv.2013.07.050>.
- Granados, H.D., Miranda, P.J., Núñez, G.C., Alzate, B.P., Mothes, P., Roa, H.M., Correa, B.E.C., Ramos, J.C., 2021. Hazards at ice-clad volcanoes: phenomena, processes, and examples from Mexico, Colombia, Ecuador, and Chile, in: *Snow and Ice-Related Hazards, Risks, and Disasters*. Elsevier, pp. 597–639.

- Gruber, S., 2007. A mass-conserving fast algorithm to parameterize gravitational transport and deposition using digital elevation models. *Water Resour. Res.* 43.
- Gruber, S., 2012. Derivation and analysis of a high-resolution estimate of global permafrost zonation. *The Cryosphere* 6, 221–233. <https://doi.org/10.5194/tc-6-221-2012>.
- Gruber, S., Haeberli, W., 2007. Permafrost in steep bedrock slopes and its temperature-related destabilization following climate change. *J. Geophys. Res.* 112. <https://doi.org/10.1029/2006JF000547>.
- Gruber, S., Hoelzle, M., Haeberli, W., 2004. Permafrost thaw and destabilization of Alpine rock walls in the hot summer of 2003. *Geophys. Res. Lett.* 31, n/a-n/a. <https://doi.org/10.1029/2004GL020051>.
- Guthrie, R.H., Friele, P., Allstadt, K., Roberts, N., Evans, S.G., Delaney, K.B., Roche, D., Clague, J.J., Jakob, M., 2012. The 6 August 2010 Mount Meager rock slide-debris flow, Coast Mountains, British Columbia: characteristics, dynamics, and implications for hazard and risk assessment. *Nat. Hazards Earth Syst. Sci.* 12, 1277–1294. <https://doi.org/10.5194/nhess-12-1277-2012>.
- Haeberli, W., Huggel, C., Kääb, A., Zraggen-Oswald, S., Polkvoj, A., Galushkin, I., Zotikov, I., Osokin, N., 2004. The Kolka-Karmadon rock/ice slide of 20 September 2002: an extraordinary event of historical dimensions in North Ossetia, Russian Caucasus. *J. Glaciol.* 50, 533–546. <https://doi.org/10.3189/172756504781829710>.
- Haeberli, W., Kääb, A., Mühll, D.V., Teyssie, P., 2001. Prevention of outburst floods from periglacial lakes at Grubengletscher, Valais, Swiss Alps. *J. Glaciol.* 47, 111–122.
- Haeberli, W., Schaub, Y., Huggel, C., 2017. Increasing risks related to landslides from degrading permafrost into new lakes in de-glaciating mountain ranges. *Geomorphology* 293, 405–417. <https://doi.org/10.1016/j.geomorph.2016.02.009>.
- Hancox, G.T., McSaveney, M.J., Manville, V.R., Davies, T.R., 2005. The October 1999 Mt Adams rock avalanche and subsequent landslide dam-break flood and effects in Poerua river, Westland, New Zealand. *New Zealand Journal of Geology and Geophysics* 48, 683–705.
- Harrison, S., Kargel, J.S., Huggel, C., Reynolds, J., Shugar, D.H., Betts, R.A., Emmer, A., Glasser, N., Haritashya, U.K., Klimeš, J., Reinhardt, L., Schaub, Y., Wiltshire, A., Regmi, D., Vilímek, V., 2018. Climate change and the global pattern of moraine-dammed glacial lake outburst floods. *The Cryosphere* 12, 1195–1209. <https://doi.org/10.5194/tc-12-1195-2018>.
- Hartmann, J., Moosdorf, N., 2012. The new global lithological map database GLiM: A representation of rock properties at the Earth surface. *Geochem. Geophys. Geosyst.* 13. <https://doi.org/10.1029/2012GC004370>.
- Hasler, A., Gruber, S., Beutel, J., 2012. Kinematics of steep bedrock permafrost. *J. Geophys. Res.* 117, n/a-n/a. <https://doi.org/10.1029/2011JF001981>.
- Hauser, A., 2002. Rock avalanche and resulting debris flow in Estero Parraguirre and Rio Colorado, Regio'n Metropolitana, Chile. *Catastrophic landslides: effects, occurrence and mechanisms. Geological Society of America Reviews in Engineering Geology* 15, 135–148.
- Häusler, H., Ng, F., Kopecny, A., Leber, D., 2016. Remote-sensing-based analysis of the 1996 surge of Northern Inylchek Glacier, central Tien Shan, Kyrgyzstan. *Geomorphology* 273, 292–307. <https://doi.org/10.1016/j.geomorph.2016.08.021>.
- Hock, R., Rasul, G., Adler, C., Cáceres, B., Gruber, S., Hirabayashi, Y., Jackson, M., Kääb, A., Kang, S., Kutuzov, S., Milner, A., Molau, U., Morin, S., Orlove, B., Steltzer, H., 2019. High Mountain Areas, in: Pörtner, H.-O., Roberts, D.C., Masson-Delmotte, V., Zhai, P., Tignor, M., Poloczanska, E., Mintenbeck, K., Alegría, A., Nicolai, M., Okem, A., Petzold, J., Rama, B., Weyer, N.M. (Eds.), *IPCC special report on the ocean and cryosphere in a changing climate*, pp. 131–202.
- Holm, K., Bovis, M., Jakob, M., 2004. The landslide response of alpine basins to post-Little Ice Age glacial thinning and retreat in southwestern British Columbia. *Geomorphology* 57, 201–216. [https://doi.org/10.1016/S0169-555X\(03\)00103-X](https://doi.org/10.1016/S0169-555X(03)00103-X).
- Hong, Y., Adhikari, P., Gourley, J.J., 2013. Flood Hazard and Disaster, in: Bobrowsky, P.T. (Ed.), *Encyclopedia of natural hazards: Includes case studies*. Springer Reference, Dordrecht, pp. 326–336.

- Huang, R., Li, W., 2014. Post-earthquake landsliding and long-term impacts in the Wenchuan earthquake area, China. *Engineering Geology* 182, 111–120. <https://doi.org/10.1016/j.enggeo.2014.07.008>.
- Huggel, C., 2009. Recent extreme slope failures in glacial environments: effects of thermal perturbation. *Quaternary Science Reviews* 28, 1119–1130. <https://doi.org/10.1016/j.quascirev.2008.06.007>.
- Huggel, C., Carey, M., Emmer, A., Frey, H., Walker-Crawford, N., Wallimann-Helmer, I., 2020. Anthropogenic climate change and glacier lake outburst flood risk: local and global drivers and responsibilities for the case of lake Palcacocha, Peru. *Natural Hazards and Earth System Sciences* 20, 2175–2193. <https://doi.org/10.5194/nhess-20-2175-2020>.
- Huggel, C., Ceballos, J.L., Pulgarín, B., Ramírez, J., Thouret, J.-C., 2007. Review and reassessment of hazards owing to volcano–glacier interactions in Colombia. *Ann. Glaciol.* 45, 128–136. <https://doi.org/10.3189/172756407782282408>.
- Huggel, C., Haeblerli, W., Käab, A., Bieri, D., Richardson, S., 2004. An assessment procedure for glacial hazards in the Swiss Alps. *Can. Geotech. J.* 41, 1068–1083. <https://doi.org/10.1139/T04-053>.
- Huggel, C., Käab, A., Haeblerli, W., Krummenacher, B., 2003. Regional-scale GIS-models for assessment of hazards from glacier lake outbursts: evaluation and application in the Swiss Alps. *Nat. Hazards Earth Syst. Sci.* 3, 647–662.
- Huggel, C., Zraggen-Oswald, S., Haeblerli, W., Käab, A., Polkvoj, A., Galushkin, I., Evans, S.G., 2005. The 2002 rock/ice avalanche at Kolka/Karmadon, Russian Caucasus: assessment of extraordinary avalanche formation and mobility, and application of QuickBird satellite imagery. *Natural Hazards and Earth System Sciences*, 173–187.
- Hungr, O., 2013. Debris Flow, in: Bobrowsky, P.T. (Ed.), *Encyclopedia of natural hazards: Includes case studies*. Springer Reference, Dordrecht, pp. 149–151.
- Hungr, O., 2016. A review of landslide hazard and risk assessment methodology, in: Aversa, S., Cascini, L., Picarelli, L., Scavia, C. (Eds.), *Landslides and engineered slopes: Experience, theory and practice : proceedings of the 12th International Symposium on Landslides, Napoli, Italy, 12-19 June 2016*. CRC Press, Boca Raton, London, New York, Leiden, pp. 3–27.
- Hungr, O., Evans, S.G., 2004. Entrainment of debris in rock avalanches: An analysis of a long run-out mechanism. *Geol Soc America Bull* 116, 1240. <https://doi.org/10.1130/B25362.1>.
- Hungr, O., Leroueil, S., Picarelli, L., 2014. The Varnes classification of landslide types, an update. *Landslides* 11, 167–194. <https://doi.org/10.1007/s10346-013-0436-y>.
- Hungr, O., McDougall, S., Bovis, M., 2005. Entrainment of material by debris flows, in: *Debris-flow hazards and related phenomena*. Springer, pp. 135–158.
- Hutchinson, J.N., 1990. General report: morphological and geotechnical parameters of landslides in relation to geology and hydrogeology., in: Bonnard, C. (Ed.), *Landslides: Proceedings of the Fifth International Symposium on Landslides, 10 - 15 July 1988, Lausanne = Glissements de terrain*. Balkema, Rotterdam, pp. 3–35.
- IPCC, 2019. *IPCC Special Report on the Ocean and Cryosphere in a Changing Climate*.
- Iturbide, M., Fernández, J., Gutiérrez, J.M., Bedia, J., Cimadevilla, E., Díez-Sierra, J., Manzanar, R., Casanueva, A., Baño-Medina, J., Milovac, J., Herrera, S., Cofiño, A.S., San Martín, D., García-Díez, M., Hauser, M., Huard, D., Yelekci, Ö., 2021. Repository supporting the implementation of FAIR principles in the IPCC-WGI Atlas. Zenodo.
- Iturrizaga, L., 2011. Glacier Lake Outburst Floods, in: Singh, V.P., Singh, P., Haritashya, U.K. (Eds.), *Encyclopedia of Snow, Ice and Glaciers*. Springer Science+Business Media B.V, Dordrecht, pp. 381–399.
- Iverson, R.M., 1997. The physics of debris flows. *Reviews of geophysics*, 245–296.
- Iverson, R.M., 2014. Debris flows: behaviour and hazard assessment. *Geology Today*, 15–20.
- Iverson, R.M., George, D.L., Logan, M., 2016. Debris flow runup on vertical barriers and adverse slopes. *J. Geophys. Res. Earth Surf.* 121, 2333–2357. <https://doi.org/10.1002/2016JF003933>.

- Jiskoot, H., 2011. Glacier Surging, in: Singh, V.P., Singh, P., Haritashya, U.K. (Eds.), *Encyclopedia of Snow, Ice and Glaciers*. Springer Science+Business Media B.V, Dordrecht, pp. 415–428.
- Jordan, P., Slaymaker, O., 1991. Holocene sediment production in Lillooet River basin, British Columbia: A sediment budget approach. *Géographie physique et Quaternaire* 45, 45–57.
- Kääb, A., Jacquemart, M., Gilbert, A., Leinss, S., Girod, L., Huggel, C., Falaschi, D., Ugalde, F., Petrakov, D., Chernomorets, S., Dokukin, M., Paul, F., Gascoïn, S., Berthier, E., Kargel, J.S., 2021. Sudden large-volume detachments of low-angle mountain glaciers – more frequent than thought? *The Cryosphere* 15, 1751–1785. <https://doi.org/10.5194/tc-15-1751-2021>.
- Kapos, V., Rhind, J., Edwards, M., Price, M.F., Ravilious, C., 2000. Developing a map of the world’s mountain forests, in: Price, M.F., Butt, N. (Eds.), *Forests in sustainable mountain development: a state of knowledge report for 2000*. Task Force on Forests in Sustainable Mountain Development. CABI, Wallingford, pp. 4–19.
- Kappes, M.S., Keiler, M., Elverfeldt, K. von, Glade, T., 2012. Challenges of analyzing multi-hazard risk: a review. *Nat Hazards* 64, 1925–1958. <https://doi.org/10.1007/s11069-012-0294-2>.
- Kappes, M.S., Keiler, M., Glade, T., 2010. Mountain risks: bringing science to society, in: *Proceedings of the international conference, Florence, chapter from single-to multi-hazard risk analyses: a concept addressing emerging challenges*.
- Kargel, J., Leonard, G., Paudel, L., Regmi, D., Bajracharya, S., Fort, M., Joshi, S., Poudel, K., Thapa, B., Watanabe, T., 2014. The 2012 Seti River flood disaster and alpine cryospheric hazards facing Pokhara, Nepal. *EGU General Assembly Conference Abstracts*, 12448.
- Kargel, J.S., 2014. Notes from the Field: One Scientist’s Search for the Causes of the Deadly Seti River Flash Flood. *NASA Earth Observatory*, Jan. 24, 20-14. <https://earthobservatory.nasa.gov/blogs/fromthefield/2014/01/24/setiriverclues/>.
- Kargel, J.S., Leonard, G.J., Shugar, D.H., Haritashya, U.K., Bevington, A., Fielding, E.J., Fujita, K., Geertsema, M., Miles, E.S., Steiner, J., Anderson, E., Bajracharya, S., Bawden, G.W., Breashears, D.F., Byers, A., Collins, B., Dhital, M.R., Donnellan, A., Evans, T.L., Geai, M.L., Glasscoe, M.T., Green, D., Gurung, D.R., Heijenk, R., Hilborn, A., Hudnut, K., Huyck, C., Immerzeel, W.W., Liming, J., Jibson, R., Kääb, A., Khanal, N.R., Kirschbaum, D., Kraaijenbrink, P.D.A., Lamsal, D., Shiyin, L., Mingyang, L., McKinney, D., Nahirnick, N.K., Zhuotong, N., Ojha, S., Olsenholler, J., Painter, T.H., Pleasants, M., Pratima, K.C., Yuan, Q.I., Raup, B.H., Regmi, D., Rounce, D.R., Sakai, A., Donghui, S., Shea, J.M., Shrestha, A.B., Shukla, A., Stumm, D., van der Kooij, M., Voss, K., Xin, W., Weihs, B., Wolfe, D., Lizong, W., Xiaojun, Y., Yoder, M.R., Young, N., 2016. Geomorphic and geologic controls of geohazards induced by Nepal’s 2015 Gorkha earthquake. *Science (New York, N.Y.)* 351, aac8353. <https://doi.org/10.1126/science.aac8353>.
- Kershaw, J.A., Clague, J.J., Evans, S.G., 2005. Geomorphic and sedimentological signature of a two-phase outburst flood from moraine-dammed Queen Bess Lake, British Columbia, Canada. *Earth Surf. Process. Landforms* 30, 1–25.
- Kirschbaum, D., Watson, C.S., Rounce, D.R., Shugar, D., Kargel, J.S., Haritashya, U.K., Amatya, P., Shean, D., Anderson, E.R., Jo, M., 2019. The State of Remote Sensing Capabilities of Cascading Hazards over High Mountain Asia. *Frontiers in earth science* 7. <https://doi.org/10.3389/feart.2019.00197>.
- Konagai, K., Sattar, A., 2012. Partial breaching of Hattian Bala Landslide Dam formed in the 8th October 2005 Kashmir Earthquake, Pakistan. *Landslides* 9, 1–11. <https://doi.org/10.1007/s10346-011-0280-x>.
- Kornilova, E.D., Krylenko, I.N., Rets, E.P., Motovilov, Y.G., Bogachenko, E.M., Krylenko, I.V., Petrakov, D.A., 2021. Modeling of Extreme Hydrological Events in the Baksan River Basin, the Central Caucasus, Russia. *Hydrology* 8, 24. <https://doi.org/10.3390/hydrology8010024>.
- Kortiev, L.I., Kortieva, V.L., Chochiev, S.V., 2009. Analysis of the social, environmental and economic damage caused by Kolka Glacier collapse. *Vestnik Vladikavkazskogo Nauchnogo* 9, 41–42.
- Kotlyakov, V.M., Rototaeva, O.V., Nosenko, G.A., 2004. The September 2002 Kolka Glacier Catastrophe in North Ossetia, Russian Federation: Evidence and Analysis. *Mountain Research and Development* 24, 78–83. [https://doi.org/10.1659/0276-4741\(2004\)024\[0078:TSKGCI\]2.0.CO;2](https://doi.org/10.1659/0276-4741(2004)024[0078:TSKGCI]2.0.CO;2).

- Krautblatter, M., Funk, D., Günzel, F.K., 2013. Why permafrost rocks become unstable: a rock-ice-mechanical model in time and space. *Earth Surf. Process. Landforms* 38, 876–887. <https://doi.org/10.1002/esp.3374>.
- Kropáček, J., Vilímek, V., Mehrishi, P., 2021. A preliminary assessment of the Chamoli rock and ice avalanche in the Indian Himalayas by remote sensing. *Landslides* 18, 3489–3497. <https://doi.org/10.1007/s10346-021-01742-1>.
- Lacroix, P., 2016. Landslides triggered by the Gorkha earthquake in the Langtang valley, volumes and initiation processes. *Earth Planets Space* 68. <https://doi.org/10.1186/s40623-016-0423-3>.
- Lambiel, C., Reynard, E., Corboz, P., Bardou, E., Payot, C., Deslarzes, B., 2020. Reconstructing past flood events from geomorphological and historical data. The Giétro outburst flood in 1818. *Journal of Maps* 16, 500–511. <https://doi.org/10.1080/17445647.2020.1763487>.
- Leinss, S., Bernardini, E., Jacquemart, M., Dokukin, M., 2021. Glacier detachments and rock-ice avalanches in the Petra Pervogo range, Tajikistan (1973–2019). *Nat. Hazards Earth Syst. Sci.* 21, 1409–1429. <https://doi.org/10.5194/nhess-21-1409-2021>.
- Liu, B., Siu, Y.L., Mitchell, G., 2016. Hazard interaction analysis for multi-hazard risk assessment: a systematic classification based on hazard-forming environment. *Nat. Hazards Earth Syst. Sci.* 16, 629–642. <https://doi.org/10.5194/nhess-16-629-2016>.
- Maharjan, S.B., Steiner, J.F., Shrestha, A.B., Maharjan, A., Nepal, S., Shrestha, M.S., Bajracharya, B., Rasul, G., Shrestha, M., Jackson, M., Gupta, N., 2021. The Melamchi flood disaster: Cascading hazard and the need for multihazard risk management. *ICIMOD*, 21 pp. (accessed 16 August 2021).
- Major, J.J., Newhall, C.G., 1989. Snow and ice perturbation during historical volcanic eruptions and the formation of lahars and floods. *Bulletin of volcanology* 52, 1–27.
- Mal, S., Allen, S.K., Frey, H., Huggel, C., Dimri, A.P., 2021. Sectorwise assessment of glacial lake outburst flood danger in the Indian Himalayan region. *Mountain Research and Development* 41, R1–R12.
- Mani, P., Dobmann, J., Caduff, U., 2014. Unwetter vom 10. Oktober 2011: Hydrometeorologische Analyse Berner Oberland: Report for the attention of Oberingenieurkreis I, Thun. geo7 AG.
- Margret, S., Funk, M., 1999. Hazard mapping for ice and combined snow/ice avalanches — two case studies from the Swiss and Italian Alps. *Cold Regions Science and Technology* 30, 159–173.
- Martha, T.R., Reddy, P.S., Bhatt, C.M., Raj, K.B.G., Nalini, J., Padmanabha, E.A., Narender, B., Kumar, K.V., Muralikrishnan, S., Rao, G.S., Diwakar, P.G., Dadhwal, V.K., 2017. Debris volume estimation and monitoring of Phuktal river landslide-dammed lake in the Zaskar Himalayas, India using Cartosat-2 images. *Landslides* 14, 373–383. <https://doi.org/10.1007/s10346-016-0749-8>.
- Mavrouli, O.-C., Abbruzzese, J., Corominas, J., Labiouse, V., 2014. Review and Advances in Methodologies for Rockfall Hazard and Risk Assessment, in: van Asch, T., Corominas, J., Greiving, S., Malet, J.-P., Sterlacchini, S. (Eds.), *Mountain Risks: From Prediction to Management and Governance*, vol. 34. Springer Netherlands, Dordrecht, pp. 179–199.
- McClung, D., Schaerer, P.A., 2006. *The avalanche handbook*. The Mountaineers Books.
- McCull, S.T., Draebing, D., 2019. Rock Slope Instability in the Proglacial Zone: State of the Art, in: Heckmann, T., Morche, D. (Eds.), *Geomorphology of Proglacial Systems*. Springer International Publishing, Cham, pp. 119–141.
- McSaveney, M.J., 2002. Recent rockfalls and rock avalanches in Mount Cook national park, New Zealand., in: Evans, S.G., DeGraff, J.V. (Eds.), *Catastrophic landslides: Effects, occurrence, and mechanisms*. Geological Soc. of America, Boulder, Colo.
- Medeu, A.R., Baimoldaev, T.A., Kirenskaya, T.L., 2016. Debris Flow Phenomena of Southeastern Kazakhstan: *Anthology of Debris Flow Phenomena and Their Investigations*. Almaty: Gylm.
- Mergili, M., Emmer, A., Juřicová, A., Cochachin, A., Fischer, J.-T., Huggel, C., Pudasaini, S.P., 2018a. How well can we simulate complex hydro-geomorphic process chains? The 2012 multi-lake outburst flood in the

- Santa Cruz Valley (Cordillera Blanca, Perú). *Earth Surf. Process. Landforms* 43, 1373–1389. <https://doi.org/10.1002/esp.4318>.
- Mergili, M., Frank, B., Fischer, J.-T., Huggel, C., Pudasaini, S.P., 2018b. Computational experiments on the 1962 and 1970 landslide events at Huascarán (Peru) with r. avafLOW: Lessons learned for predictive mass flow simulations. *Geomorphology* 322, 15–28.
- Mergili, M., Jaboyedoff, M., Pullarello, J., Pudasaini, S.P., 2020a. Back-calculation of the 2017 Piz Cengalo-Bondo landslide cascade with r. avafLOW. *Nat. Hazards Earth Syst. Sci.* <https://doi.org/10.5194/nhess-20-505-2020>.
- Mergili, M., Pudasaini, S.P., Emmer, A., Fischer, J.-T., Cochachin, A., Frey, H., 2020b. Reconstruction of the 1941 GLOF process chain at Lake Palcacocha (Cordillera Blanca, Peru). *Hydrol. Earth Syst. Sci.* 24, 93–114. <https://doi.org/10.5194/hess-24-93-2020>.
- Mergili, M., Schneider, J.F., 2011. Regional-scale analysis of lake outburst hazards in the southwestern Pamir, Tajikistan, based on remote sensing and GIS. *Nat. Hazards Earth Syst. Sci.* 11, 1447–1462. <https://doi.org/10.5194/nhess-11-1447-2011>.
- Morán-Tejeda, E., López-Moreno, J.I., Stoffel, M., Beniston, M., 2016. Rain-on-snow events in Switzerland: recent observations and projections for the 21st century. *Clim. Res.* 71, 111–125. <https://doi.org/10.3354/cr01435>.
- Moreiras, S., Lisboa, M.S., Mastrantonio, L., 2012. The role of snow melting upon landslides in the central Argentinean Andes. *Earth Surf. Process. Landforms* 37, 1106–1119. <https://doi.org/10.1002/esp.3239>.
- Mostbauer, K., Kaitna, R., Prenner, D., Hrachowitz, M., 2018. The temporally varying roles of rainfall, snowmelt and soil moisture for debris flow initiation in a snow-dominated system. *Hydrol. Earth Syst. Sci.* 22, 3493–3513. <https://doi.org/10.5194/hess-22-3493-2018>.
- Murray, T., Strozzi, T., Luckman, A., Jiskoot, H., Christakos, P., 2003. Is there a single surge mechanism? Contrasts in dynamics between glacier surges in Svalbard and other regions. *J. Geophys. Res.* 108. <https://doi.org/10.1029/2002JB001906>.
- Musselman, K.N., Lehner, F., Ikeda, K., Clark, M.P., Prein, A.F., Liu, C., Barlage, M., Rasmussen, R., 2018. Projected increases and shifts in rain-on-snow flood risk over western North America. *Nat. Clim. Chang.* 8, 808–812. <https://doi.org/10.1038/s41558-018-0236-4>.
- Nair, A., Singh, S.K., 2014. Understanding the Causes of Uttarakhand Disaster of June 2013: A Scientific Review, in: Pradeepkumar, A.P. (Ed.), *Proceedings of the 2nd Disaster, Risk, and Vulnerability Conference: 24-26 April, 2014*. Dept. of Geology, University of Kerala, [Thiruvananthapuram], pp. 57–64.
- Narama, C., Daiyrov, M., Duishonakunov, M., Tadono, T., Sato, H., Kääh, A., Ukita, J., Abdrakhmatov, K., 2018. Large drainages from short-lived glacial lakes in the Teskey Range, Tien Shan Mountains, Central Asia. *Nat. Hazards Earth Syst. Sci.* 18, 983–995. <https://doi.org/10.5194/nhess-18-983-2018>.
- Narama, C., Duishonakunov, M., Kääh, A., Daiyrov, M., Abdrakhmatov, K., 2010. The 24 July 2008 outburst flood at the western Zyndan glacier lake and recent regional changes in glacier lakes of the Teskey Ala-Too range, Tien Shan, Kyrgyzstan. *Nat. Hazards Earth Syst. Sci.* 10, 647–659. <https://doi.org/10.5194/nhess-10-647-2010>.
- Nibanupudi, H.K., Gupta, A.K., Rawat, P.K., 2015. Mitigating climatic and human induced disaster risks through ecosystem resilience: Harmonizing built and natural environments in the HKH region, in: *Mountain hazards and disaster risk reduction*. Springer, pp. 139–157.
- O'Connor, J.E., Hardison, J.H., Costa, J.E., 2001. Debris flows from failures of Neoglacial-age moraine dams in the Three Sisters and Mount Jefferson Wilderness areas, Oregon. US Department of the Interior, US Geological Survey.
- Oppikofer, T., Jaboyedoff, M., Keusen, H.-R., 2008. Collapse at the eastern Eiger flank in the Swiss Alps. *Nature Geosci* 1, 531–535. <https://doi.org/10.1038/ngeo258>.

- Paranunzio, R., Laio, F., Chiarle, M., Nigrelli, G., Guzzetti, F., 2016. Climate anomalies associated with the occurrence of rockfalls at high-elevation in the Italian Alps. *Nat. Hazards Earth Syst. Sci.* 16, 2085–2106. <https://doi.org/10.5194/nhess-16-2085-2016>.
- Payrastré, O., Nicolle, P., 2021. Estimation des débits de pointe atteints par les petits cours d'eau des Alpes Maritimes lors de la tempête Alex, le 2 octobre 2020: Action 8.2. [Rapport de recherche]. IFSTTAR - Institut Français des Sciences et Technologies des Transports, de l'Aménagement et des Réseaux. <https://hal.archives-ouvertes.fr/hal-03327094> (accessed 23 September 2021).
- Pescaroli, G., Alexander, D., 2015. A definition of cascading disasters and cascading effects: Going beyond the “toppling dominos” metaphor. *Planet@Risk* 3, 58–67.
- Petersen, M.D., Harmsen, S.C., Jaiswal, K.S., Rukstales, K.S., Luco, N., Haller, K.M., Mueller, C.S., Shumway, A.M., 2018. Seismic Hazard, Risk, and Design for South America. *Bulletin of the Seismological Society of America*. <https://doi.org/10.1785/0120170002>.
- Petley, D., 2012. Using seismic data to analyse the Seti River landslide in Nepal. *The Landslide Blog*. Accessed May 30, 2012.
- Petrakov, D.A., Chernomorets, S.S., Evans, S.G., Tutubalina, O.V., 2008. Catastrophic glacial multi-phase mass movements: a special type of glacial hazard. *Adv. Geosci.* 14, 211–218.
- Petrakov, D.A., Chernomorets, S.S., Viskhadzhieva, K.S., Dokukin, M.D., Savernyuk, E.A., Petrov, M.A., Erokhin, S.A., Tutubalina, O.V., Glazyrin, G.E., Shpuntova, A.M., Stoffel, M., 2020. Putting the poorly documented 1998 GLOF disaster in Shakhimardan River valley (Alay Range, Kyrgyzstan/Uzbekistan) into perspective. *The Science of the total environment* 724, 138287. <https://doi.org/10.1016/j.scitotenv.2020.138287>.
- Pierson, T.C., 2005. Hyperconcentrated flow — transitional process between water flow and debris flow, in: Jakob, M., Hungr, O. (Eds.), *Debris-flow Hazards and Related Phenomena*. Praxis Publishing Ltd, Berlin, Heidelberg, pp. 159–202.
- Pierson, T.C., Costa, J.E., Vancouver, W., 1987. A rheologic classification of subaerial sediment-water flows, in: Costa, J.E. (Ed.), *Debris flows/ avalanches: Process, recognition, and mitigation*. The Geological Society of America, Boulder, Col., pp. 1–12.
- Pierson, T.C., JANDA, R.J., Thouret, J.-C., Borrero, C.A., 1990. Perturbation and melting of snow and ice by the 13 November 1985 eruption of Nevado del Ruiz, Colombia, and consequent mobilization, flow and deposition of lahars. *Journal of Volcanology and Geothermal Research* 41, 17–66.
- Pomeroy, J.W., Fang, X., Marks, D.G., 2016. The cold rain-on-snow event of June 2013 in the Canadian Rockies - characteristics and diagnosis. *Hydrological Processes* 30, 2899–2914. <https://doi.org/10.1002/hyp.10905>.
- Popovnin, V.V., Petrakov, D.A., Tutubalina, O.V., Chernomorets, S.S., 2003. The glacial disaster of 2002 in North Ossetia. *Earth's Cryosphere* VII, 3–17.
- Raymond, M., Wegmann, M., Funk, M., 2003. Inventar gefährlicher Gletscher in der Schweiz, Mitt. VAW/ETH, reprot, 368.
- Rickenmann, D., Badoux, A., Hunzinger, L., 2016. Significance of sediment transport processes during piedmont floods: the 2005 flood events in Switzerland. *Earth Surf. Process. Landforms* 41, 224–230. <https://doi.org/10.1002/esp.3835>.
- Roback, K., Clark, M.K., West, A.J., Zekkos, D., Li, G., Gallen, S.F., Chamlagain, D., Godt, J.W., 2018. The size, distribution, and mobility of landslides caused by the 2015 Mw7. 8 Gorkha earthquake, Nepal. *Geomorphology* 301, 121–138.
- Roberti, G., Friele, P., van Wyk de Vries, B., Ward, B., Clague, J.J., Perotti, L., Giardino, M., 2017. Rheological evolution of the Mount Meager 2010 debris avalanche, southwestern British Columbia. *Geosphere* 13, 369–390. <https://doi.org/10.1130/GES01389.1>.
- Roberti, G., Ward, B., van Wyk De Vries, B., Falorni, G., Menounos, B., Friele, P., Williams-Jones, G., Clague, J.J., Perotti, G., Giardino, M., 2018. Landslides and glacier retreat at Mt. Meager volcano: Hazard and risk challenges. *Geohazards7 Engineering Resiliency in a Changing Climate*.

- Round, V., Leinss, S., Huss, M., Haemmig, C., Hajnsek, I., 2017. Surge dynamics and lake outbursts of Kyagar Glacier, Karakoram. *The Cryosphere* 11, 723–739.
- Ruiz-Villanueva, V., Allen, S., Arora, M., Goel, N.K., Stoffel, M., 2017. Recent catastrophic landslide lake outburst floods in the Himalayan mountain range. *Progress in Physical Geography: Earth and Environment* 41, 3–28. <https://doi.org/10.1177/0309133316658614>.
- Sattar, A., Haritashya, U.K., Kargel, J.S., Karki, A., 2022. Transition of a small Himalayan glacier lake outburst flood to a giant transborder flood and debris flow. *Scientific reports* 12, 12421.
- Schaub, Y., Huggel, C., Cochachin, A., 2016. Ice-avalanche scenario elaboration and uncertainty propagation in numerical simulation of rock-/ice-avalanche-induced impact waves at Mount Hualcán and Lake 513, Peru. *Landslides* 13, 1445–1459. <https://doi.org/10.1007/s10346-015-0658-2>.
- Schauwecker, S., Gascón, E., Park, S., Ruiz-Villanueva, V., Schwarb, M., Sempere-Torres, D., Stoffel, M., Vitolo, C., Rohrer, M., 2019. Anticipating cascading effects of extreme precipitation with pathway schemes - Three case studies from Europe. *Environment international* 127, 291–304. <https://doi.org/10.1016/j.envint.2019.02.072>.
- Schneider, D., Huggel, C., Cochachin, A., Guillén, S., García, J., 2014. Mapping hazards from glacier lake outburst floods based on modelling of process cascades at Lake 513, Carhuaz, Peru. *Adv. Geosci.* 35, 145–155. <https://doi.org/10.5194/adgeo-35-145-2014>.
- Schneider, D., Huggel, C., Haerberli, W., Kaitna, R., 2011. Unraveling driving factors for large rock-ice avalanche mobility. *Earth Surf. Process. Landforms* 36, 1948–1966. <https://doi.org/10.1002/esp.2218>.
- Schneider, J.F., Gruber, F.E., Mergili, M., 2013. Recent cases and geomorphic evidence of landslide-dammed lakes and related hazards in the mountains of Central Asia, in: *Landslide science and practice*. Springer, pp. 57–64.
- Selby, M.J., 1993. *Hillslope materials and processes*, 2nd ed. Oxford Univ. Press, Oxford, 451 pp.
- Seynova, I.B., Chernomorets, S., Dokukin, M., Petrakov, D., Savernyuk, E., Lukashov, A., Belousova, E., 2017. Formation of water flow in lahars from active glacier-clad volcanoes. *Earths Cryosphere* 21, 103–111.
- Shrestha, A.B., Bajracharya, S.R., Kargel, J.S., Khanal, N.R., 2016. The impact of Nepal's 2015 Gorkha earthquake-induced geohazards. *International Centre for Integrated Mountain Development (ICIMOD)*.
- Shrestha, AB, Steiner, J., Nepal, S., Maharjan, S.B., Jackson, M., Rasul, G., Bajracharya, B., 2021. Understanding the Chamoli flood: Cause, process, impacts, and context of rapid infrastructure development. *RIVER BASINS AND CRYOSPHERE, ICIMOD, Kathmandu, Nepal*.
- Shugar, D.H., Burr, A., Haritashya, U.K., Kargel, J.S., Watson, C.S., Kennedy, M.C., Bevington, A.R., Betts, R.A., Harrison, S., Strattman, K., 2020. Rapid worldwide growth of glacial lakes since 1990. *Nat. Clim. Chang.* 10, 939–945.
- Shugar, D.H., Jacquemart, M., Shean, D., Bhushan, S., Upadhyay, K., Sattar, A., Schwanghart, W., McBride, S., van Vries, M.W. de, Mergili, M., Emmer, A., Deschamps-Berger, C., McDonnell, M., Bhambri, R., Allen, S., Berthier, E., Carrivick, J.L., Clague, J.J., Dokukin, M., Dunning, S.A., Frey, H., Gascoin, S., Haritashya, U.K., Huggel, C., Kääb, A., Kargel, J.S., Kavanaugh, J.L., Lacroix, P., Petley, D., Rupper, S., Azam, M.F., Cook, S.J., Dimri, A.P., Eriksson, M., Farinotti, D., Fiddes, J., Gnyawali, K.R., Harrison, S., Jha, M., Koppes, M., Kumar, A., Leinss, S., Majeed, U., Mal, S., Muhuri, A., Noetzli, J., Paul, F., Rashid, I., Sain, K., Steiner, J., Ugalde, F., Watson, C.S., Westoby, M.J., 2021. A massive rock and ice avalanche caused the 2021 disaster at Chamoli, Indian Himalaya. *Science (New York, N.Y.)*. <https://doi.org/10.1126/science.abh4455>.
- Siddique, T., Haris, P.M., Pradhan, S.P., 2022. Unraveling the geological and meteorological interplay during the 2021 Chamoli disaster, India. *Natural Hazards Research*. <https://doi.org/10.1016/j.nhres.2022.04.003>.
- Sigurdsson, H., Houghton, B., McNutt, S., Rymer, H., Stix, J., 2015. *The encyclopedia of volcanoes*. Elsevier.
- Singh, D., Horton, D.E., Tsiang, M., Haugen, M., Ashfaq, M., Mei, R., Rastogi, D., Johnson, N.C., Charland, A., Rajaratnam, B., 2014. Severe precipitation in Northern India in June 2013: Causes, historical context, and changes in probability. *Bull Am Meteorol Soc* 95, S58-S61.

- Singh, R., Shekhar, M., Pandey, V.K., Kumar, R., Sharma, R.K., 2018. Causes and geomorphological effects of large debris flows in the lower valley areas of the Meru and Gangotri glaciers, Bhagirathi basin, Garhwal Himalaya (India). *Remote Sensing Letters* 9, 809–818. <https://doi.org/10.1080/2150704X.2018.1484956>.
- Somos-Valenzuela, M.A., Oyarzún-Ulloa, J.E., Fustos-Toribio, I.J., Garrido-Urzuá, N., Chen, N., 2020. The mudflow disaster at Villa Santa Lucía in Chilean Patagonia: understandings and insights derived from numerical simulation and postevent field surveys. *Nat. Hazards Earth Syst. Sci.* 20, 2319–2333. <https://doi.org/10.5194/nhess-20-2319-2020>.
- Sosio, R., 2015. Rock–Snow–Ice Avalanches, in: *Landslide Hazards, Risks and Disasters*. Elsevier, pp. 191–240.
- Srivastava, P., Namdev, P., Singh, P.K., 2022. 7 February Chamoli (Uttarakhand, India) Rock-Ice Avalanche Disaster: Model-Simulated Prevailing Meteorological Conditions. *Atmosphere* 13, 267. <https://doi.org/10.3390/atmos13020267>.
- Stanley, T., Kirschbaum, D.B., Pascale, S., Kapnick, S., 2020. Extreme Precipitation in the Himalayan Landslide Hotspot, in: Levizzani, V., Kidd, C., Kirschbaum, D.B., Kummerow, C.D., Nakamura, K., Turk, F.J. (Eds.), *Satellite Precipitation Measurement*, vol. 69. Springer International Publishing, Cham, pp. 1087–1111.
- Stäubli, A., Nussbaumer, S.U., Allen, S.K., Huggel, C., Arguello, M., Costa, F., Hergarten, C., Martínez, R., Soto, J., Vargas, R., Zambrano, E., Zimmermann, M., 2018. Analysis of Weather- and Climate-Related Disasters in Mountain Regions Using Different Disaster Databases, in: Mal, S., Singh, R., Huggel, C. (Eds.), *Climate Change, Extreme Events and Disaster Risk Reduction*, vol. 47. Springer International Publishing, Cham, pp. 17–41.
- Stethem, C., 2013. Avalanches, in: Bobrowsky, P.T. (Ed.), *Encyclopedia of natural hazards: Includes case studies*. Springer Reference, Dordrecht, pp. 31–34.
- Stoffel, M., Bollschweiler, M., Beniston, M., 2011. Rainfall characteristics for periglacial debris flows in the Swiss Alps: past incidences–potential future evolutions. *Climatic Change* 105, 263–280. <https://doi.org/10.1007/s10584-011-0036-6>.
- Stoffel, M., Corona, C., 2018. Future winters glimpsed in the Alps. *Nature Geosci* 11, 458–460. <https://doi.org/10.1038/s41561-018-0177-6>.
- Stoffel, M., Huggel, C., 2012. Effects of climate change on mass movements in mountain environments. *Progress in Physical Geography: Earth and Environment* 36, 421–439. <https://doi.org/10.1177/0309133312441010>.
- Stoffel, M., Mendlik, T., Schneuwly-Bollschweiler, M., Gobiet, A., 2014a. Possible impacts of climate change on debris-flow activity in the Swiss Alps. *Climatic Change* 122, 141–155. <https://doi.org/10.1007/s10584-013-0993-z>.
- Stoffel, M., Tiranti, D., Huggel, C., 2014b. Climate change impacts on mass movements—case studies from the European Alps. *The Science of the total environment* 493, 1255–1266. <https://doi.org/10.1016/j.scitotenv.2014.02.102>.
- Strahler, A.N., 1957. Quantitative analysis of watershed geomorphology. *Eos, Transactions American Geophysical Union* 38, 913–920.
- Sun, Q., Zhang, X., Zwiers, F., Westra, S., Alexander, L.V., 2021. A Global, Continental, and Regional Analysis of Changes in Extreme Precipitation. *Journal of Climate* 34, 243–258. <https://doi.org/10.1175/JCLI-D-19-0892.1>.
- Tanyaş, H., van Westen, C.J., Allstadt, K.E., Anna Nowicki Jessee, M., Görüm, T., Jibson, R.W., Godt, J.W., Sato, H.P., Schmitt, R.G., Marc, O., Hovius, N., 2017. Presentation and Analysis of a Worldwide Database of Earthquake-Induced Landslide Inventories. *J. Geophys. Res. Earth Surf.* 122, 1991–2015. <https://doi.org/10.1002/2017JF004236>.

- Tapia Baldis, C., Trombotto Liaudat, D., 2019. Rockslides and rock avalanches in the Central Andes of Argentina and their possible association with permafrost degradation. *Permafrost and Periglac. Process.* 30, 330–347.
- The Hindu, 2012. 10 killed, 60 missing as glacial lake burst in Nepal. May 5, 2012. <https://www.thehindu.com/news/international/10-killed-60-missing-as-glacial-lake-burst-in-nepal/article3387581.ece>.
- Thouret, J.C., Ramírez C., J., Gibert-Malengreau, B., Vargas, C.A., Naranjo, J.L., Vandemeulebrouck, J., Valla, F., Funk, M., 2007. Volcano–glacier interactions on composite cones and lahar generation: Nevado del Ruiz, Colombia, case study. *Ann. Glaciol.* 45, 115–127. <https://doi.org/10.3189/172756407782282589>.
- Tielidze, L.G., Kumladze, R.M., Wheate, R.D., Gamkrelidze, M., 2019. The Devdoraki Glacier Catastrophes, Georgian Caucasus. *HunGeoBull*, 21–35. <https://doi.org/10.15201/hungeobull.68.1.2>.
- Tobler, D., Kull, I., Jacquemart, M., Haehlen, N., 2014. Hazard Management in a Debris Flow Affected Area: Case Study from Spreitgraben, Switzerland, in: Sassa, K., Canuti, P., Yin, Y. (Eds.), *Landslide Science for a Safer Geoenvironment*, vol. 6. Springer International Publishing, Cham, pp. 25–30.
- Tobler, D., Mani, P., Riner, R., Haehlen, N., Raetzo, H., 2015. Prediction of Climate Change Forced Mass Movement Processes Induced in Periglacial Areas, in: Lollino, G., Manconi, A., Clague, J., Shan, W., Chiarle, M. (Eds.), *Engineering Geology for Society and Territory - Volume 1*. Springer International Publishing, Cham, pp. 143–147.
- UNEP, 2007. *Tourism and mountains: A practical guide to managing the environmental and social impacts of mountain tours*. UNEP; Conservation International; Tour Operators’ Initiative, Paris, Arlington, Va., Madrid, 1 volume (various pagings).
- United Nations Office for Disaster Risk Reduction. *Sendai Framework for Disaster Risk Reduction 2015 - 2030* 2015.
- Uuemaa, E., Ahi, S., Montibeller, B., Muru, M., Kmoch, A., 2020. Vertical Accuracy of Freely Available Global Digital Elevation Models (ASTER, AW3D30, MERIT, TanDEM-X, SRTM, and NASADEM). *Remote Sensing* 12, 3482. <https://doi.org/10.3390/rs12213482>.
- van Wyk de Vries, M., Bhushan, S., Jacquemart, M., Deschamps-Berger, C., Berthier, E., Gascoïn, S., Shean, D.E., Shugar, D.H., Kääb, A., 2021. Pre-collapse motion of the February 2021 Chamoli rock-ice avalanche, Indian Himalaya.
- Veh, G., Korup, O., Specht, S. von, Roessner, S., Walz, A., 2019. Unchanged frequency of moraine-dammed glacial lake outburst floods in the Himalaya. *Nat. Clim. Chang.* 9, 379–383. <https://doi.org/10.1038/s41558-019-0437-5>.
- Veh, G., Lützwow, N., Kharlamova, V., Petrakov, D., Hugonnet, R., Korup, O., 2022. Trends, Breaks, and Biases in the Frequency of Reported Glacier Lake Outburst Floods. *Earth’s Future* 10. <https://doi.org/10.1029/2021EF002426>.
- Vergara Dal Pont, I., Moreiras, S.M., Santibañez Ossa, F., Araneo, D., Ferrando, F., 2020. Debris flows triggered from melt of seasonal snow and ice within the active layer in the semi-arid Andes. *Permafrost and Periglac. Process.* 31, 57–68. <https://doi.org/10.1002/ppp.2020>.
- Vilca, O., Mergili, M., Emmer, A., Frey, H., Huggel, C., 2021. The 2020 glacial lake outburst flood process chain at Lake Salkantaycocha (Cordillera Vilcabamba, Peru). *Landslides* 18, 2211–2223. <https://doi.org/10.1007/s10346-021-01670-0>.
- Villalba, R., Boninsegna, J.A., Veblen, T.T., Schmelter, A., Rubulis, S., 1997. Recent Trends in Tree-Ring Records from High Elevation Sites in the Andes of Northern Patagonia, in: Diaz, H.F., Beniston, M., Bradley, R.S. (Eds.), *Climatic Change at High Elevation Sites*. Springer Netherlands, Dordrecht, pp. 193–222.
- Voight, B., 1990. The 1985 Nevado del Ruiz volcano catastrophe: anatomy and retrospection. *Journal of Volcanology and Geothermal Research* 42, 151–188.
- Vuichard, D., Zimmermann, M., 1987. The 1985 catastrophic drainage of a moraine-dammed lake, Khumbu Himal, Nepal: cause and consequences. *Mountain Research and Development*, 91–110.

- Walter, F., Amann, F., Kos, A., Kenner, R., Phillips, M., Preux, A. de, Huss, M., Tognacca, C., Clinton, J., Diehl, T., Bonanomi, Y., 2020. Direct observations of a three million cubic meter rock-slope collapse with almost immediate initiation of ensuing debris flows. *Geomorphology* 351, 106933. <https://doi.org/10.1016/j.geomorph.2019.106933>.
- Werder, M.A., Bauder, A., Funk, M., Keusen, H.-R., 2010. Hazard assessment investigations in connection with the formation of a lake on the tongue of Unterer Grindelwaldgletscher, Bernese Alps, Switzerland. *Nat. Hazards Earth Syst. Sci.* 10, 227–237. <https://doi.org/10.5194/nhess-10-227-2010>.
- Westoby, M.J., Glasser, N.F., Brasington, J., Hambrey, M.J., Quincey, D.J., Reynolds, J.M., 2014. Modelling outburst floods from moraine-dammed glacial lakes. *Earth-Science Reviews* 134, 137–159. <https://doi.org/10.1016/j.earscirev.2014.03.009>.
- Wever, N., Jonas, T., Fierz, C., Lehning, M., 2014. Model simulations of the modulating effect of the snow cover in a rain-on-snow event. *Hydrol. Earth Syst. Sci.* 18, 4657–4669. <https://doi.org/10.5194/hess-18-4657-2014>.
- Wilhelm, C., Feuerstein, G.C., Huwiler, A., Kühne, R., 2019. Bergsturz Cengalo und Murgänge Bondo: Erfahrungen der kantonalen Fachstelle, in: Bründl, M., Schweizer, J. (Eds.), *Forum für Wissen 2019. Lernen aus Extremereignissen.*, pp. 53–66.
- Worni, R., Huggel, C., Clague, J.J., Schaub, Y., Stoffel, M., 2014. Coupling glacial lake impact, dam breach, and flood processes: A modeling perspective. *Geomorphology* 224, 161–176. <https://doi.org/10.1016/j.geomorph.2014.06.031>.
- Worni, R., Stoffel, M., Huggel, C., Volz, C., Casteller, A., Luckman, B., 2012. Analysis and dynamic modeling of a moraine failure and glacier lake outburst flood at Ventisquero Negro, Patagonian Andes (Argentina). *Journal of Hydrology* 444–445, 134–145. <https://doi.org/10.1016/j.jhydrol.2012.04.013>.
- Worni, R.P., 2012. Characteristics of glacial lake hazards and extreme flow events: advanced approaches to model processes and process chains.
- Würzer, S., Jonas, T., Wever, N., Lehning, M., 2016. Influence of Initial Snowpack Properties on Runoff Formation during Rain-on-Snow Events. *Journal of Hydrometeorology* 17, 1801–1815. <https://doi.org/10.1175/JHM-D-15-0181.1>.
- Yafyazova, R.K., 2007. Nature of Debris Flows in the Zailiysky Alatau Mountains. *Problems of Adaptation. Almaty* (in Russian).
- Yafyazova, R.K., 2011. Disastrous debris flows connected with glacial processes and defense methods against them in Kazakhstan. *Italian Journal of Engineering Geology and Environment Special issue: V Conference Debris Flow*, 1101–1110.
- Yin, B., Zeng, J., Zhang, Y., Huai, B., Wang, Y., 2019. Recent Kyagar glacier lake outburst flood frequency in Chinese Karakoram unprecedented over the last two centuries. *Nat Hazards* 95, 877–881.
- Zaginaev, V., Ballesteros-Cánovas, J.A., Erokhin, S., Matov, E., Petrakov, D., Stoffel, M., 2016. Reconstruction of glacial lake outburst floods in northern Tien Shan: Implications for hazard assessment. *Geomorphology* 269, 75–84. <https://doi.org/10.1016/j.geomorph.2016.06.028>.
- Zaginaev, V., Petrakov, D., Erokhin, S., Meleshko, A., Stoffel, M., Ballesteros-Cánovas, J.A., 2019. Geomorphic control on regional glacier lake outburst flood and debris flow activity over northern Tien Shan. *Global and Planetary Change* 176, 50–59. <https://doi.org/10.1016/j.gloplacha.2019.03.003>.
- Zhang, M., Chen, F., Tian, B., Liang, D., Yang, A., 2020. Characterization of Kyagar Glacier and Lake Outburst Floods in 2018 Based on Time-Series Sentinel-1A Data. *Water* 12, 184. <https://doi.org/10.3390/w12010184>.
- Zhang, S., Zhang, L., Lacasse, S., Nadim, F., 2016. Evolution of Mass Movements near Epicentre of Wenchuan Earthquake, the First Eight Years. *Scientific reports* 6, 36154. <https://doi.org/10.1038/srep36154>.
- Zhang, T., Yin, Y., Li, B., Liu, X., Wang, M., Gao, Y., Wan, J., Gnyawali, K.R., 2022. Characteristics and dynamic analysis of the February 2021 long-runout disaster chain triggered by massive rock and ice avalanche at

Chamoli, Indian Himalaya. *Journal of Rock Mechanics and Geotechnical Engineering*.
<https://doi.org/10.1016/j.jrmge.2022.04.003>.

Zhao, B., 2016. April 2015 Nepal earthquake: observations and reflections. *Nat Hazards* 80, 1405–1410.
<https://doi.org/10.1007/s11069-015-2001-6>.

Zheng, G., Allen, S.K., Bao, A., Ballesteros-Cánovas, J.A., Huss, M., Zhang, G., Li, J., Yuan, Y., Jiang, L., Yu, T., Chen, W., Stoffel, M., 2021a. Increasing risk of glacial lake outburst floods from future Third Pole deglaciation. *Nat. Clim. Chang.* 11, 411–417. <https://doi.org/10.1038/s41558-021-01028-3>.

Zheng, G., Mergili, M., Emmer, A., Allen, S., Bao, A., Guo, H., Stoffel, M., 2021b. The 2020 glacial lake outburst flood at Jinwuco, Tibet: causes, impacts, and implications for hazard and risk assessment. *The Cryosphere* 15, 3159–3180. <https://doi.org/10.5194/tc-15-3159-2021>.

Zscheischler, J., Westra, S., van den Hurk, B.J.J.M., Seneviratne, S.I., Ward, P.J., Pitman, A., AghaKouchak, A., Bresch, D.N., Leonard, M., Wahl, T., Zhang, X., 2018. Future climate risk from compound events. *Nature Clim Change* 8, 469–477. <https://doi.org/10.1038/s41558-018-0156-3>.